



Article

Real-World Driving Cycles Adaptability of Electric Vehicles

Zhicheng Sun ^{1,2}, Zui Wen ¹, Xin Zhao ¹, Yunpeng Yang ¹ and Su Li ^{2,*}

¹ China Automotive Technology&Research Center Co. Ltd., Tianjin 300401, China;
sunshine649@163.com (Z.S.); wenzui@catarc.ac.cn (Z.W.); zhaoxin2019@catarc.ac.cn (X.Z.);
yangyunpeng@catarc.ac.cn (Y.Y.)

² School of Energy and Environmental Engineering, Hebei University of Technology, Tianjin 300401, China

* Correspondence: 13352067329@189.cn; Tel.: +86-133-5206-7329

Received: 28 October 2019; Accepted: 26 February 2020; Published: 3 March 2020



Abstract: Electric vehicles (EVs) include battery electric vehicles (BEVs), fuel-cell vehicles (FCVs) and fuel-cell hybrid electric vehicles (FCHEVs). The performance of vehicles is usually evaluated using standardized driving cycle tests; however, the results from standardized driving cycle tests deviate from the real-world driving cycle. In order to test the adaptability of EVs to real-world driving cycles, conditions of three typical routes in Tianjin are collected and their characteristics analyzed; then BEV and FCV models are created based on a type of FCHEV to simulate 0–100 km/h acceleration and cruising performance under a real-world driving cycle; finally, a motor bench is used to test the performance of FCHEV under the NEDC (New European Driving Cycle). After the adaptability of the three models to real-world driving cycle is compared based on the simulation and test results, it is found that FCHEV can recycle braking energy and has quick dynamic response, which can be well adapted to the real-world driving cycle.

Keywords: electric vehicles; driving cycle; energy consumption

1. Introduction

China has now become one of the largest energy consumers and importers in the world [1]. While continuous environmental pollution and the energy security crisis have attracted increasing public attention, vehicle exhaust emissions have ranked to be a major source of air pollution in some cities in China because transportation is responsible for about 1/3 of greenhouse gas emissions [2]. The proportion is same in EU (European Union), US and other regions in the world [3]. Currently, countries worldwide are taking various measures to address transportation emissions, such as promoting public transportation and inventing more energy-saving transmission technology.

New-energy vehicles represented by battery electric vehicles (BEVs) and fuel-cell electric vehicles (FCEVs) are ideal solutions to this problem. In 2017, global sales of BEVs exceeded 1 million, increasing by 54 % compared to that in 2016. By now, global ownership of EVs has reached over 5 million [4]. There are many factors contributing to the continuous increase in EV ownership. Firstly, governments in many countries have introduced relevant policies and incentives [5]. For example, the EU proposes to cut greenhouse gas emission by 60% by 2030; California offers to subsidize consumers purchasing EVs [6]; the Chinese government provides subsidies of various levels based on technological levels of EVs—the longer the mileage and the higher the energy density, the greater the subsidy [7]. Secondly, EVs powered by a ternary lithium battery or lithium iron phosphate battery feature faster dynamic response, are more environmentally friendly and more energy-saving than traditional fuel vehicles [8]. Thirdly, electric energy production today can satisfy future transportation needs. For instance, China produces most electric power resources for itself. Although there are some problems in cost and

battery technology, EVs usually charge during off-peak power consumption hours at night, hence the development needs of EVs in the near future can be satisfied as long as electric power resources are reasonably allocated [9]. Therefore, vigorous promotion of application of EVs is one of the effective ways to address the energy and environmental crisis brought about by the transportation system of today.

However, large amounts of lithium, cobalt and nickel are used to produce batteries for EVs and permanent magnet motors require a lot of rare earth elements such as dysprosium, terbium, praseodymium and neodymium [10]. This has a great negative impact on sustainable development of the environment. Meanwhile, as rare earth elements are unevenly distributed worldwide, their yield is greatly affected by geopolitics and this significantly limits production of BEVs [11]. FCEVs are powered by proton exchange membrane fuel cells. Compared with other fuel cells, proton exchange membrane fuel cells have high density, great efficiency and low operating temperature, and are suitable as a power source for vehicles. Moreover, as fuel cells use hydrogen as fuel, water is the only reaction product and they produce no emission, which is the greatest advantage [12]. But a great quantity of greenhouse gas will be generated when hydrogen is produced for FCEVs and such a quantity is no less than the emission of traditional fuel vehicles. Luckily, as technologies progress, primary energy resources will no longer be the main source of electric power when electric power is to be produced by renewable energy sources including nuclear energy, biomass energy, solar energy and wind energy. By that time, greenhouse gas emissions from FCEVs will be 99.2 % lower than that of traditional fuel vehicles. Sadly, fuel cells are unable to work under heavy load for a long time and have response time, making them unsuitable for violent varying-duty operations. Also, long-time operation will seriously compromise the service life of fuel cells. In order to adapt to varying-duty operations, a FCEV is usually equipped with a hybrid power system consisting of fuel cells and power batteries. When the vehicles are accelerating or conditions change abruptly, power batteries will produce some of their energy to reduce energy supply pressure of fuel cells and thus extend their service life [13].

Every EV model has its advantages. For example, a BEV, although designed in simple way with fewer parts, has short mileage and long charging time. PHEVs have greater cruising ability thanks to their engines, but they emit greenhouse gas [14]. Fuel-cell vehicles (FCVs) and fuel-cell hybrid electric vehicles (FCHEVs) are both powered mainly by fuel cells without emission or pollution. But they cannot be promoted on a large scale due to restrictions in cost and technology.

Many Chinese and foreign scholars have studied the operating status of EVs and FCEVs via micro-simulation and macro-test. Xiaodan Xu et al. developed an EV model to simulate its energy consumption under various road conditions. Test results show that if PHEVs can account for 50% market share, energy consumption will be cut by 30% [15]. Xinkai Wu et al. collected energy consumption data of one EV driving on three different routes and analyzed the relations between its power and velocity and its accelerated velocity and road gradient to come up with a estimation model of EV power [16]. Xinmei Yuan et al. proposed a method to evaluate EV energy consumption under real driving cycles and proved the effectiveness of such a method by simulation and test data. The results showed that such method can accurately evaluate EV energy consumption under different road conditions and serve as a possible alternative mechanism to EV energy consumption evaluation [17]. John Brady et al. developed a driving cycle by real-world data from electric vehicle, over a six-month period. Real-world driving cycles are essential for EV powertrain design, battery management systems, battery range estimation and the provision of better information to EV users [18]. Marta Faria et al. monitored 40 drivers for a period of six months, The data obtained allowed for testing of the impacts of increasing the percentage of traffic shifting from peak to off-peak hours in energy consumption [19]. Shangfeng Jiang et al. included the quality of FCVs and road grade as influencing factors of an energy management strategy and used a forward-looking control strategy based on road conditions to reduce lag of fuel cells and cut fuel consumption rate [20]. Roberto Álvarez Fernández et al. studied mileage and energy consumption of EVs under various energy management strategies. The authors believed that before enough infrastructure was provided, a combination of two

power modes (hydrogen and electric energy) could be an effective method to power vehicles with low risk [21]. Z. Mokrani et al. studied the fuel cell/accumulator power systems used in PHEVs and verified the effectiveness of the EV energy management and control strategy they came up with via a hybrid system simulation model based on Matlab/Simulink [22]. Morrison G, et al. estimated the costs of all BEVs and FCEVs to be created from now to 2040. The results showed that the costs of these two power systems become similar quickly from 2025 to 2030; after 2040, the cost of FCEVs will drop below that of BEVs and gain remarkable advantages in larger models and longer traveling distance [23].

Most of the above studies focused on the factors affect the energy consumption of electric vehicles, and studied the effects of speed, acceleration and gradient on electric vehicles, but did not consider the characteristics of the vehicle itself. This paper studies the performance of different types of electric vehicles under different road conditions. As the same time standard cycles cannot accurately reflect the performance of the vehicle, it is necessary to study the performance of electric vehicles to real-world driving cycles. Firstly, a BEV was used to collect three typical routes in Tianjin. Then, BEV and FCV models were established based on a certain FCHEV, and the adaptability of the BEV and FCV to three real-world cycle was simulated using AVL CRUISE. Lastly, the 100 km/h acceleration performance, cruising performance, and energy consumption of the FCHEV were tested with a motor bench. The simulation and test results of the three vehicles were comprehensively compared, and the real-world driving cycle adaptability of electric vehicles was analyzed.

BEVs and FCEVs have many different modeling methods, depending on the purposes of simulation and degree of accuracy. The forward model is more accurate and complex since it uses drivers' instructions as input parameters and creates models for all vehicle parts (such as transmission and direct current/direct current (DC/DC)) to simulate and estimate energy consumption. Its deficiency lies in heavy calculation burden and great difficulty in micro-analysis of energy flow [24]. Reverse simulation is another way. It uses vehicle motion parameters (such as velocity and accelerated velocity) as input and simulates power required for vehicles to move forward via the efficiency diagram and power model, and hence is suitable for the micro-analysis of energy flow process [25]. In this paper, we mainly use reverse simulation to calculation FCVs and BEVs.

The paper is organized as follows. Section 2 describes the process of collecting a real-world driving cycle. Section 3 introduces the mathematical model of vehicles, fuel cell, battery and so on. Experiment and simulation results are analyzed in Section 5.

2. Real-World Driving Cycles

2.1. Collect Information of Real-World Driving Cycle

In order to simulate energy consumption and performance of vehicles under real-world driving cycles, an EV is used to collect information of real-world driving cycles in Tianjin in this paper. To eliminate the impact of single road condition on vehicle energy consumption, three routes are selected in Tianjin based on traffic condition and traveling pattern of local residents, covering roads of different grades and as many areas as possible (such as business districts, residential areas and suburb areas) in the entire road network. While collecting road conditions, energy consumption of the vehicle used is also tested on the routes. The first route is located in the downtown area where there are many traffic lights and junctions. Besides, highly populated places such as shopping malls, hospitals and schools are also located along this route. Information collection time is at the busy hour in the morning and this route is congested with average velocity of 22.4 km/h (hereinafter referred to as R1). The second route is located in a suburban area with a few traffic lights and junctions. The traffic is smooth with average velocity of 44.6 km/h (hereinafter referred to as R2). The third route is a high-velocity road and the test vehicle runs constantly at high velocity with average velocity of 64.6 km/h (hereinafter referred to as R3). The information of the three routes is shown in Figure 1.

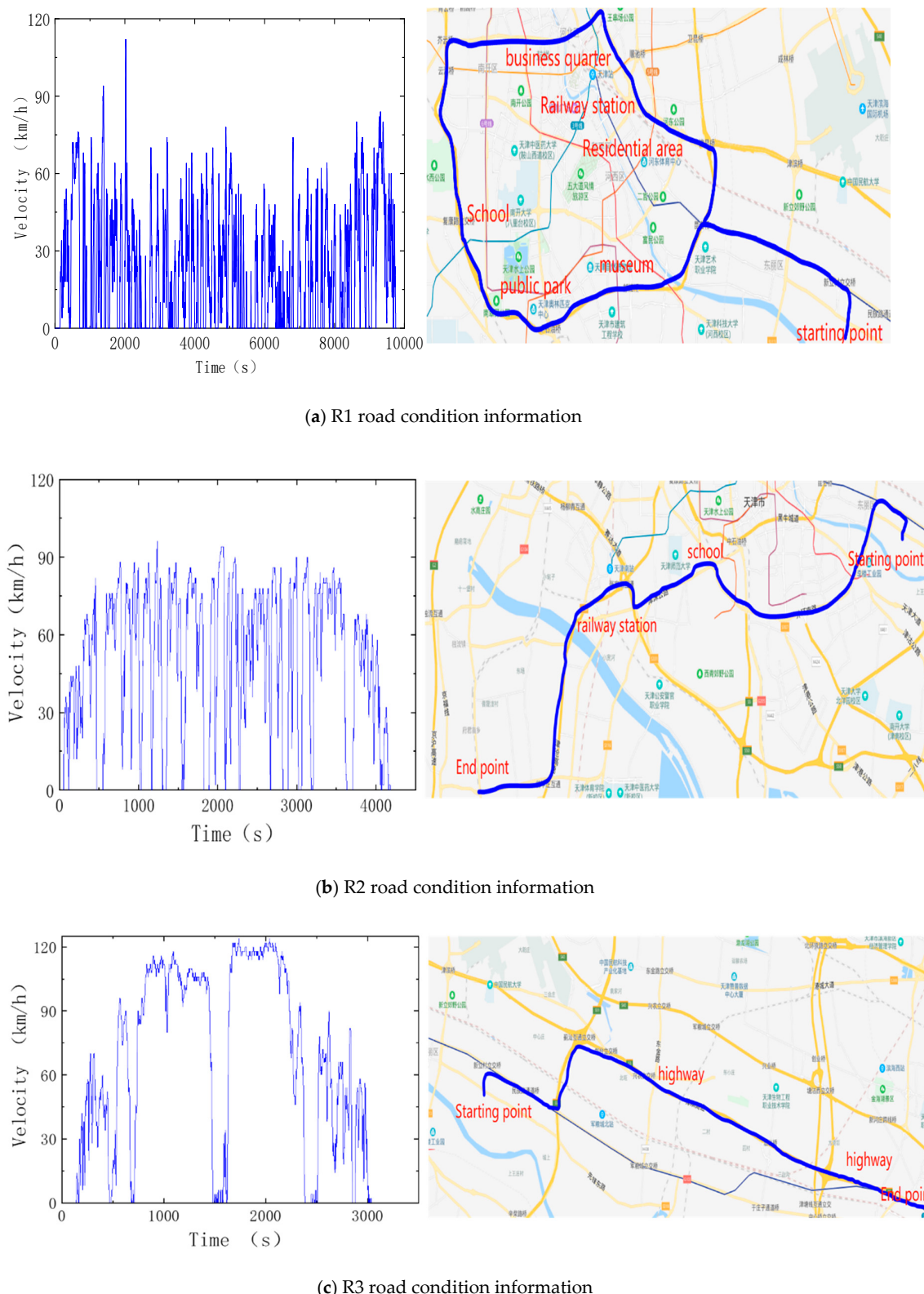


Figure 1. Curve of conditions of three real routes.

2.2. Characteristics of Real-World Driving Cycle

Characteristics of real-world driving cycles include velocity, acceleration and time. In this paper, the conditions of three routes and characteristics of CLTC-P (China light-duty vehicle test

cycle-passenger car) and NEDC (New European Driving Cycle) are compared. CLTC-P is a passenger car driving cycle based on the traffic conditions in China, including three velocity ranges of high, medium and low velocity with average velocity of 28.9 km/h.

Figure 2 describes percentage of time that driving at such speed, including uniform speed, acceleration, deceleration and idle speed (when the electric motor is uncoupled from the drivetrain) in three real-world driving cycles. We can see from the picture that R1 has the highest percentage of idle speed and R3 has the highest percentage of uniform speed. R1 and R2 have similar percentage of acceleration and deceleration.

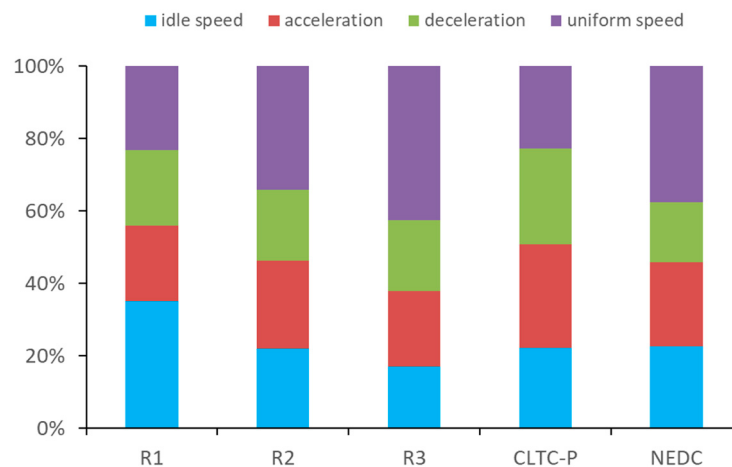


Figure 2. Comparison of conditions of each route.

Figure 3 describes the probability distribution of velocity and acceleration under three real-world driving cycles. We can tell from Figure 3a,b that the probability is the highest for velocity range from 0 to 10 km/h and the acceleration is mainly distributed between -1 – 1 m/s 2 under R1 condition. We can see from Figure 3e,f that the probability of velocity is the highest between 60–80 km/h and the acceleration is mainly distributed between -1 – 1 m/s 2 under R2 condition. From Figure 3e,f we know that the probability of velocity is the highest between 110–120 km/h and the acceleration is mainly distributed between -0.5 – 0.5 m/s 2 under R3 condition.

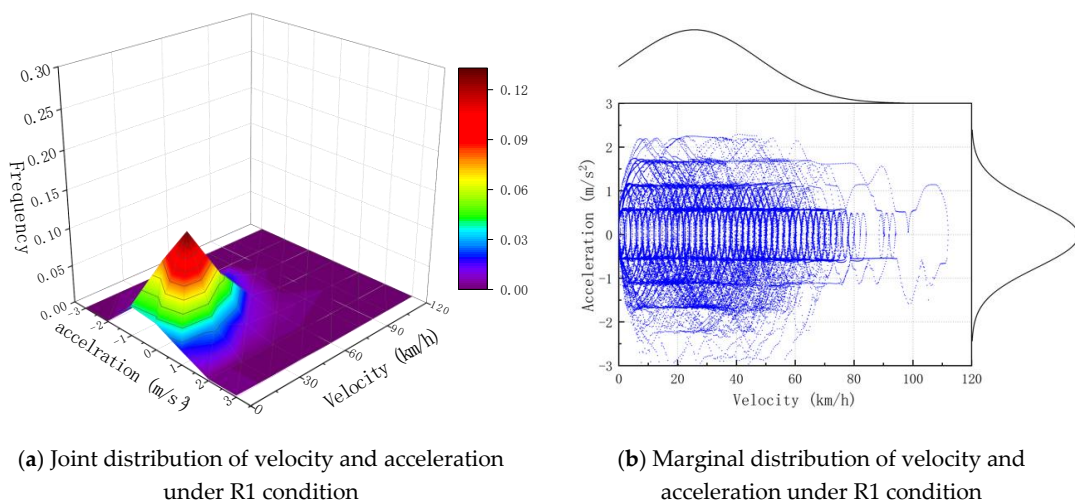


Figure 3. Cont.

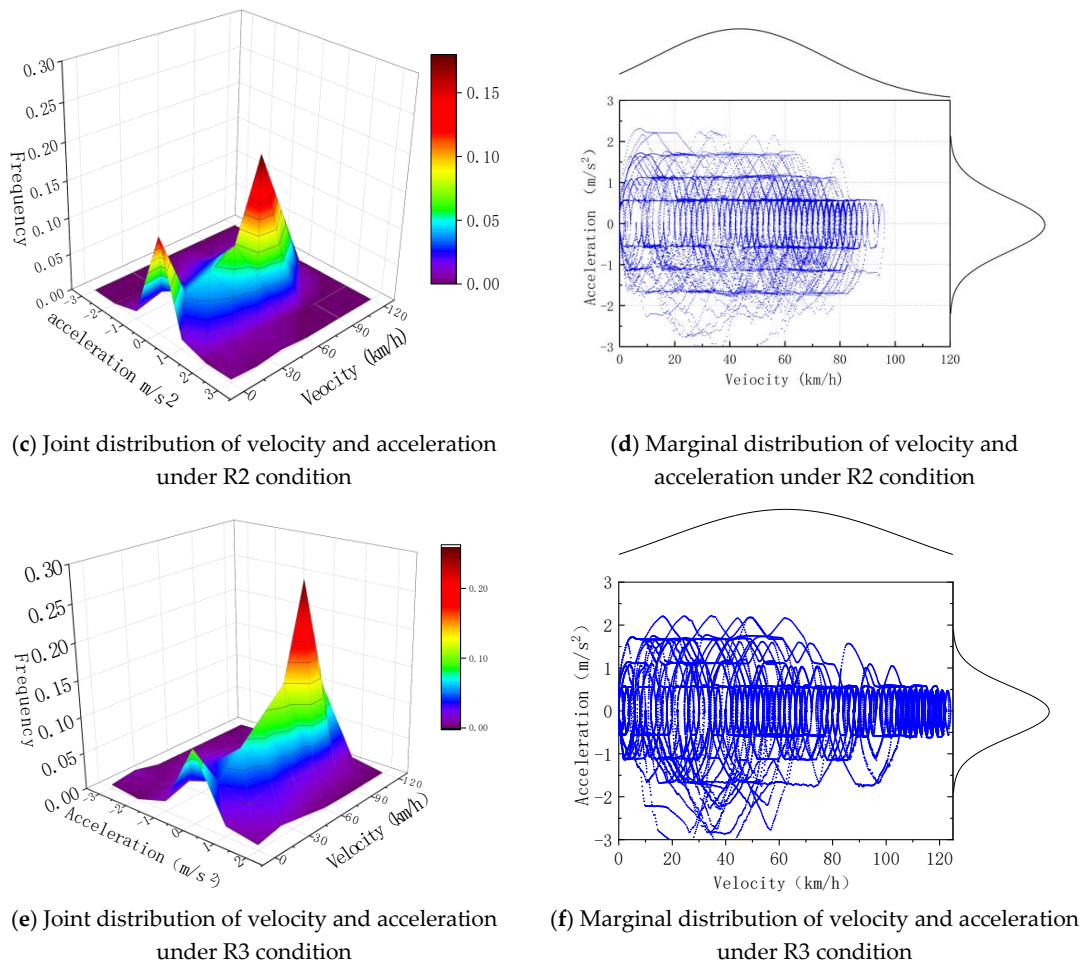


Figure 3. Probability distribution of velocity and acceleration in three road conditions.

Through the comparative analysis of Figures 2 and 3, we know that vehicles start and stop more times, acceleration and deceleration are frequent, and the velocity is low to medium under the R1 condition; the velocity is medium to high and velocity distribution is in polarization under the R2 condition; and the velocity is mainly high with high percentage of constant velocity and small change in acceleration under the R3 condition.

3. Mathematical Model of Vehicles

In order to compare difference in performance of BEV, FCV and FCHEV, simulation models of BEV and FCV are created based on a model of FCHEV made by a certain country. Such simulation models have identical parameters such as curb weight, windward area and tire radius with the FCHEV model and only differ in power systems. Therefore, consistent vehicle performance can be ensured. The basic parameters of the vehicle are shown in Table 1.

Table 1. Basic parameters of fuel-cell hybrid electric vehicle (FCHEV).

Parameter	Value
Overall height	1537 mm
Overall width	1816 mm
Overall length	4890 mm
Curb weight	1848 kg
Hydrogen tank volume	122.4 L
Maximum power	114 kW

3.1. Power System Structure Model

BEVs or FCVs are subject to air, gradient and rolling resistance during driving and overcome such resistance to move forward.

$$F_{v,res} = F_\alpha + F_r + F_g \quad (1)$$

In the formula above, $F_{v,res}$ is the total resistance of vehicles during driving, F_α is air resistance, F_r is rolling resistance and F_g is gradient resistance [26].

$$F_\alpha = \frac{1}{2}\rho AC_x v^2 \quad (2)$$

$$F_r = m_v C_r g \cos(\alpha) \quad (3)$$

$$F_g = m_v g \sin(\alpha) \quad (4)$$

In the three formulas above, v is the vehicle velocity, ρ is the air density, A is the front surface of vehicle, m_v is the vehicle mass, g is the acceleration of gravity, C_x is the drag coefficient, C_r is the aerodynamic coefficient and α is the road gradient.

To sum up, vehicle wheel propulsion power P_{wheel} can be calculated with the formula below [27]:

$$P_{wheel} = v(m_v(t) \frac{d}{dt} v(t) + F_\alpha(t) + F_r(t) + F_g(t)) \quad (5)$$

Vehicle wheel power comes from power battery and some energy loses during transmission. Thus, power P_B provided by the battery should be:

$$P_B = \frac{P_{wheel}}{\varphi_{DC/AC} \times \varphi_{motor}} \quad (6)$$

where $\varphi_{DC/AC}$ is DC/AC conversion efficiency and φ_{motor} mechanical efficiency of drive motor [28,29].

3.2. Lithium Battery Model

In this simulation, a lithium ion battery model is used for the BEV. A lithium ion battery consists of cathode, anode and electrolyte. During discharging, lithium ions (Li^+) break free from the anode, spread to the cathode via electrolyte and join the cathode. The charging process is the opposite. The total voltage of the battery is the difference between cathode and anode voltages [30]. The battery model is as shown in Figure 4.

Battery voltage can be expressed by the formula below:

$$V(t) = V_u - V_n - V_p - V_s - V_e - V_o - V_c \quad (7)$$

In the formula above, V_u and V_n are cathode and anode potentials; V_o and V_c are voltage drop caused by surface resistance due to charge transfer between the cathode and the anode; V_p , V_s and V_e are voltage drop caused by intrinsic resistance of the cathode and the anode and electrolytic resistance [31,32].

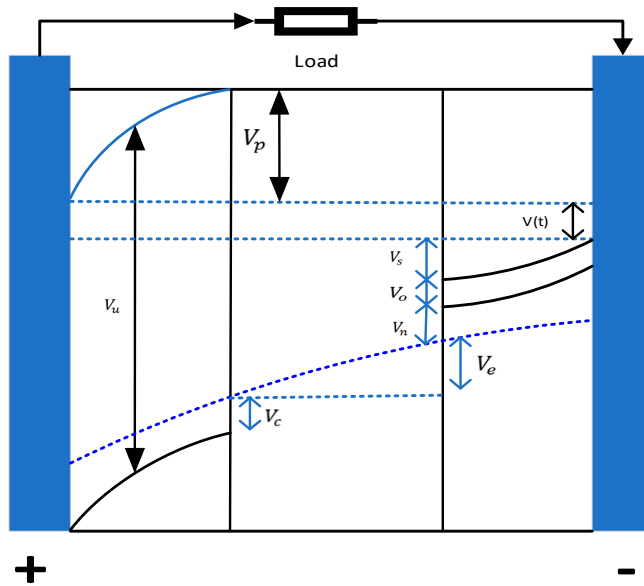


Figure 4. Physical model of a lithium battery.

3.3. Proton Exchange Membrane Fuel-Cell Model

Proton exchange membrane fuel cell is a major power source of FCVs and its voltage can be described by the formula [33] below:

$$E = N_{FC}(E_{rev} - E_{act} - E_{ohm} - E_{con}) \quad (8)$$

In the formula above, N_{FC} is the number of fuel cell stack current, E_{rev} is thermodynamic reversible potential, E_{act} is activation loss, E_{ohm} is ohmic loss and E_{con} is concentration loss.

Among them, thermodynamic reversible potential can be calculated with the formula [34] below:

$$E_{rev} = E_0 - 0.85e^{-3}(T - T_c) + \frac{RT}{2F} \ln(\sqrt{P_{O_2}}P_{H_2}) \quad (9)$$

where E_0 is reversible nearest potential of single battery, T is battery temperature, T_c is temperature correction offset, P_{O_2} and P_{H_2} are partial pressure of oxygen and hydrogen.

Activation loss can be expressed by the formula [35] below:

$$\frac{dE_{act}}{dt} = \frac{I_{FC}}{C_{dl}}(1 - \frac{E_{act}}{\eta_{act}}) \quad (10)$$

where C_{dl} is double-layer capacitance of single fuel cell.

When static activation loss is large, it can be simplified into the formula [36] below:

$$\eta_{act} = \frac{RT}{2\alpha F} \ln(\frac{I_{FC}}{I_o}) \quad (11)$$

where I_o is AC density and α is symmetrical factor.

Ohmic loss can be expressed by the formula [37] below:

$$E_{ohm} = I_{FC} \times R_{FC} \quad (12)$$

where R_{FC} is internal resistance.

Concentration loss can be calculated via the formula [38] below:

$$E_{con} = -B \times \ln \left(1 - \frac{I_{FC}}{I_{max}} \right) \quad (13)$$

where B is empirical constant and I_{max} is maximum allowable current. The equation above can be used to identify relation between fuel cell voltage and current.

In fuel cells, oxygen and hydrogen react to transform chemical energy to electric energy. Energy transformation efficiency is defined as the ratio of output energy against input energy. The output energy of fuel cells is electric energy and the input energy is chemical energy. Additionally, some auxiliary equipment such as an air compressor and cooling fan are required to ensure normal and stable operation of a fuel-cell system. The ratio of energy consumed by such auxiliary equipment against total energy is referred to as auxiliary efficiency. Therefore, the efficiency of a fuel cell system can be defined as:

$$\eta_{FCS} = \eta_{TH} \times \eta_{AUX} = \frac{V_{FC}}{1.254} \left(\frac{P_{FC} - P_{AUX}}{P_{FC}} \right) \quad (14)$$

where η_{TH} is theoretical efficiency, η_{AUX} is auxiliary efficiency and P_{AUX} is auxiliary power.

An air compressor system and cooling system in a fuel cell are major auxiliary equipment and power required by the air compressor can be calculated according to the formula [39] below:

$$P_{com} = \frac{C_p T_{air}}{\eta_{mec} \eta_{mot}} \left(\left(\frac{P_{out}}{P_{in}} \right)^{\frac{\gamma-1}{\gamma}} - 1 \right) F_{cp} \quad (15)$$

where P_{com} is air compressor efficiency, η_{mec} is compressor mechanical efficiency, C_p is specific heat capacity of air, T_{air} is air inlet temperature, P_{in} and P_{out} are air inlet and outlet pressures and γ is the value of air specific heat capacity.

Flow of the air compressor is determined by current output by fuel cells, as shown by the formula [40] below:

$$F_{cp} = S \times M_{air} \frac{N_{cell} \times I_{FC}}{4X_{O_2} \times F} \quad (16)$$

where S is stoichiometric ratio, M_{air} is molar coefficient of air and X_{O_2} is molar coefficient of oxygen.

Hydrogen consumption of fuel cells is determined by output current of relevant system, as shown by the formula [41] below:

$$m_{H_2} = \int_0^t \frac{M_{H_2} N_{cell}}{2F} I_{FC}(t) dt \quad (17)$$

where m_{H_2} is hydrogen mass consumption rate and M_{H_2} is molar mass of hydrogen.

4. Model Validation

In this paper, the performances of three vehicle models under CLTC-P are used as examples to validate the model. The models of BEV and FCV are established by AVL CRUISE, the power changes of BEV and FCV under cltc-p are simulated, and the power changes of FCHEV under CLTC-P are tested by a motor test bench. The power changes of the three models are shown in Figure 5. It can be seen from the figure that the wheel power of the vehicle changes with the change of speed. When the vehicle decelerates, the power of BEV and FCHEV will be less than 0, FCV cannot recover the energy when braking, so its wheel power is always greater than 0.

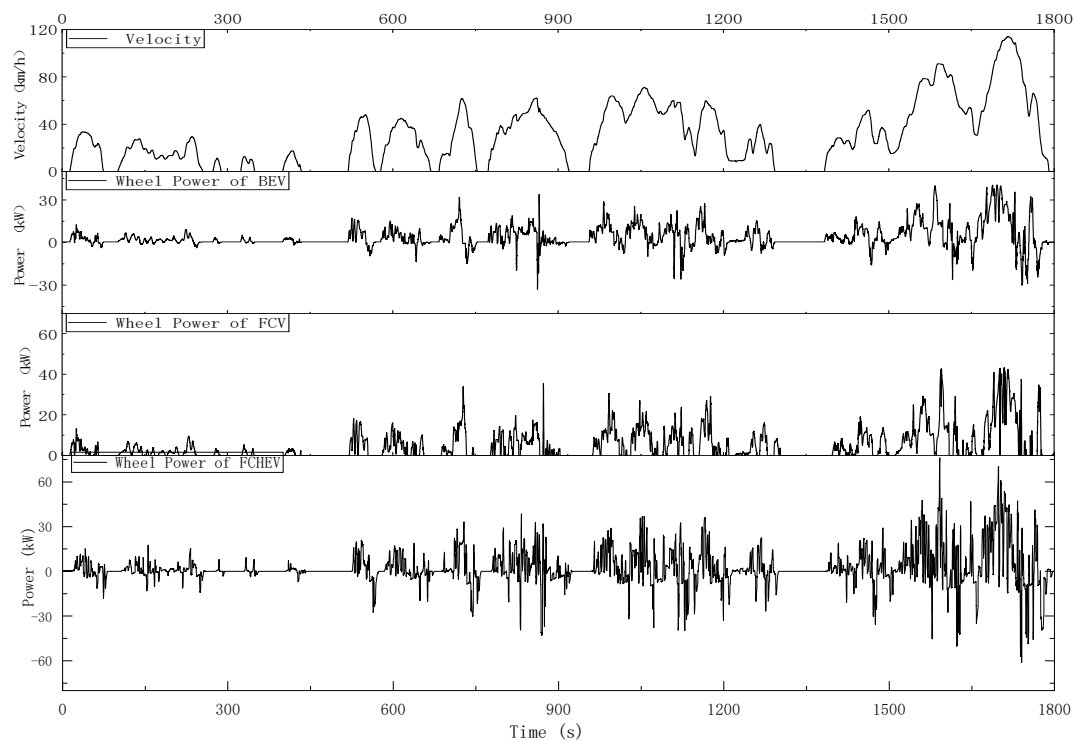


Figure 5. Changes in power of three models under CLTC-P (China light-duty vehicle test cycle-passenger car).

The energy consumption of the three models described in Figure 6 under CLTC-P. It can be seen from the figure that the difference between the gross energy consumption of the three models is within 5%. BEV and FCHEV can recover part of the energy, and the difference between energy recover is less than 5 %. The above results prove the reliability of the simulation model.

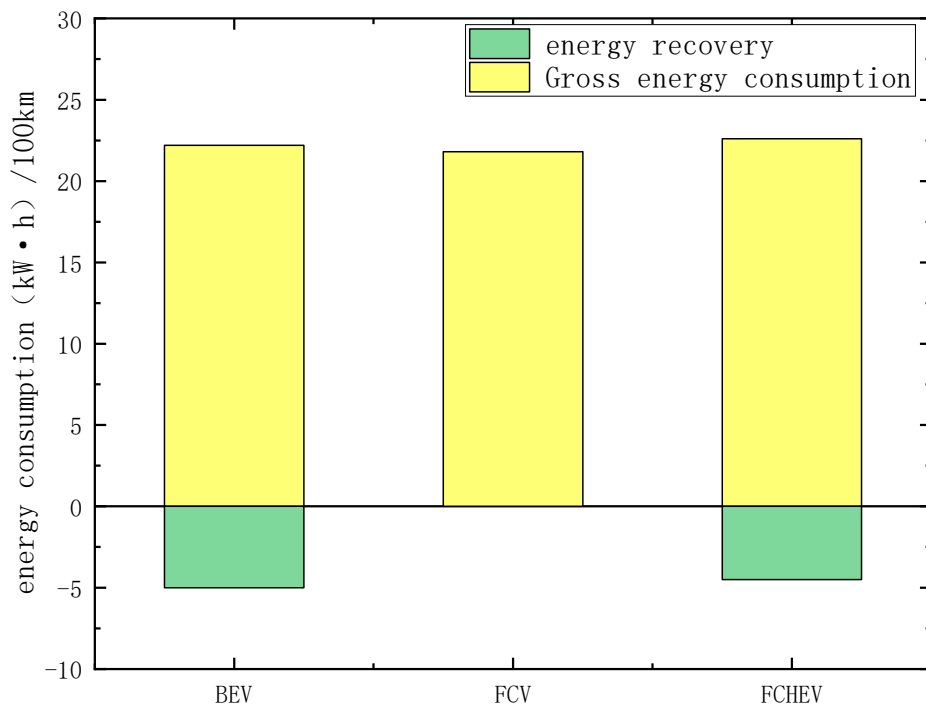


Figure 6. Energy consumption of three models under CLTC-P.

5. Results and Analysis

5.1. Simulation Results of Battery Electric Vehicle (BEV)

BEVs have a power system structure as shown in Figure 7 which mainly consists of a power battery, DC/DC and motor. Current input from lithium batteries flows to DC/alternating current (AC) after boosting at DC/DC and then into a three-phase AC motor for it to drive EVs to move.

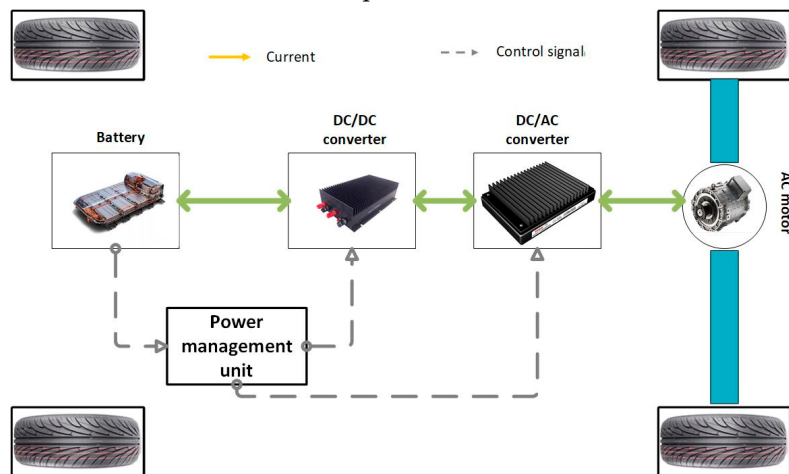


Figure 7. Battery electric vehicle (BEV) power system structure model.

5.1.1. Joint Distribution of Velocity, Accelerated Velocity and Battery Power of BEV under Three Road Conditions

A significant advantage EVs have over traditional fuel vehicles is that the energy recycling system of the former can recover energy during deceleration. Figure 8 describes joint distribution of velocity, accelerated velocity and power of BEV under three real-world driving cycles. In this figure, a power larger than 0 indicates discharging of the vehicle; a power smaller than 0 indicates charging of its battery; an accelerated velocity larger than 0 indicates acceleration of the vehicle; an accelerated velocity smaller than 0 indicates deceleration of the vehicle. We can see from the figure that power distribution range of the vehicle increases along with the increase in velocity under these three road conditions. Under the R1 condition, the power of the vehicle falls into the range of -20 – 20 kw; under the R2 condition, the power of the vehicle falls into the range of -40 – 40 kw; under the R3 condition, the power of the vehicle falls into the range of -60 – 60 kw.

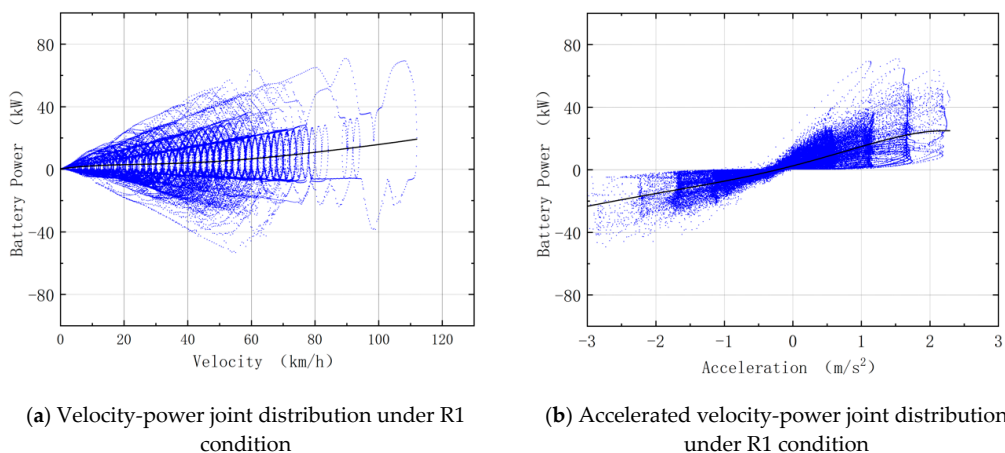


Figure 8. Cont.

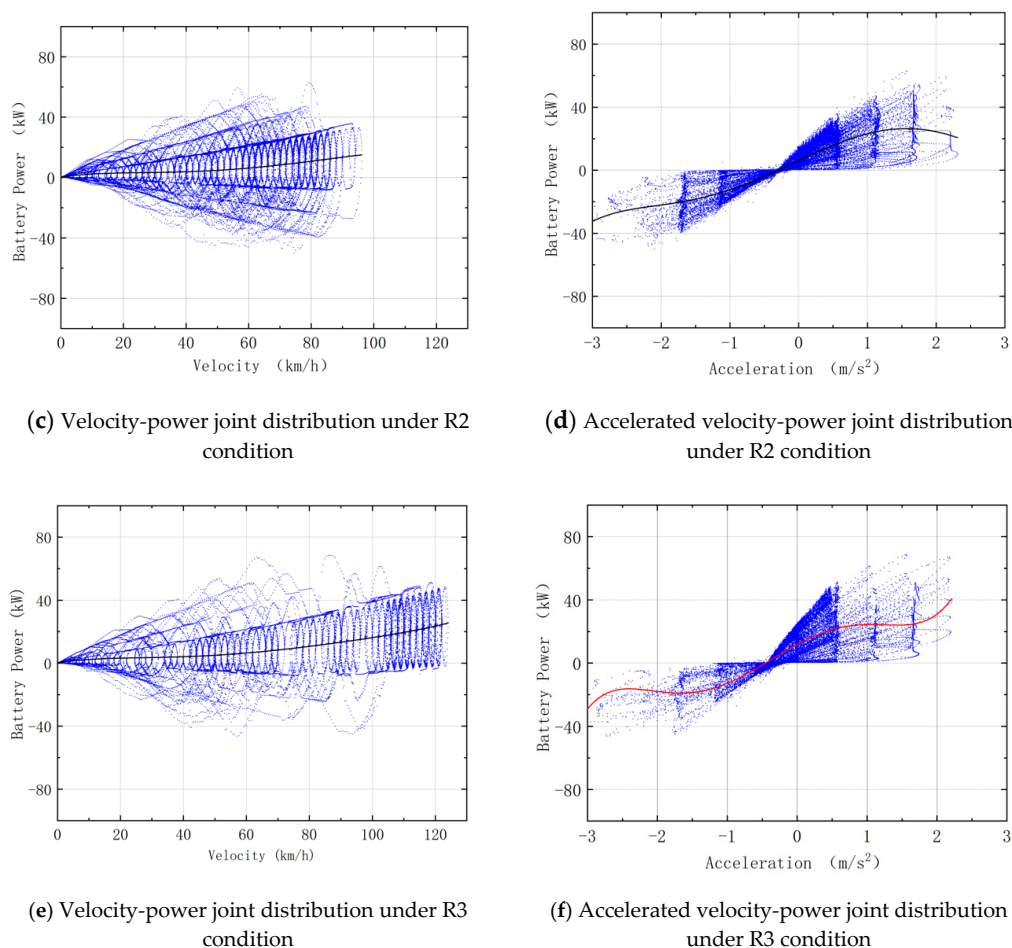


Figure 8. Distribution of BEV velocity and accelerated velocity under different road conditions.

5.1.2. BEV 0–100 km/h Acceleration Performance Test

Figure 9 describes the process of BEV accelerating from 0 km/h to 100 km/h. Its battery output power keeps increasing in the process. When the velocity of the vehicle reaches steady state, battery output power quickly drops to steady state as well. When the vehicle starts decelerating, its energy recycle system charges the battery. The charging power decreases as the velocity drops until the velocity reaches 0 km/h and the charging power also reaches 0 kW.

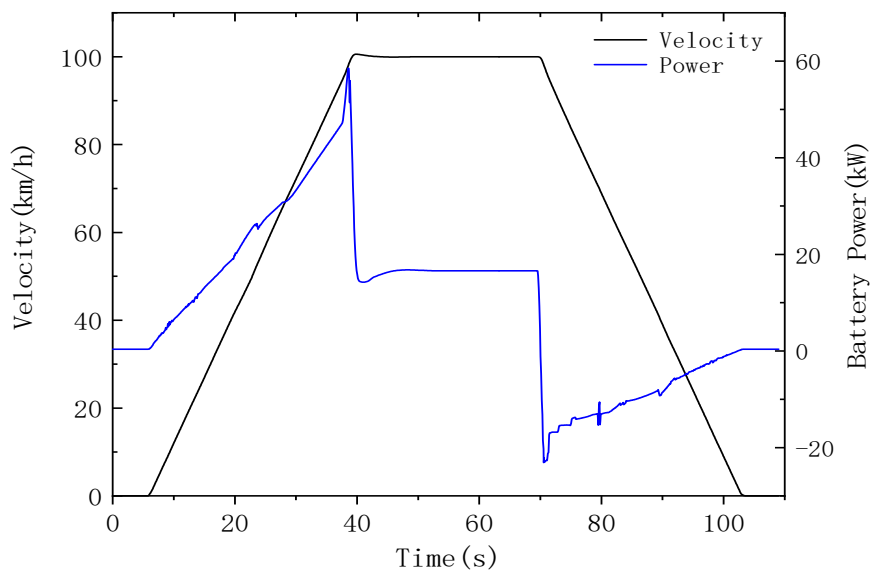


Figure 9. Changes in battery output power of BEV under 0–100 km/h acceleration condition.

5.1.3. BEV Cruising Performance Test

Figure 10 describes changes in output power when BEV is tested in cruising mode with a velocity from 0 to 160 km/h. We can tell from the figure that the battery output power keeps increasing during acceleration of the BEV. When its velocity reaches steady state, the battery output power reaches steady state as well. When the vehicle decelerates, its energy recycle system starts working. At such a moment, its battery power is lower than 0, until the vehicle velocity turns to 0 km/h.

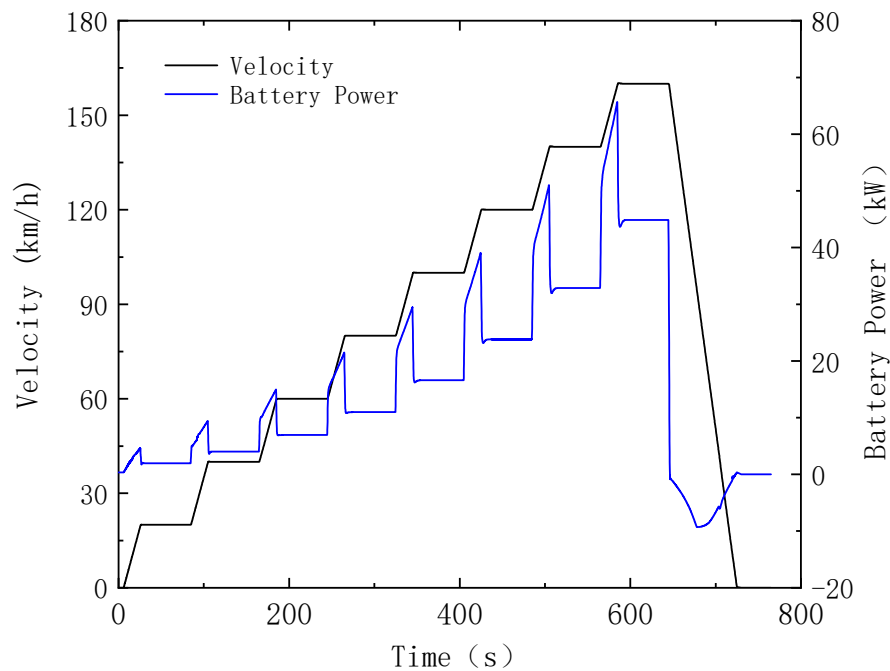


Figure 10. Changes in battery output power of BEV in cruising mode.

5.2. Simulation Results of Fuel-Cell Vehicle (FCV)

A FCV mainly consists of a proton exchange membrane fuel cell, DC/DC and motor and its power system structure is as shown in Figure 11. The current generated by fuel cells flows to DC/AC to

be converted into AC after boosting at DC/DC and then runs to three-phase AC motor to drive the vehicle forward.

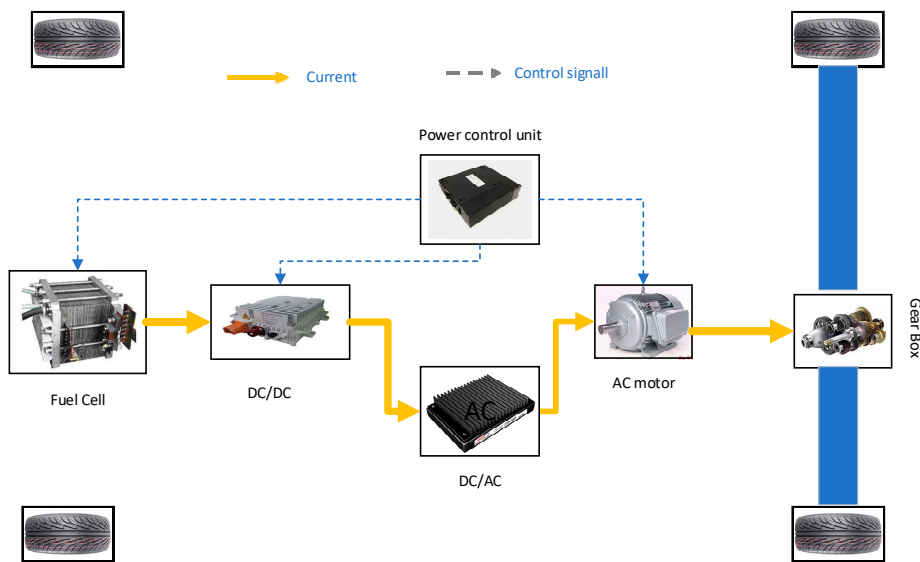
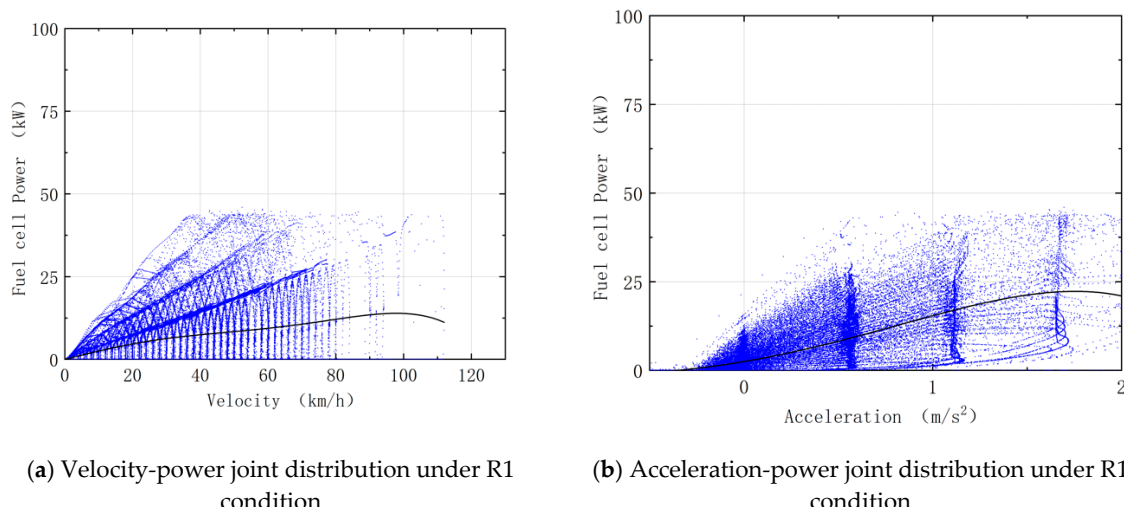


Figure 11. Fuel-cell vehicle (FCV) power system structure model.

5.2.1. Joint Distribution of Velocity, Accelerated Velocity and Fuel-Cell Power of FCV under Three Road Conditions

Figure 12 describes relations between velocity, accelerated velocity and power of a fuel cell under three real-world driving cycles. Since a FCV has no energy-storing device, it has no energy recycle system and therefore, its fuel cell output power is larger than 0. We can tell from the figure that power range increases as the velocity increases. Under the R1 condition, the power mainly falls into the range of 0–30 kW; under the R2 condition, the power mainly falls into the range of 0–40 kW; under the R3 condition, the power mainly falls into the range of 0–50 kW.



(a) Velocity-power joint distribution under R1 condition

(b) Acceleration-power joint distribution under R1 condition

Figure 12. Cont.

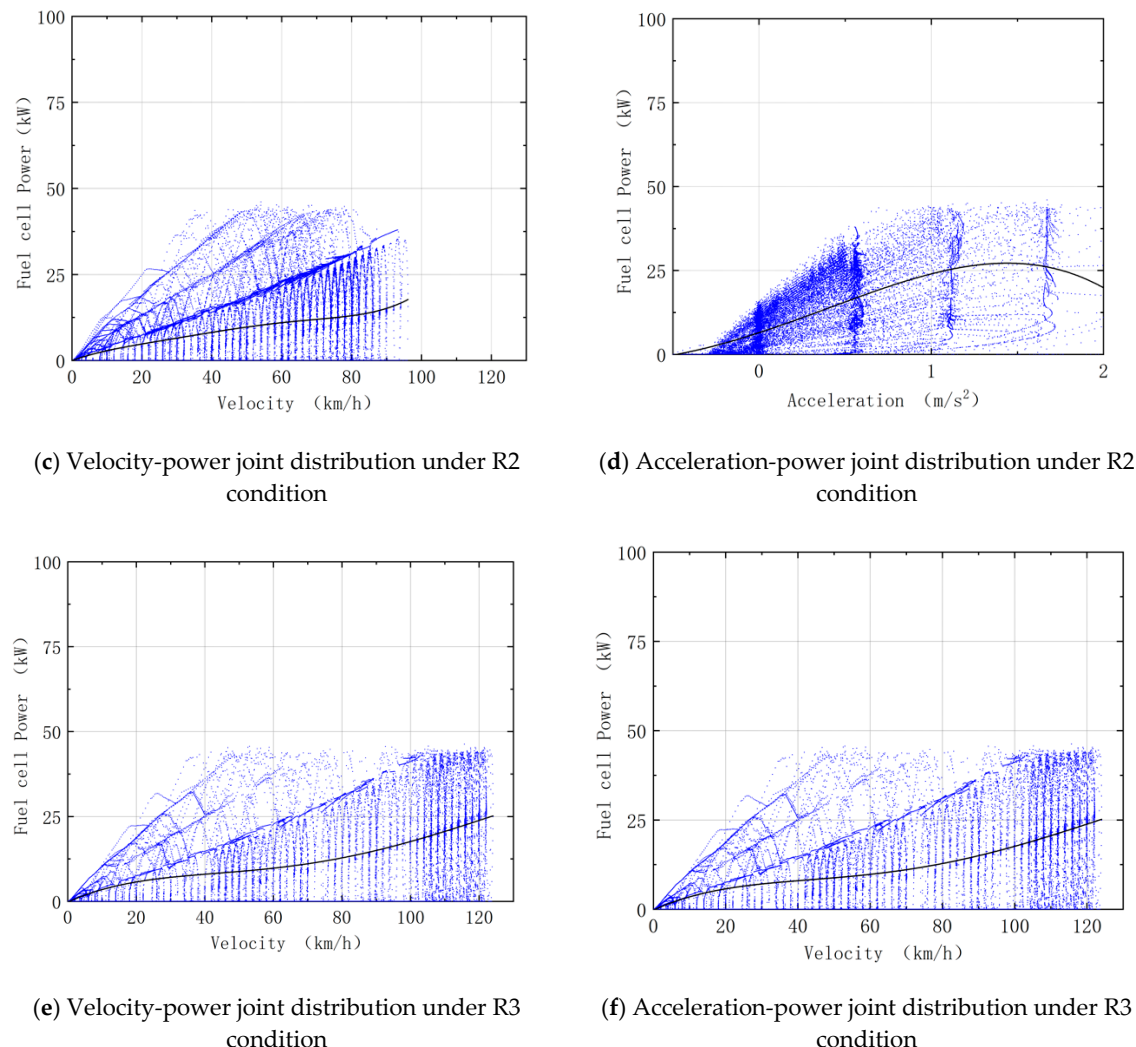


Figure 12. Joint distribution of velocity, acceleration and power of FCV under three real-world driving cycles.

After a comprehensive comparison of Figures 8 and 12, we find that power distribution range of a BEV or FCV increases along with its velocity. The BEV has an energy recycle system and can recover some energy during deceleration; while the FCV has no such device and cannot recover its braking energy. Therefore, the FCV has larger energy consumption than BEV.

5.2.2. 0–100 km/h Acceleration Performance Test

Figure 13 describes changes in fuel cell power when FCV accelerates from 0 to 100 km/h. We can see from the figure that when the vehicle starts accelerating, fuel-cell power increases gradually; when the velocity continues to increase, fuel-cell power fluctuates. When the velocity stabilizes at 100 km/h, fuel-cell power also stabilizes. When the velocity drops, fuel-cell power drops to zero, which means no power is output.

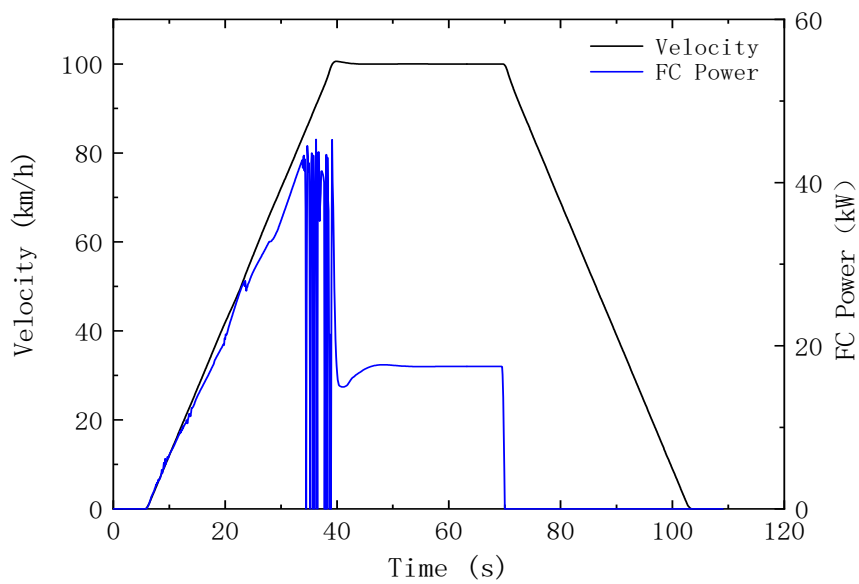


Figure 13. Changes in fuel cell power during 0–100 km/h acceleration of FCV.

5.2.3. FCV Cruising Performance Test

Figure 14 describes changes in fuel-cell power of the FCV in cruising mode. We can see from the figure that when the vehicle starts accelerating, its fuel-cell power increases. When the vehicle accelerates from 120 km/h to 140 km/h or when its velocity reaches 160 km/h, fuel-cell power fluctuates and the fuel cell works unstably.

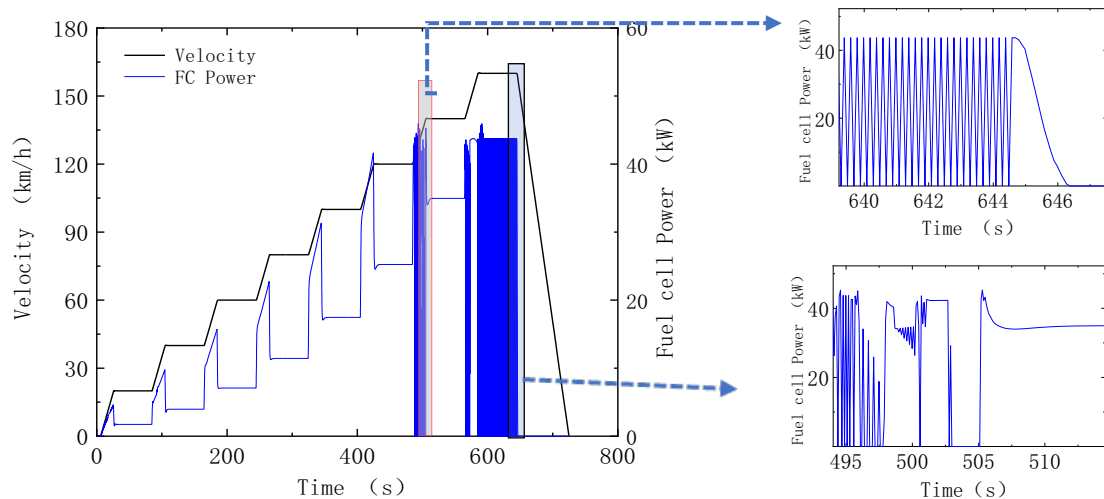


Figure 14. Changes in fuel-cell power of the FCV in cruising mode.

5.3. Test Results of Fuel-Cell Hybrid Electric Vehicle (FCHEV)

In the test, a model of a FCHEV from a certain country is used whose main structure is as shown in the Figure 15. The fuel cell is its main source of power. It outputs energy when the vehicle accelerates and recovers energy when the vehicle decelerates. This guarantees power performance and cruising ability and reduces emission to zero. Due to restrictions in test conditions, performance of the vehicle is tested under NEDC instead of R1, R2 and R3 conditions.

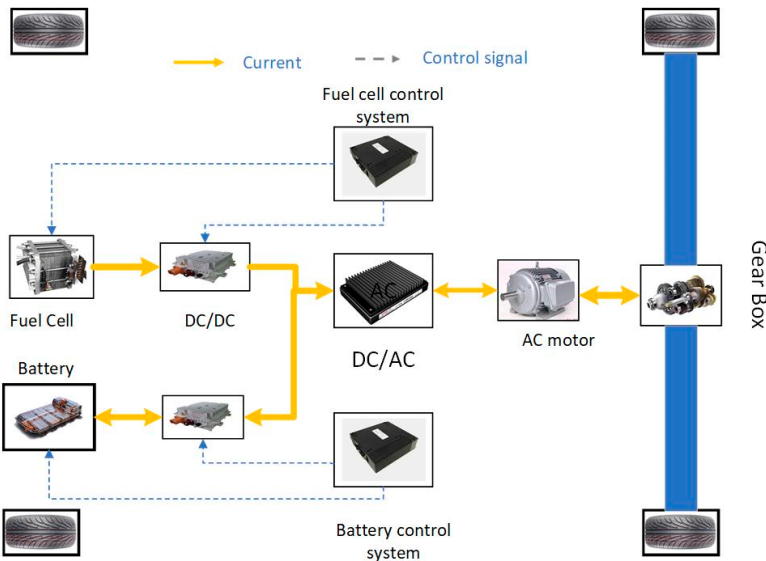


Figure 15. Fuel-cell hybrid electric vehicle (FCHEV) power system structure model.

5.3.1. New European Driving Cycle (NEDC) Condition

Figure 16 describes changes in power of main components of FCHEV under NEDC. We can see from the figure that as the velocity of the vehicle increases, its fuel cell power increases; when the vehicle decelerates, its fuel cell power drops to zero. When the vehicle keeps accelerating at high velocity, its fuel-cell power fluctuates.

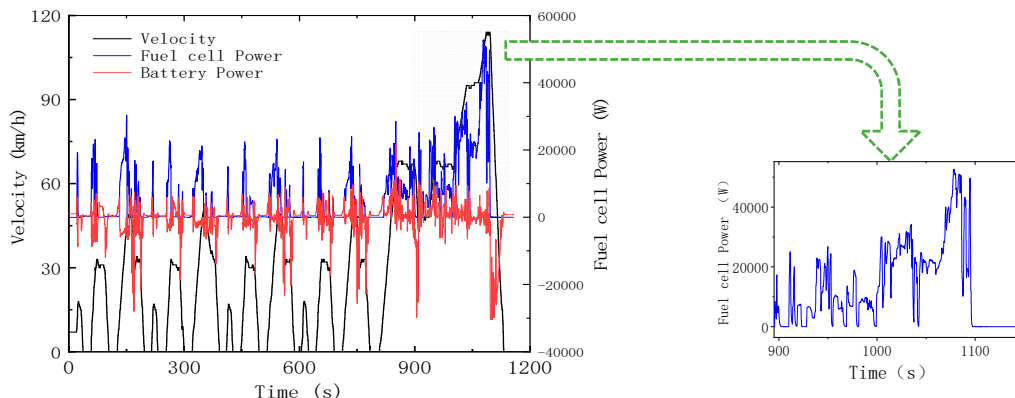


Figure 16. Changes in fuel cell and lithium battery power of FCHEV under New European Driving Cycle (NEDC).

A comprehensive comparison of Figures 13, 14 and 16 reveals that, when FCV keeps accelerating or runs at high velocity, its fuel cell output power fluctuates. This is because the fuel cell is not suitable for operation under high load and long-time operation under high load will seriously compromise its service life.

5.3.2. 0–100 km/h Acceleration Performance

Figure 17 describes changes in the power of the main components of the FCHEV when it accelerates from 0 km/h to 100 km/h. We can see from the figure that at the beginning of the acceleration, lithium battery power increases first and then fuel-cell power starts to increase, because fuel cell has some lag. During acceleration, fuel-cell power keeps increasing and the percentage of lithium battery power decreases. When velocity of the vehicle stabilizes at 100 km/h, lithium battery output power drops to zero, while fuel-cell output power stabilizes and the the fuel cell drives the vehicle forwards alone.

During deceleration, fuel-cell power drops to zero, motor power is smaller than zero and basically matches with the power battery power curve. This means that the energy recycle system of the vehicle starts working. When the velocity of the vehicle drops to zero, output power of the fuel cell and lithium battery drops to zero as well.

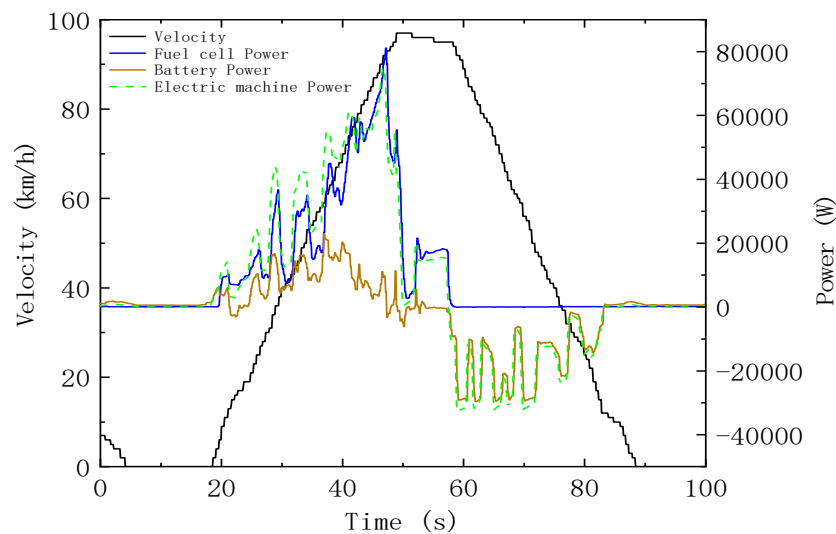


Figure 17. Changes in power of main components of FCHEV during 0–100 km/h acceleration.

5.3.3. FCHEV Cruising Performance Test

Figure 18 describes changes in the power of main components of a FCHEV during cruising mode test. We can see from the figure that when the vehicle runs stably at 20 km/h and 40 km/h, its fuel-cell power is basically zero, which means it is the lithium battery driving the vehicle forwards. When velocity of the vehicle stabilizes at over 40 km/h, the fuel cell provides the power and lithium battery output power is basically zero. This indicates that when the vehicle runs at low velocity, its power battery provides the power; when the vehicle has great power demand, the fuel cell provides the power. During acceleration of the vehicle, both the lithium battery and fuel cell provide the power; when the velocity stabilizes, battery power is basically zero and the fuel cell provides the main power.

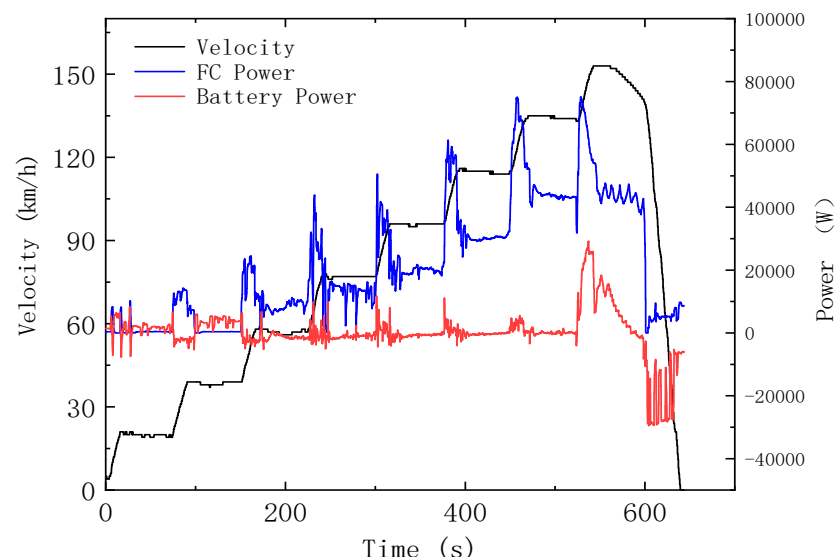


Figure 18. Changes in power of fuel cell and lithium battery of FCHEV in cruising mode.

5.3.4. Energy Consumption

The energy consumption of the BEV and FCV under NEDC is simulated, compared with the energy consumption of FCHEV under NEDC. Figure 19 describes the energy consumption of the three models under NEDC. The energy consumption of the vehicle is the sum of the gross energy consumption and the energy recovery. It can be seen from the figure that the gross energy consumption of the three models is about equal, the energy recovery of the BEV accounts for 26.8% of the gross energy consumption, and the energy recovery of FCHEV accounts for 20.3% of the gross energy consumption. The FCV has no energy recovery, so the FCV has the highest energy consumption.

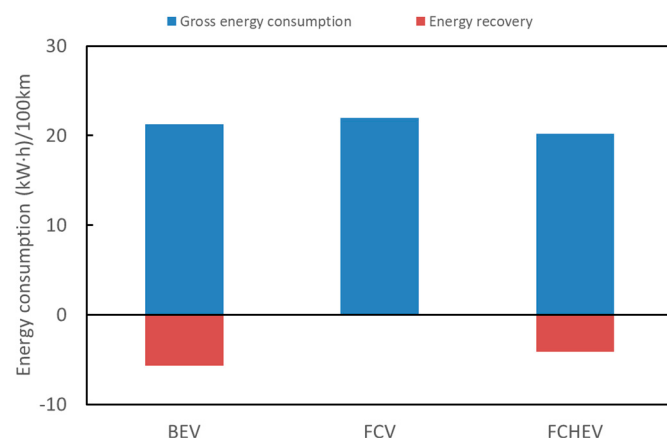


Figure 19. Energy consumption of three models under NEDC.

6. Conclusions

In this paper, conditions of three typical real roads in Tianjin are collected, including time, velocity and acceleration. Then, basic parameters of a FCHEV model from a certain country are used to build the BEV and FCV models. Later, performance of such BEV and FCV models is simulated under real-world driving cycles, 0–100 km/h acceleration condition and steady-state condition. A comprehensive comparison of BEV and FCV simulation results and FCHEV test result shows:

(1) The BEV power system has simple structure and quicker dynamic response and can recover braking energy. The recovery efficiency is different under different traffic conditions. The energy recovery efficiency is 33.4% under R1 condition, the energy recovery efficiency is 29.2% under R2 condition, and the energy recovery efficiency is 12.6% under R3 condition. However, due to restrictions such as battery capacity, the BEV is not suitable for long-distance travel.

(2) The only source of energy of the FCV is hydrogen, which is environmentally friendly without pollution and emission. But FCVs have slow dynamic response and unstable power output under high load. The output power under high load is unstable. During the 0–100 km/h acceleration performance test when the speed exceeds 80 km/h, the output power of the fuel cell starts to oscillate. During the cruising performance test, when the speed exceeds 120 km/h, the output power of fuel cell starts to oscillate.

(3) The FCHEV uses hydrogen as source of power and at the same time is equipped with a lithium battery. During acceleration, the power battery can intervene in a timely way to power the vehicle and improve dynamic response; during deceleration, power battery can timely store extra energy produced by fuel cell and reduce energy consumption. The energy recovery efficiency is 20.3% under NEDC condition. During the 0–100 km/h acceleration performance test the output power of the fuel cell does not oscillate. During the cruising performance test, when the speed exceeds 160 km/h, the output power of fuel cell starts to oscillate. The FCHEV combines the advantages of BEV and FCV and features great adaptability to real roads as well as reduced energy consumption thanks to a dual driving power of fuel cell and power battery. Therefore, it is a suitable model worth promoting.

However, a complex control strategy is required for coupling of the fuel cell and power battery due to the high cost of fuel-cell production and lack of sound infrastructure such as hydrogen refueling stations. Thus, a future study should focus on a control strategy for the FCHEV to improve adaptability to real-world cycles and lower energy consumption. In addition, we should improve the development policies, laws and regulations related to fuel cells, and pay attention to the construction of infrastructure and supporting industries.

Author Contributions: Conceptualization, Z.W. and X.Z.; methodology, Z.S., S.L.; software, Z.S.; validation, Y.Y., and X.Z.; formal analysis, Z.S.; investigation, Z.W.; resources, Z.S.; data curation, Z.S.; writing—original draft preparation, Z.S.; writing—review and editing, X.Z.; project administration, Z.W.; funding acquisition, Z.W. All authors have read and agreed to the published version of the manuscript.

Funding: The research was supported by the National Key Research and Development Program of China (Grant No. 2018YFB0105603).

Conflicts of Interest: The authors declare no conflict of interest. Zhicheng Sun, Zui Wen, Xin Zhao, Yunpeng Yang are from China Automotive Technology & Research Center Co. Ltd., the company, China Automotive Technology Research Center Co., Ltd., provided the test equipment.

References

1. Song, Y.; Zhang, M.; Sun, R. Using a new aggregated indicator to evaluate China's energy security. *Energy Policy* **2019**, *132*, 167–174. [[CrossRef](#)]
2. Das, H.S.; Tan, C.W.; Yatim, A.H.M. Fuel cell hybrid electric vehicles: A review on power conditioning units and topologies. *Renew. Sustain. Energy Rev.* **2017**, *76*, 268–291. [[CrossRef](#)]
3. Zhang, C.; Yang, F.; Ke, X.; Liu, Z.; Yuan, C. Predictive modeling of energy consumption and greenhouse gas emissions from autonomous electric vehicle operations. *Appl. Energy* **2019**. [[CrossRef](#)]
4. Zhili, D.; Boqiang, L.; Chunxu, G. Development path of electric vehicles in China under environmental and energy security constraints. *Resour. Conserv. Recycl.* **2019**, *143*, 17–26. [[CrossRef](#)]
5. Li, Y.; Zhong, Z.; Zhang, K.; Zheng, T. A car-following model for electric vehicle traffic flow based on optimal energy consumption. *Phys. A Stat. Mech. Its Appl.* **2019**. [[CrossRef](#)]
6. Pagani, M.; Korosec, W.; Chokani, N.; Abhari, R.S. User behaviour and electric vehicle charging infrastructure: An agent-based model assessment. *Appl. Energy* **2019**. [[CrossRef](#)]
7. Du, J.; Ouyang, D. Progress of Chinese electric vehicles industrialization in 2015: A review. *Appl. Energy* **2017**, *188*, 529–546. [[CrossRef](#)]
8. Berecibar, M.; Gandiaga, I.; Villarreal, I.; Omar, N.; van Mierlo, J.; Van den Bossche, P. Critical review of state of health estimation methods of Li-ion batteries for real applications. *Renew. Sustain. Energy Rev.* **2016**, *56*, 572–587. [[CrossRef](#)]
9. Albanese, L.; Ciriminna, R.; Meneguzzo, F.; Pagliaro, M. The impact of electric vehicles on the power market. *Energy Sci. Eng.* **2015**, *3*, 300–309. [[CrossRef](#)]
10. Ballinger, B.; Stringer, M.; Schmeda-Lopez, D.R.; Kefford, B.; Parkinson, B.; Greig, C.; Smart, S. The vulnerability of electric vehicle deployment to critical mineral supply. *Appl. Energy* **2019**, *255*, 113844. [[CrossRef](#)]
11. Naumanen, M.; Uusitalo, T.; Huttunen-Saarivirta, E.; van der Have, R. Development strategies for heavy duty electric battery vehicles: Comparison between China, EU, Japan and USA. *Resour. Conserv. Recycl.* **2019**. [[CrossRef](#)]
12. Fathabadi, H. Novel fuel cell/battery/supercapacitor hybrid power source for fuel cell hybrid electric vehicles. *Energy* **2018**, *143*, 467–477. [[CrossRef](#)]
13. Fathabadi, H. Fuel cell hybrid electric vehicle (FCHEV): Novel fuel cell/SC hybrid power generation system. *Energy Convers. Manag.* **2018**, *156*, 192–201. [[CrossRef](#)]
14. Harvey, L.D.D. Cost and energy performance of advanced light duty vehicles: Implications for standards and subsidies. *Energy Policy* **2018**, *114*, 1–12. [[CrossRef](#)]
15. Xu, X.; Aziz, H.M.A.; Guensler, R. A modal-based approach for estimating electric vehicle energy consumption in transportation networks. *Transp. Res. Part D Transp. Environ.* **2019**, *75*, 249–264. [[CrossRef](#)]
16. Wu, X.; Freese, D.; Cabrera, A.; Kitch, W.A. Electric vehicles' energy consumption measurement and estimation. *Transp. Res. Part D Transp. Environ.* **2015**, *34*, 52–67. [[CrossRef](#)]

17. Yuan, X.; Zhang, C.; Hong, G.; Huang, X.; Li, L. Method for evaluating the real-world driving energy consumptions of electric vehicles. *Energy* **2017**, *141*, 1955–1968. [[CrossRef](#)]
18. Brady, J.; O’Mahony, M. Development of a driving cycle to evaluate the energy economy of electric vehicles in urban areas. *Appl. Energy* **2016**, *177*, 165–178. [[CrossRef](#)]
19. Faria, M.; Rolim, C.; Duarte, G.; Farias, T.; Baptista, P. Assessing energy consumption impacts of traffic shifts based on real-world driving data. *Transp. Res. Part D Transp. Environ.* **2018**, *62*, 489–507. [[CrossRef](#)]
20. Jiang, S.; Wang, C.; Zhang, C.; Bai, H.; Xu, L. Adaptive estimation of road slope and vehicle mass of fuel cell vehicle. *eTransportation* **2019**. [[CrossRef](#)]
21. Fernández, R.Á.; Caraballo, S.C.; Cilleruelo, F.B.; Lozano, J.A. Fuel optimization strategy for hydrogen fuel cell range extender vehicles applying genetic algorithms. *Renew. Sustain. Energy Rev.* **2018**, *81*, 655–668. [[CrossRef](#)]
22. Mokrani, Z.; Rekioua, D.; Mebarki, N.; Rekioua, T.; Bacha, S. Proposed energy management strategy in electric vehicle for recovering power excess produced by fuel cells. *Int. J. Hydrogen Energy* **2017**, *42*, 19556–19575. [[CrossRef](#)]
23. Morrison, G.; Stevens, J.; Joseck, F. Relative economic competitiveness of light-duty battery electric and fuel cell electric vehicles. *Transp. Res. Part C Emerg. Technol.* **2018**, *87*, 183–196. [[CrossRef](#)]
24. Carey, A.M.; Paige, G.B.; Carr, B.J.; Dogan, M. Forward modeling to investigate inversion artifacts resulting from time-lapse electrical resistivity tomography during rainfall simulations. *J. Appl. Geophys.* **2017**, *145*, 39–49. [[CrossRef](#)]
25. Sepúlveda, F.D.; Lucay, F.; González, J.F.; Cisternas, L.A.; Gálvez, E.D. A methodology for the conceptual design of flotation circuits by combining group contribution, local/global sensitivity analysis, and reverse simulation. *Int. J. Miner. Process.* **2017**, *164*, 56–66. [[CrossRef](#)]
26. Lekshmi, S.; Lal Priya, P.S. Mathematical modeling of Electric vehicles—A survey. *Control Eng. Pract.* **2019**, *92*, 104138.
27. Liu, H.; Zhang, X.; Chen, Y.; Taha, M.; Xu, H. Active damping of driveline vibration in power-split hybrid vehicles based on model reference control. *Control Eng. Pract.* **2019**. [[CrossRef](#)]
28. Karaoglan, M.U.; İnce, A.C.; Colpan, C.O.; Glüsen, A.; Kuralay, N.S.; Müller, M.; Stolten, D. Simulation of a hybrid vehicle powertrain having direct methanol fuel cell system through a semi-theoretical approach. *Int. J. Hydrogen Energy* **2019**, *44*, 18981–18992. [[CrossRef](#)]
29. Zhou, X.; Qin, D.; Hu, J. Multi-objective optimization design and performance evaluation for plug-in hybrid electric vehicle powertrains. *Appl. Energy* **2017**, *208*, 1608–1625. [[CrossRef](#)]
30. Richardson, R.R.; Osborne, M.A.; Howey, D.A. Gaussian process regression for forecasting battery state of health. *J. Power Sources* **2017**, *357*, 209–219. [[CrossRef](#)]
31. Wilke, C.; Bensmann, A.; Martin, S.; Utz, A.; Hanke-Rauschenbach, R. Optimal design of a district energy system including supply for fuel cell electric vehicles. *Appl. Energy* **2018**, *226*, 129–144. [[CrossRef](#)]
32. Li, H.; Ravey, A.; N’Diaye, A.; Djerdir, A. A novel equivalent consumption minimization strategy for hybrid electric vehicle powered by fuel cell, battery and supercapacitor. *J. Power Sources* **2018**, *395*, 262–270. [[CrossRef](#)]
33. Kim, J.; Kim, M.; Kang, T.; Sohn, Y.-J.; Song, T.; Choi, K.H. Degradation modeling and operational optimization for improving the lifetime of high-temperature PEM (proton exchange membrane) fuel cells. *Energy* **2014**, *66*, 41–49. [[CrossRef](#)]
34. Ahmadi, S.; Bathaei, S.M.T. Multi-objective genetic optimization of the fuel cell hybrid vehicle supervisory system: Fuzzy logic and operating mode control strategies. *Int. J. Hydrogen Energy* **2015**, *40*, 12512–12521. [[CrossRef](#)]
35. Fadel, A.; Zhou, B. An experimental and analytical comparison study of power management methodologies of fuel cell-battery hybrid vehicles. *J. Power Sources* **2011**, *196*, 3271–3279. [[CrossRef](#)]
36. Lachhab, I.; Krichen, L. An improved energy management strategy for FC/UC hybrid electric vehicles propelled by motor-wheels. *Int. J. Hydrogen Energy* **2014**, *39*, 571–581. [[CrossRef](#)]
37. Aouzellag, H.; Ghedamsi, K.; Aouzellag, D. Energy management and fault tolerant control strategies for fuel cell/ultra-capacitor hybrid electric vehicles to enhance autonomy, efficiency and life time of the fuel cell system. *Int. J. Hydrogen Energy* **2015**, *40*, 7204–7213. [[CrossRef](#)]
38. Li, T.; Huang, L.; Liu, H. Energy management and economic analysis for a fuel cell supercapacitor excavator. *Energy* **2019**, *172*, 840–851. [[CrossRef](#)]

39. Hwang, J.-J.; Hu, J.-S.; Lin, C.-H. Design of a range extension strategy for power decentralized fuel cell/battery electric vehicles. *Int. J. Hydrogen Energy* **2015**, *40*, 11704–11712. [[CrossRef](#)]
40. Wan, Y.; Guan, J.; Xu, S. Improved empirical parameters design method for centrifugal compressor in PEM fuel cell vehicle application. *Int. J. Hydrogen Energy* **2017**, *42*, 5590–5605. [[CrossRef](#)]
41. Li, Y.; Wu, Y.; Zhang, Y.; Wang, S. A Kriging-based bi-objective constrained optimization method for fuel economy of hydrogen fuel cell vehicle. *Int. J. Hydrogen Energy* **2019**. [[CrossRef](#)]



© 2020 by the authors. Licensee MDPI, Basel, Switzerland. This article is an open access article distributed under the terms and conditions of the Creative Commons Attribution (CC BY) license (<http://creativecommons.org/licenses/by/4.0/>).

EVS28
KINTEX, Korea, May 3-6, 2015

“Measurement and Analysis of Indian Road Drive Cycles for Efficient and Economic Design of HEV Component”

Mr.Vishal Parekh¹, Dr.Varshaben Shah²

Power Electronics and Electronic Drive, Research Head, ASPERO Research, India¹
Electrical Department, Prof. SVNIT, India²

Abstract

Drive cycle pattern is different for different countries which depends on their traffic density, road condition and driver discipline. Drive cycle influences HEV's components design, sizing and their ratings. Standard drive cycle data doesn't reveal much information to determine efficient and economic design of HEV's components. In this research paper measurement and analysis of real time Indian road drive cycles (IRDC) are carried out for urban roads, state highway, national highway and express Highway where vehicles have their most run. Real time drive cycle data will expose impact of driver's skills, traffic, road conditions and short acceleration / deceleration period, which can be represented on drive cycle chart. Analysis of IRDC in terms of rate of acceleration and deceleration, top speed, average speed with road length and analysed mathematically to find energy and power required for acceleration, normal operation and energy harvested during deceleration. Based on information from IRDC HEV's components initial size are estimated. Initial estimated size is optimized to make HEV's components design more efficient and economic. Teaching and learning based optimization algorithm (TLBO) and Multi objective genetic algorithm (MOGA) are used to optimize HEV's components. Constraint of optimization algorithm are like engine and motor rating should be selected such that it has effective top speed with enough acceleration capability and can run enough distance to reach destination according to Indian urban, state, national and express highway pattern where cities are very closed compared with other countries and its regeneration component design should able to harvest maximum deceleration energy. For economic operation of HEV's, running cost in terms of Rs. / Km. should be minimum.

Keywords: Indian Road Drive Cycle, Hybrid Electric Vehicle Component, Efficient and Economic, Analysis of Drive Cycle, Drive Cycle and HEV

NOMENCLATURE

V_{OC}	Battery open circuit voltage (V)	$\text{Exp}(t)$	Exponential zone voltage (V)
E_o	Battery constant voltage (V)	$\frac{dw}{dt_{(<0)}}$	Change in watt (W)
R	Internal resistance (Ohm)	V_{charge}	Charging voltage (V)
i	Battery current (Amp)	V_{total}	Total voltage (V)
K	Polarization constant (V/Ah)	C_{cc}	Charge constant
Q_{it}	Battery capacity (Ah) Actual battery charge (Ah)	Q_{ut}	Total charge of battery (Ah)

Q_u	Actual charge of battery (Ah)	M_v	(CG) of Car and Rear Wheel Mass of Vehicle
K	SOC level (%)	g	Gravitational Force
HP	Horse Power	α	Slant Angle of Road
W	Watt	h_g	Height of CG of Car
T	Torque	W_f	Normal Load On Front Excel
P	Power	F_f	Frictional Constant
V	Voltage	r_g	Effective Tier Radius
I	Current	M_{Meani}	Mean of Drive cycle parameters of i^{th} number population
N_m	Mechanical Speed	M_N	New Drive Cycle Parameter
N	Turn of winding	M_o	Old Drive Cycle Parameter
R_{r0}	Rotor Diameter	T_F	Teaching Factor
L_{st}	Stack Length	$M_{i,j}$	Drive cycle Parameter of i^{th} and j^{th} number
μ_0	Absolute Permeability	SOC	State of Charge
μ_r	Relative Permeability	HEV	Hybrid Electric Vehicle
C_ϕ	Flux – Construction Factor	IC	Internal Combustion
A_m	Magnate Pole Area	GA	Genetic Algorithm
A_g	Air Gap Area	MOGA	Multi Objective Genetic Algorithm
l_m	Length Of Magnet	TLBO	Teaching and Learning Based Optimization
g	Length Of Air Gap	IRDC	Indian Road Drive Cycle
L_g	Inductance Of Air Gap		
T	Motor Torque		
T_L	Load Torque		
J	Moment Of Inertia		
ω_m	Angular Velocity		
B	Friction Constant		
T_{tmax}	Maximum Tractive Force on Front Excel		
μ	Road adhesion coefficient		
L	Distance between Wheels		
L_b	Distance between Centre of Gravity		

1 Introduction

India is growing market for automobile where biggest class of consumer is middle class family. Many automobile companies have already started research in HEV which has ability to use non-convectional energy which is bestowed amply in India. HEV also become has economic choice for Indian consumer and for Indian environment. Government of India is also planning to give subsidy for HEV to motivate consumers to buy HEV. Fuel energy costs more than electric energy according to electric tariff plan. [1] Design of HEV's components is began with studying drive cycle. Drive cycle pattern depends on road condition, road type, traffic density and driver's behaviour [5]. There are different standard drive cycle available from different countries e.g. ECE-15, EUDC, EPA Federal Test [28]. These drive cycle data

are used for vehicle emission analysis and for estimation of HEV's components size. Standard drive cycles dose not reveal information like rate of acceleration & deceleration and its power, peak power demand & actual time of travelling [2]. Efficient and economic design of HEV's components cannot be done based on information and analysis from standard drive cycle. Design of motor, IC engine, battery is depended on load pattern. Different countries have different drive cycle pattern, so for actual information India road drive cycle must be measured in real travel time. Real time data of drive cycle are necessary to be measured and to reveal detailed information about drive cycle load pattern. Real time drive cycle measurement goes through natural environmental condition of all different type of roads, different type of road condition and different type of traffic condition which gives different drive cycle for different roads so it can be used for HEV's components size estimation [3].

For the selection of power train configuration different power train configurations are available. All power train serves different purpose. There are different types of configuration of power train which are series design, parallel design, and series & parallel design.

Dynamic model of vehicle is used for modelling and simulation and it is used to calculate vehicle power requirement which is close to actual performance [6, 7].

Variety of drive cycle pattern has to be considered while HEV's components initial sizing is determined. For initial sizing rule based theorem, different estimation method [27] and mean value models [29] are used. The optimum component size should be calculated by proper optimization method because direct initial sizing will not give a solution that works efficiently with different drive cycle patterns [8].

To select optimum component size optimization should be done. Certain constrain are set while optimization process is taking place.

Different optimization techniques can be used like swarm optimization, genetic algorithm optimization, multi objective genetic algorithm optimization and teaching and learning based optimization. TLBO method is never used for HEV's components optimization.

Estimated component size can be optimized by GA. It uses derivative and it achieves single objective. It selects random values from population which is data derived from drive cycle. Fittest value is found from population.

Limitation of this method is it doesn't perform multi objective tasks [9]. Multi objective genetic algorithm is evolved method or modified method from GA. This method is able to satisfy multi objective laid down in single set of iteration flow. Iteration stops when fittest values are achieved, which is considered fittest among population and is solution [10, 11]. Swarm optimization can be used to solve complex solution. It dose investigation of population by considering multi objectives as well as limitation set to those objectives. Control strategy for can also be optimized by swarm optimization technique [12, 13]. Teaching and learning based optimization method is recent development in field of optimization technique which is also inspired by nature of classroom working environment where teacher teach learners behave during study. For HEV's components optimization this method can be useful because normally population size is high and multi objective supposed to be achieved while designing HEV's components. In TLBO method learners which are drive cycle population learns to become best by comparing their data with each other and also modify them to achieve multiple objective and set control strategy.

After optimization of component size their performance parameters are checked and their running economy is also compared with conventional IC engine car which are present in India [14, 15].

Throughout the paper parallel configuration of HEV is considered which is explained in section 2. Information about real time drive cycle a method measurement on different Indian roads and its analysis cycle is done in section 3, Modelling of HEV's components is done in section 4. In section 5, initial estimation of components is done by considering parameters of drive cycle. In section 6 initial estimation value is optimized by TLBO method which is new and never used for HEV's component size optimization and MOGA method to make comparison. Economical comparison is shown in section 7. Result of all method of optimization is shown in section 8 and it is concluded in section 9.

2 System Configurations

HEV's components design is done for medium size vehicle. Various drive train configurations can be used for HEV. Selection of drive train pattern depends upon application. In this paper parallel drive train configuration is used. Parallel

drive train requires less space compared to series configuration and is suitable for use in medium sized car. Series configuration is used for heavy duty application and its drive train requires additional generator space.

Figure 1 Shows block diagram of Parallel drive train configuration.

For parallel drive train configuration battery, fuel tank, IC engine, motor and inverter, splitter which splits load between IC engine and electric motor and this entire set of components are connected to the a load.

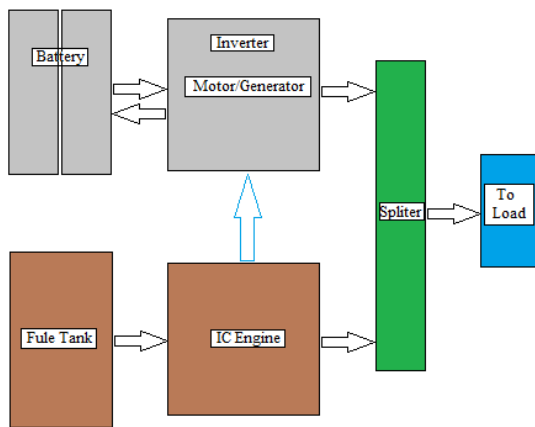


Figure 1: Parallel HEV

Here rating of IC engine and electric motor are 50% of load. Rating of IC engine can be chosen higher than 50% of load depending upon its maximum efficient point.

Dynamic model of HEV is used for modelling and analysis of vehicle parameters. Figure 2 Shows block diagram of dynamic model of HEV. As drive train component Lead-Ion battery, BLDC motor, diesel CRDi IC engine is selected.

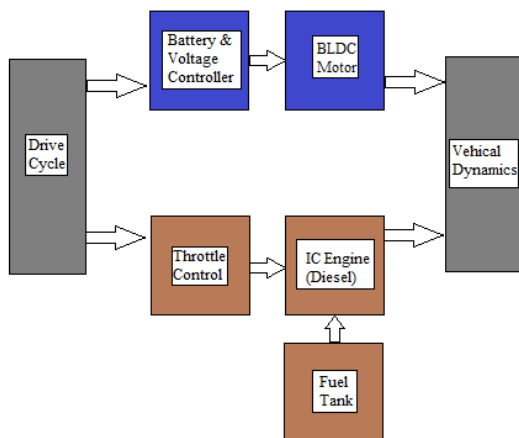


Figure 2: Dynamic Model of HEV

3 Indian road drive cycle

3.1 Drive cycle measurement

The driving cycle is sequence of vehicle operating condition i.e. idling, acceleration, cruise, creeping and declaration with respect to time for a given city, region or a country.

Indian roads are categorized in four ways which are (i) express highway (ii) national highway (iii) state highway (iv) urban roads/rural road [4].

So, the selection of population and road is very crucial while planning drive cycle measurement program. All type of Roads should be covered. Vehicle selection is also very crucial. Vehicle of similar rating should be selected as rating of HEV to be designed. Vehicle which is most economic while running is selected to start drive cycle measurement program. Table 1 shows parameters of vehicle to determine drive cycles.

Table 1: Vehicle Parameters

Vehicle HP	128HP
Vehicle RPM	6000
Tractive Effort coefficient for Indian roads	0.4 to 0.5
Mass of Vehicle	1300 Kg
Rolling resistance coefficient in this case	0.013 (asphalt road)
Height of CG from ground	87 cm
Effective radius of tire	29 cm
Distance between wheels	268.5mm

For the purpose of measurement of drive cycle medium sized car with diesel engine is used. Medium size cars are economical choice in India. Drive cycle measurement is carried out by android application which uses global positioning system by traveling in car. Data of time to speed were measured and plotted in android application and those were loaded in Microsoft excel. To collect legit drive cycle data the vehicle is driven in to natural environment.

3.2 Characteristic of IRDC

For different type of road the drive cycle parameters varies considerably as it can be observed from figure 3. It can be observed that for express highway max speed and max HP is

high but time of run is Less and from urban roads observed that acceleration and deceleration cycle is very high compared with Express highway but max HP and mac speed is low while national and state highway both requires high run time form HEV [16, 17].

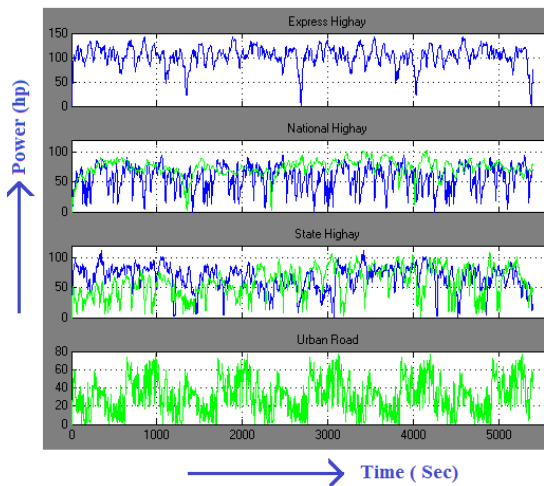


Figure 3: Drive Cycle

3.3 Analysis

Table 2 shows data of which are derived from real time drive cycle termed as drive cycle of different road (DC), average speed (AS), maximum speed (MS), Average Time (AT), Maximum Time (MT), total time(T) and distance (D). Data are categorized by means of road types E, N, S, C and U stands for express highway, national highway, state highway, state and national highway and urban road respectively.

It can be said that all drive cycle will have different requirements from power train. Express highways requires higher average HP and maximum HP while national and state highways requires vehicle to run for long time so design of HEV's components should fulfil both load drive cycle characteristic.

Table 3 shows summery values of data from table 2 which enables to understand marginal difference in characteristics of different road drive cycle measured in real time.

3.4 Vehicle Dynamics

Vehicle dynamics are considered for calculation performance parameter of HEV. Vehicle's calculates performance parameter like its horsepower requirement, speed, torque, and acceleration & deceleration power can be determined by vehicle dynamics.

Table 2: Mean Values of Drive Cycle Parameters

DC	AS	MS	AT	MT	T	D
Express Highway						
E	106	147	103	143	45	80
National Highway						
N1	57	97	57	95	23	22
N2	83	38	81	135	209	220
N3	63	135	62	122	95	100
N4	81	133	79	130	25	33
N5	70	105	68	102	140	170
State Highway						
S1	66	115	64	112	51	60
S2	60	115	58	112	171	171
S3	61	119	60	116	27	27
S4	79	141	77	138	50	65
State & National Highway						
C1	78	131	76	128	76	98
C2	76	126	74	123	186	235
Urban Road						
U1	26	63	28	60	23	9
U2	32	79	32	77	17	9
Avg	70	114	68	118	85	99

Table 3: Drive cycle summary

DC	AS	MS	AT	MT	T	D
E	106	147	103	143	45	80
N	63	101	62	98	81	96
S	71	120	69	117	118	147
U	29	71	30	68	20	9

$$F_{t\text{ total}} = F_{t\text{ max}} + F_r + F_w + F_g \quad \dots (1)$$

$F_{t\text{ total}}$ is total force required at front axle which considers resistance forces of road and car to calculate actual force required by car. From force torque, speed and horse power are calculated which are shown in table 2 and 3.

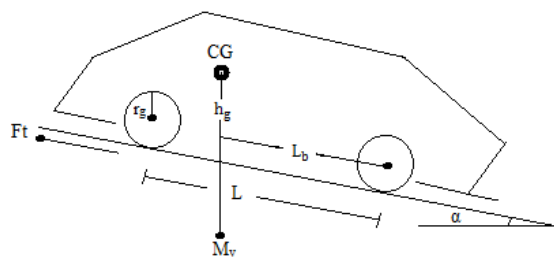


Figure 4: Vehicle dynamics

$$F_{t \max} = \mu W_f = \left[\frac{L_b}{L} M_v g \cos\alpha - \frac{h_g}{L} \left(F_{t \max} - F_r \left(1 - \frac{r_d}{h_g} \right) \right) \right] \mu \quad \dots (2)$$

Parameters of resistance force are calculated as [19]

Rolling resistance force
 $F_r = P f_r \cos\alpha \quad \dots (3)$

Aerodynamic drag force
 $F_w = \rho A_f C_D (V + Vw)^2 \quad \dots (4)$

Gradient Resistance force
 $F_g = M_v g \sin\alpha \quad \dots (5)$
 [19]

Figure 4 shows parameters of dynamic vehicle used for equations.

This resistance are summed up to get actual power used during vehicle dynamics calculation.

4 Modelling of HEV's components

From IRDC analysis battery kilo watt requirement, hour requirement, size of motor, size of IC engine and fuel tank is determined. The seizing is done for parallel configuration of HEV which is simulated in MATLAB Simulink. Data taken from table 2 are average HP and maximum HP to determine average power require by motor and IC engine and peak power required by the same and deceleration power to estimate power of battery and its recharging from deceleration energy. From those mean value of each parameter is considered [28]. All component size estimation and its optimization will be tested in MATLAB Simulink model. Parallel HEV model is modelled in MATLAB Simulink.

Brushless DC Motor, Lead-Ion Battery, IC Engine same as motor rating is selected as component of HEV.

For simulation and modelling of parallel configuration of HEV, modelling equations are mentioned below.

1. Battery charging, discharging model [21]

- Discharge Voltage Status

$$V_{OC} = E_0 - R \times i - K \frac{Q}{Q-it} (i t + i) + \text{Exp}(t) \quad \dots (6)$$

- Charging Voltage Status

$$V_{charge} = \int \left(\frac{dw}{dt_{(c0)}} \times \frac{w}{v} \times V_{total} \times C_{cc} \right) dt \quad \dots (7)$$

- SOC Calculation [22]

$$Q_{ut} = V \times I \times (T) = VIH \quad \dots (8)$$

$$Q_u = WH - \int_0^t i(t) dt \quad \dots (9)$$

$$K = \frac{Q_u}{Q_{ut}} \times 100\% \quad \dots (10)$$

2. Brushless DC motor model [23]

Modelling equations of brushless DC motor

$$I_S = \frac{P}{V} \quad \dots (11)$$

$$T = \frac{Watt}{2 \pi \times w_{sync}} \quad \dots (12)$$

$$L_{st} = \frac{T}{2 N_m N B_g R_{r0} I_s} \quad \dots (13)$$

$$T_L = 2 L_{st} N_m N B_g R_{r0} I_s \quad \dots (14)$$

$$L_g = \frac{2\pi \mu_0, R_{r0}, L_{st} N^2}{g + \frac{l_m}{\mu_r c_\theta}} \quad \dots (15)$$

$$C_\Phi = \frac{A_m}{A_g} \cong 1 \quad \dots (16)$$

$$T = J \frac{d \omega_m}{dt} + T_L + B \omega_m \quad \dots (17)$$

$$\omega_m = \int \frac{T - T_L}{J} \quad \dots (18)$$

$$T_m = \frac{P}{\omega_m} \quad \dots (19)$$

3. Throttling model [24]

Throttle model is done by making look up table from standard throttle opening to fuel output graph of IC engine.

4. IC engine model [25]

$$B_{HP} = \frac{P \times A \times L \times N \times n}{60} \quad \dots (20)$$

P_i = Indicated mean effective pressure

A = Bore area = 0.05

L = Length of displacement = 0.065

$$N = R.P.M. = 6000$$

$$n = \text{Cylinder} = 4$$

5. Fuel tank model

By calorific value model

Total energy in car,

$$\text{Diesel calorific value } D_{\text{cal}} = 46000$$

$$\text{Tank capacity } T_c = 22.5$$

$$\text{Time (sec) } T = 3600$$

$$D_{\text{cal}} \times T_c \times T = 3.726 \times 10^9 \text{ Calorie}$$

From this simulation model parameters like SOC%, fuel consumption, battery consumption torque & horsepower production will be analysed.

5 Influence of drive cycle in HEV's components sizing

The main component of HEV's power train are battery storage, power rating of electric machine and size and rating of IC engine and it's fuel tank capacity [20]. All this components mainly determines initial cost of HEV's power train. Running cost is determined by fuel/battery power consumption.

To determine components size of HEV first step is to collect data of real time drive cycles of roads where HEV is to be driven.

Influence parameter for battery ampere-hour rating is determined by how long vehicle has to be travelled which average distance of different is charging station and acceleration power requirement of motor.

Similarly size of IC engine and motor is determined by average power and peak power required to fulfil drive cycle load requirement [19].

Deceleration energy determines rating recharging circuit which should be capable of holding and harvesting deceleration power.

Deceleration and acceleration power is higher in urban roads and state highway while it is considerably less in express highway.

From figure 5 and 6 initial component size can be estimated. Initial estimation is done to begin designing process of HEV's component.

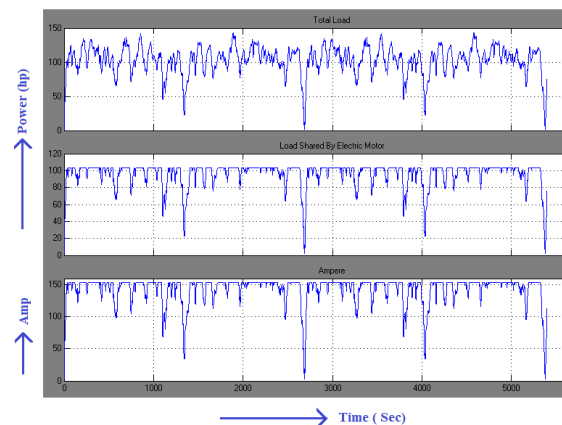


Figure 5: Electric Motor Power and Ampere

Initial estimation of components is derived without keeping any constraint by simply finding means of drive cycle parameters. Initial sizing is done by mean value method and results are;

Motor rating = 60hp

IC engine rating = 60hp

Battery rating = 22.7kw

Fuel Tank = 22lit.

Initial sizing is not done by any algorithm or any designing method but simply by considering the influence of drive cycle on HEV's component sizing and from table 3 which shows mean load demand [27].

From this initial sized data of component, optimization will be done with consideration of constraints.

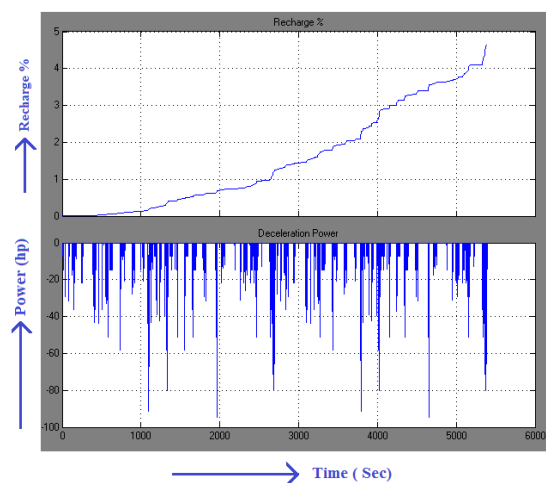


Figure 6: Recharge of Battery and Deceleration Energy

Table 5: Rating from result of optimization

Optimization Method(Final Rating)	Motor (HP)	IC Engine (HP)	Battery Rating (kw)
Mean Value	60	60	22.7
TLBO	45	45	21.5
MOGA	50	50	21.5

7 Economy

Economy of running HEV is based on electricity and fuel prices on year 2015. It is calculated in terms of Rs/km. Rs/km for convectional IC engine and HEV which contains design component are calculated [27]. How much money needed to be spent for kilometre ride for any drive cycle is compared in result.

Table 6: Running cost

Car Type	Rs/KM	Road
IC Engine	3.005	Express highway
HEV	1.45	Express highway

HEV have lower running cost as compared to conventional IC engine type car which could be prime factor to motivate Indian consumer to buy HEV technology based car.

8 Results

Table 7, 8, 9 shows result of different optimization method. Component sized from mean value method shows it to be least efficient among three.

Optimization by TLBO shows 4% in rpm drop which means 4% less acceleration than mean value method of component design while it shows efficient IC engine operation which is less efficient component in any HEV.

By results of TLBO optimization method with MOGA optimization method it shows result came from TLBO are efficient than MOGA but it shows drop of rpm of 1.5% compared with MOGA.

TLBO method reduces component size to 25% and with MOGA method to 20% compared with results from mean value method.

These optimized component size were put in to different drive cycle condition where none of the result shows any variation in its performance and TLBO is able to sustain all drive cycle

characteristics by dropping 4% in RPM even with 25% less in HP rating.

Table 7: For state highway

Designing Method	HP	Battery SOC %	Fuel Left %	RPM Drop %
Mean Value Result	120	76.08	40.12	0
MOGA Optimization Result	98	77.26	44.66	2.5
TLBO Optimization Result	90	78.7	51.12	4

Table 8: For urban highway

Designing Method	H P	Battery SOC %	Fuel Left %	RPM Drop %
Mean Value Result	120	98.06	99.47	0
MOGA Result	98	98.19	99.51	2.5
TLBO Result	90	98.25	99.57	4

Table 9: For express highway

Designing Method	HP	Battery SOC %	Fuel Left %	RPM Drop %
Mean Value Result	120	92.64	40.12	0
MOGA Optimization Result	98	92.9	90.33	2.5
TLBO Optimization Result	90	92.81	51.12	4

9 Conclusion

Drive cycle is measured for Indian road that revealed its numerous characteristics. There is major variation in drive cycle for different road type. From cycle data component size were estimated and optimized with new method which

is TLBO. To observe TLBO method's effectiveness it was compared with MOGA method of optimization. Results were simulated in MATLAB on with dynamic model of vehicle and modelling of parallel HEV's components. Component selected by different optimization methods were put through different drive cycle and it did show that optimization done by TLBO method selects component size that is less than other two component size result derived with different methods. TLBO component rating is less than other two but still it is able to sustain different drive cycle load characteristics by only 4% drop in RPM. TLBO method proves to be optimizing HEV component more effectively because it has capability to modify data that suits different criteria. By optimal reduction in HEV component size with TLBO method the running cost of vehicle is reduced up to 50% by reducing rating of component. TLBO method is very effective tool of optimization of HEV for versatile drive cycle characteristics as Indian road have.

References

- [1] Vaibhav Aaradhi, Ketaki Gaidhani, Plug In Hybrid Electric Vehicle- Indian Transport Sector Perspective,, ISSN 2229-5518, International Journal of Scientific & Engineering Research,2013
- [2] Sanghpriya H. Kamble, Tom V. Mathew, G.K. Sharma, Development of real-world driving cycle: Case study of Pune, India,ISSN 1396-9209,Elsevier Science,2009.
- [3] Varsha Shah, Patel Pritesh, Patel Sagar, Prasanta Kundu Ranjan, Maheshwari, Measurement of Real Time Drive Cycle for Indian Roads and Estimation of Component Sizing for HEV using LABVIEW, World Academy of Science, Engineering and Technology 58 2011
- [4] Lok Sabha Secretariat, National Highways Development Project: An Overview, parliament Library and reference, research, documentation and information service, August/2013
- [5] Staackmann, M.Liau, B.Y., Dynamic driving cycle analyses using electric vehicle time-series data, Energy Conversion Engineering Conference 0-7803-4515-0 ,1997
- [6] Chen, K.,Villeneuve-d'Ascq, Lhomme, W., Bouscayrol, A., Berthon, A., Comparison of two series-parallel Hybrid Electric Vehicles focusing on control structures and operation modes, Vehicle Power and Propulsion Conference,2009
- [7] Xin Li; Dept. of Electr. & Computer Eng. Concordia Univ., Montreal, QC ; Williamson, S.S., Comparative Investigation of Series and Parallel Hybrid Electric Vehicle (HEV) Efficiencies Based on Comprehensive Parametric Analysis, Vehicle Power and Propulsion Conference,2007
- [8] Massimo Ceraolo, Antonio di Donato, and Giulia Franceschi, A General Approach to Energy Optimization of Hybrid Electric Vehicles, IEEE transactions on vehicular technology, vol. 57, no. 3, may 2008
- [9] Lei Zhang, David G. Dorrell,, Genetic Algorithm Based Optimal Component Sizing For an Electric Vehicle, IEEE, 2013
- [10] Bufu Huang, Zhancheng Wang and Yangsheng Xu, Multi-Objective Genetic Algorithm for Hybrid Electric Vehical Parameter Optimization International Conference on Intelligent Robots And Systems, 2006
- [11] Thomas J. Boehme, Benjamin Frank, Markus Schori and Torsten Jeinsch, Multi-Objective Optimal Powertrain Design of Parallel Hybrid Vehicles with Respect to Fuel Consumption and Driving Performance, European Control Conference,2014
- [12] Chirag Desai, Student Member, IEEE, and Sheldon S. Williamson, Member, IEEE, Particle Swarm Optimization for Efficient Selection, Of Hybrid Electric Vehicle Design Parameters, Power and Energy Lab, 2010
- [13] Omar Hegazy, Student Member, IEEE, and Joeri Van Mierlo , Particle Swarm Optimization for Optimal Powertrain Component Sizing and Design of Fuel Cell Hybrid Electric Vehicle, 12th International Conference on Optimization of Electrical and Electronic Equipment, 2010
- [14] R.V. Rao, V.J. Savsani, D.P. Vakharia, Teaching-learning-based optimization: A novel Method for constrained mechanical design Optimization problems, Computer-Aided Design, 2015
- [15] David L. González-Álvarez, Miguel A. Vega-Rodríguez, Juan A. Gómez-Pulido, And Juan M. Sánchez-Pérez, Multi-objective Teaching-Learning-Based Optimization (MO-TLBO) for Motif Finding, International Symposium on Computational Intelligence and Informatics, 2014

- [16] Sanjeev SINHA, Ravindra KUMAR, Driving Cycle Pattern for Cars in Medium Sized City of India, Proceedings of the Eastern Asia Society for Transportation Studies, Vol.9, 2013
- [17] Atyam mukherjee, Statistical analysis of the road network of India, Indian Academy of
- [18] Mehrdad Ehsani,Yimin Gao,Sebastien E. Gay,Ali Emadi, Modern Electric Hybrid Electric, and Fuel Cell Vehicles, Fundamentals, Theory, and Design,Ch 2,Crc Press,2000
- [19] J. Kwon, J. Kim, E. Fallas, S. Pagerit, and A. Rousseau, Impact of Drive Cycles on PHEV Component Requirements, SAE International, 2008
- [20] Ayman Moawad, Gurhari Singh, Simeon Hagspiel, Mohamed Fellah, Aymeric Rousseau, Impact of Real World Drive Cycles on PHEV Fuel Efficiency and Cost for Different Powertrain and Battery Characteristics, EVS24,2009
- [21] Olivier Tremblay1, Louis-A. Dessaint, Experimental Validation of a Battery Dynamic Model for EV Applications, EVS 24,2009
- [22] Sabine Piller, Marion Perrin,Andreas Jossen,Methods for state-of-charge determination and their applications, Journal of Power Sources,2001
- [23] T.J.E. Miller, Brushless Permanent-Magnet and Reluctance Motor Drives, Oxford Science Publication, 1989
- [24] Willard W. Pulkrabek, Engineering Fundamentals of the Internal Combustion Engine Ch3,Prentice Hall,2003
- [25] Willard W. Pulkrabek, Engineering Fundamentals of the Internal Combustion Engine Ch5,Prentice Hall,2003
- [26] Kalyanmoy Deb., Multi-Objective Optimization Using Evolutionary Algorithm,Ch 3,Wiley,2010
- [27] Kumari M, Thakura, P.R. Badodkar, D.N. Design and estimation of drive train components of Hybrid Electric Vehicle, Non-Conventional Energy (ICONCE), 2014
- [28] Sanjeev SINHA, Ravindra KUMAR, Driving Cycle Pattern for Cars in Medium Sized City of India, Proceedings of the Eastern Asia Society for Transportation Studies, Vol.9, 2013
- [29] Clement Fauvel, Vikesh Napal, Aymeric Rousseau, Medium and Heavy Duty Hybrid Electric Vehicle Sizing to Maximize Fuel Consumption Displacement on Real World Drive Cycles, EVS26, May 6-9-2012

Authors

Dr. Varsha Shah received Master of Engineering degree in Power System from SVRCET (Surat, Gujarat) in 1986. PhD. Degree from SVNIT (Surat, Gujarat). Currently she is Associate Professor at SVNIT in electrical department. Field of Research: HEV, EV, energy storage technology, power system and electrical drives.

Vishal Sanjaybhai Parekh received Master of Engineering degree in Power Electronics and Electrical Drive from MEFGI (Rajkot, Gujarat) in 2012. Currently he is Research Head at ASPERO research (Rajkot, Gujarat). Field of research: Power electronics, electric drive, hybrid electric vehicle, embedded system.

Review

Analysis of the Current Electric Battery Models for Electric Vehicle Simulation

Gaizka Saldaña ¹, José Ignacio San Martín ¹, Inmaculada Zamora ², Francisco Javier Asensio ^{1,*} and Oier Oñederra ²

¹ Department of Electrical Engineering, University of the Basque Country (UPV/EHU), Avda. Otaola 29, 20600 Eibar, Spain

² Department of Electrical Engineering, University of the Basque Country (UPV/EHU), Pza. Ingeniero Torres Quevedo s/n, 48013 Bilbao, Spain

* Correspondence: franciscojavier.asensio@ehu.eus; Tel.: +34-94-303-3052

Received: 3 June 2019; Accepted: 16 July 2019; Published: 18 July 2019



Abstract: Electric vehicles (EVs) are a promising technology to reduce emissions, but its development enormously depends on the technology used in batteries. Nowadays, batteries based on lithium-ion (Li-Ion) seems to be the most suitable for traction, especially nickel-manganese-cobalt (NMC) and nickel-cobalt-aluminum (NCA). An appropriate model of these batteries is fundamental for the simulation of several processes inside an EV, such as the state of charge (SoC) estimation, capacity and power fade analysis, lifetime calculus, or for developing control and optimization strategies. There are different models in the current literature, among which the electric equivalent circuits stand out, being the most appropriate model when performing real-time simulations. However, impedance models for battery diagnosis are considered very attractive. In this context, this paper compares and contrasts the different electrical equivalent circuit models, impedance models, and runtime models for battery-based EV applications, addressing their characteristics, advantages, disadvantages, and usual applications in the field of electromobility. In this sense, this paper serves as a reference for the scientific community focused on the development of control and optimization strategies in the field of electric vehicles, since it facilitates the choice of the model that best suits the needs required.

Keywords: batteries; electric vehicle; equivalent circuit; impedance model; Li-Ion; battery modelling

1. Introduction

Nowadays, electric vehicles (EVs) are booming, due to the existing environmental problems. Among the different storage technologies in electromobility, batteries stand out the most. Although there are other alternatives such as hydrogen storage, a battery is also required for DC bus voltage stabilization and switching on of other essential or auxiliary devices of the fuel cell system [1]. High capital costs, limited lifetime, and relatively poor performance at low temperatures are the most important issues in EVs [2–5]. Therefore, the development of efficient storage technologies is an essential part for electromobility [6].

Lithium technology is highlighted for electromobility among the studied batteries options [7]. Its specific power and energy density are the highest, with the lowest self-discharge ratio [8]. In addition, voltage by cell is higher, which is the major drawback of the low overcharging tolerance. Therefore, a specifically designed charging system is required for this type of battery.

Lithium is the material basis of this type of battery, since lithium ions are carried from cathode to anode (charging) through a separator, and vice versa (discharging). However, lithium-ion (Li-Ion) batteries can be classified among different categories based on other elements, mainly those corresponding

to the cathode chemical composition. Figure 1 shows a comparative summary of the best-known lithium ion batteries.

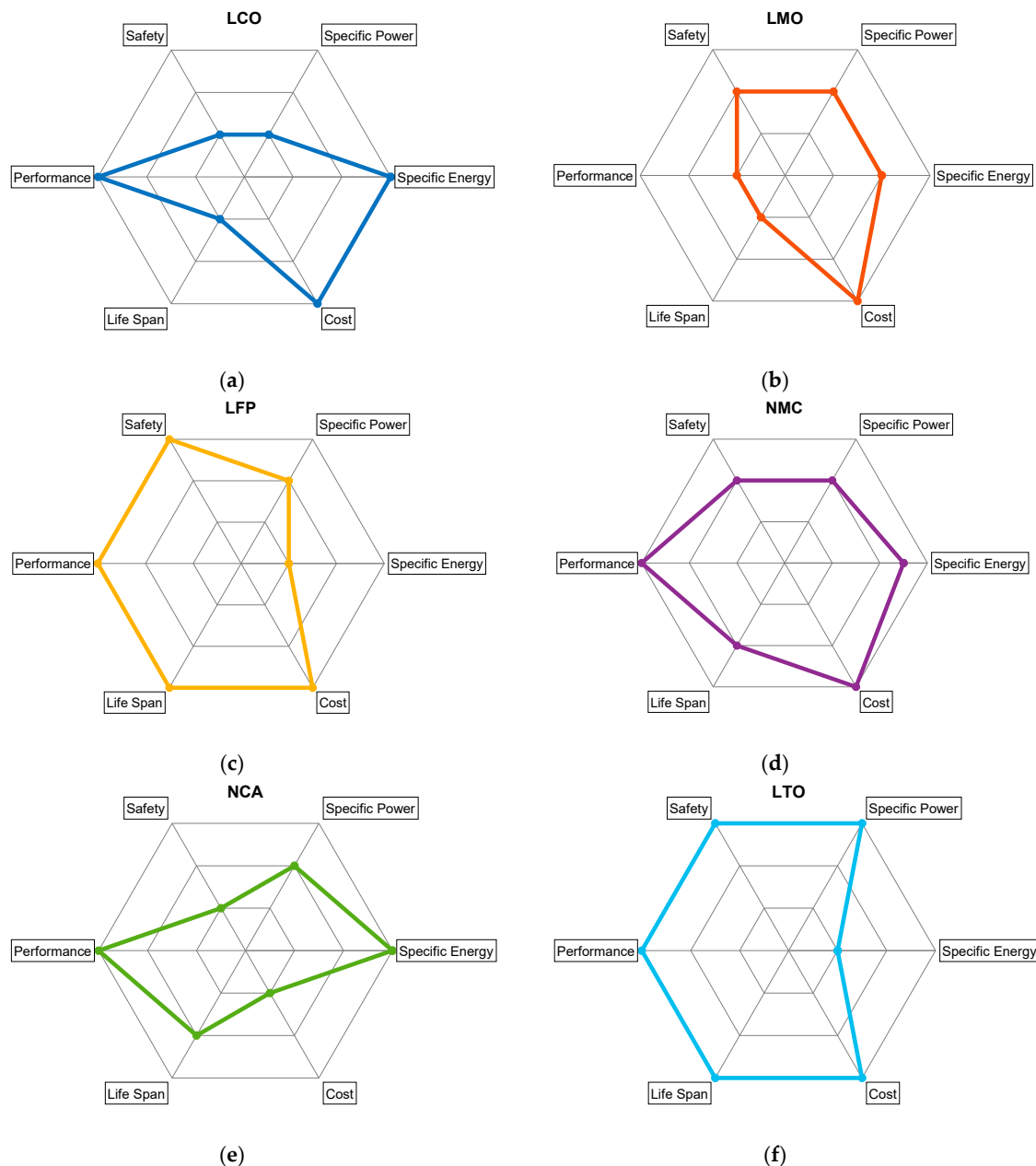


Figure 1. Lithium-ion (Li-Ion) technology comparison. (a) LCO; (b) LMO; (c) LFP; (d) NMC; (e) NCA; (f) LTO.

Specific energy is a key factor in storage, as it defines the driving range of an EV. As it can be seen in Figure 1, lithium-cobalt-oxide (LCO), nickel-cobalt-aluminum (NCA), and nickel-manganese-cobalt (NMC) technologies stand out within specific energy, but LCO can practically be discarded due to Solid Electrolyte Interphase (SEI) problems and toxicity [9]. Figure 2 shows the expected advances in specific energy for different types of battery [10].

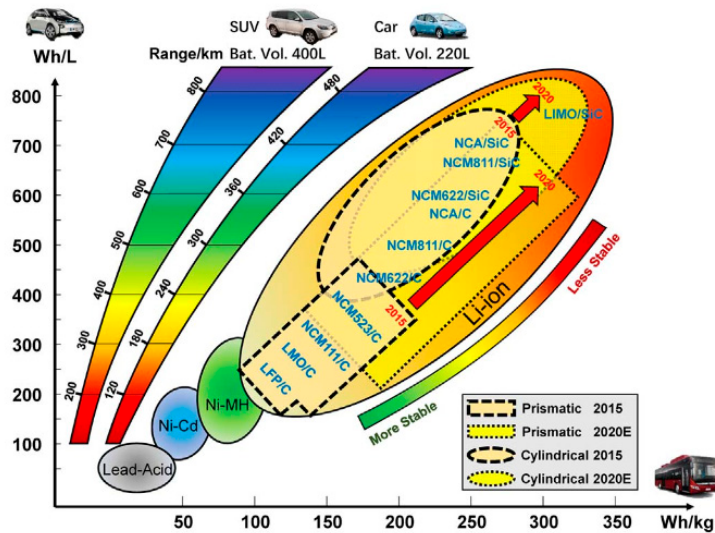


Figure 2. Li Ion Battery roadmap.

The average lifetime of batteries in EVs tends to be approximately 8 to 10 years, which is defined by a 20–30% degradation in battery capacity compared to its initial capacity [3]. In practice, the lifetime of a battery is reduced due to the high-power profile of the vehicle during acceleration and braking, which can be more than ten times higher than the average power. To overcome this drawback, not only innovation in battery technology to increase the specific energy is required, but also advanced control and optimization techniques are necessary. In this context, the use of a reliable model of the battery becomes a key factor when improving the techno-economic efficiency of the system. The Battery Management System (BMS) is responsible for the correct management of the energy stored in the batteries, and indirectly for the safety of the passengers of the vehicle [11].

The choice of the adequate battery model according to the purpose or application for which it will be used is essential. Some of the most common applications are battery design, their characterization, state of charge (SoC) or state of health (SoH) estimation, and thermal analysis or mechanical stress studies in specific applications. Depending on the field of study, there are several battery models, which are gathered in Table 1.

Models usually known as electrochemical models, as presented in [12], are aimed at describing the electrochemical reactions that occur within cell level. Thus, they are the most detailed models, but also the costliest in terms of developing and suiting. Besides, they require many computing resources.

Electrical models, however, are commonly based on an equivalent circuit to reproduce the effects of the batteries under operation, being faster than electrochemical ones by neglecting some high levels of detail.

Mathematical or analytical models depict operation effects by complex differential equations of second or greater order. Considering that many parameters are not necessary, they are sufficiently fast. However, these models do not have physical correspondence, so they are not appropriate either. Abstract models use several analysis tools such as artificial intelligence to predict the batteries performance. Accuracy depends majorly on data amount at training stage. Interpretability is practically impossible since only experimental results are used.

Combined models are composed by several sub-models to depict effects of variables from different nature. Thermoelectric models stand out within these models as their effects are related to each other.

Table 1. General classification of battery models.

Model Nature	Model	Data	Physical Interpretability	Analogy	Accuracy	Complexity	Suited Application
Electro-chemical	Pure Electro-Chemical ECM/Reduced order Electro-Chemical	P SE	H M	White box Grey box	VH H	H M	Battery design
Analytical	Peukert's model	E	L		M	M	Prediction
	Rakhmatov and Vrudhula	SE	M		M	M	
	Sheperd other iterations	SE	M	Black box	M	M	
	State-Space	E	L		M	M	
Electrical	Simples	Simple Rint	E	M		L	L
		Enhanced Rint	SE	M		L	
		RC	SE	M		L	
	Thevenin	1st order	SE	M	Grey box	L-H	Real time control, SoC estimation, ...
		2nd order	SE	M			
		3rd order	SE	M			
		nth order	SE	M			
	PNGV	1st order	SE	M		L-H	Real time control, SoC estimation, ...
		2nd order	SE	M			
		nth order	SE	M			
	Noshin Neural nets	Noshin	SE	M		M	Characterization and real time operation
		Neural nets	E	L		H	
Impedance	Frequency domain	SE	L-M	Grey box	M	M	Characterization and real time operation
Thermal	Analytical Thermal ECM Thermal	P-SE SE	H M	White box Grey box	H M	H M	
Mechanical/Fatigue	Fatigue/Mechanical	P-SE	H	Grey box		H	Design
Abstract model	Artificial Intelligence	E	L	Black box	M	M	Offline analysis
Combined models	Electro-Thermal	SE	M			M	Real time
	Thermo-electrochemical	P	H			H	
	Thermo-Mechanical	SE	H	Grey box	L-H	H	

* E: Empirical, H: High, L: Low, M: Medium, P: Physical, SE: Semi-Empirical, VH: Very High.

Thus, electrical and combined models are predominant in electromobility studies, as electrochemical ones are too complex, and mathematical ones do not have physical correspondence. Therefore, they are not suitable for real-time control. In this sense, this paper focuses on the analysis and description of the most relevant existing electrical models that are suitable to be implemented in a BMS of an EV. In this paper, simple models, Thevenin models, partnership for a new generation of vehicles (PNGV) models, impedance models, and runtime models are considered.

Simple models are the most basic models, which are only appropriate for steady-state analysis, Thevenin and PNGV models are suitable for transient state simulation, Impedance models focus on AC behavior, and runtime models depict DC behavior while runtime of the battery is predicted. These applications are collected in Table 2 [13].

Table 2. Batteries electrical model classification.

Predicting Capability	Thevenin Based/PNGV Models (ECM)	Impedance Based Models	Runtime-Combined Based Models
DC	No	No	Yes
AC	Limited	Yes	No
Transient	Yes	Limited	Limited
Battery Runtime	No	No	Yes

This paper is organized as follows: Section 2 analyzes several electrical models currently applied to Li-Ion batteries within electromobility. These models are subcategorized as simple models, Thevenin models, PNGV models, and Noshin model, arranged from the simplest, which considers only ideal elements, to the most complex, which could be a third-order model or a model considering a large number of elements. Section 3 explains impedance models, which can also be useful for other models' parameter definition. Section 4 introduces runtime models, and V-I performance of the models is explained in Section 5. Finally, conclusions are shown in Section 6.

2. Equivalent Circuit Models

In this section, several equivalent circuit models (ECMs) available in the literature that are used in electromobility applications are described, arranged from simpler to more complex.

2.1. Simple Models

2.1.1. Ideal Battery Model

The first electrical model of a battery was developed in PSpice by Hageman in [14], which allows the simulation of Pb-acid, nickel-cadmium, and alkaline batteries. Later, Gold developed a similar model for Li-Ion models with errors of up to 12% [15].

An ideal model is the simplest model, with only a constant voltage source and neglecting other internal parameters. Terminal voltage matches the open-circuit voltage in every moment. Thus, this model does not consider voltage variation under load variation, SoC changes, or any other transient phenomena.

General specifications of an ideal battery are given in capacity (Ah) and voltage (V). Stored amount of energy is given by their product (Wh). This model maintains a constant voltage independently from other factors until it is fully discharged, when the voltage drops to zero [16]. However, in real batteries, voltage is affected by the SoC, since the capacity lowers when the load is increased.

Results of this model are acceptable for steady-state analyses where the battery performance is not the scope. The most common application is the feeding of power devices, usually converters.

An improvement of this model could be the replacement of the voltage source by a SoC-controlled voltage source. Thus, voltage is varied depending on the SoC based on a look-up table, which improves the accuracy while its simplicity is maintained.

2.1.2. Simple or Linear Battery Model

The simple model, linear battery model, or internal resistance model (IR) [17], contains a resistance R_{int} , apart from the voltage source, V_{oc} (Figure 3).

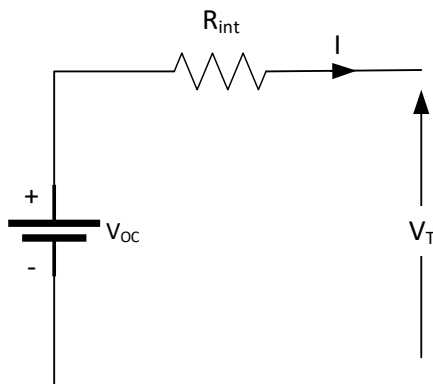


Figure 3. Simple or linear battery model.

The resistance R_{int} represents the energy losses, which make batteries heat up. Terminal voltage V_T matches up with open-circuit voltage V_{OC} only when it is in open circuit. However, when a load is connected, this voltage is given by:

$$V_T = V_{OC} - R_{int} \cdot I. \quad (1)$$

Therefore, this model can emulate the instantaneous voltage drop when the circuit is completed, which is directly proportional to the circulating current. The higher the internal resistance in a battery, the greater the losses, and the lower the available maximum power.

The main drawback of this model, as well as of the previous one, is that neither the terminal voltage V_T nor the open-circuit voltage V_{oc} vary according to the SoC or others, as this can be electrolyte

concentration. Resistance is constant too, independent from SoC or temperature. In this sense, it has to be noted that, in a real battery, the resistance is highly dependent on battery type, SoC and SoH state, and temperature (Figure 4 [18,19]). Generally, resistance increases when SoC lowers (Figure 4a), SoH lowers (degradation increases) (Figure 4b), and temperature lowers (Figure 4c).

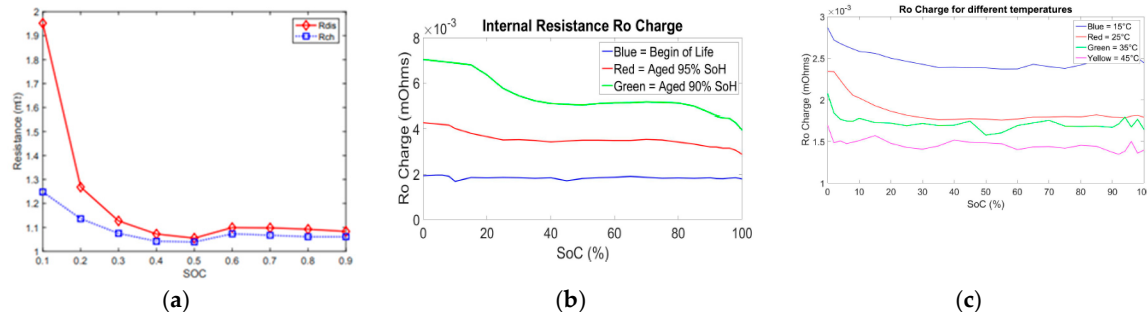


Figure 4. R_{int} variation in NMC with (a) state of charge (SoC); (b) state of health (SoH); and (c) temperature.

Applicability of this model is restricted to studies where the battery operates at the middle range of SoC, where the internal resistance and temperature are almost constant. At low SoC, however, resistance varies too much. Available energy to be released, that is, capacity, cannot be depicted, and it is supposed to be unlimited [20]. The most common application is the feeding of power devices as converters or inverters [21].

Within EVs applications, this model is used in maintenance studies, as battery preheating at cold environment [22], and dynamic simulations of hybrid and electric vehicles. Dynamic simulation can be improved by considering a SoC-controlled voltage source [23,24].

Resistance from Figure 3, R_{int} , differs in charging or discharging mode, as shown in Figure 5a. Therefore, different resistances can be considered for better accuracy, R_c for charging and R_d for discharging, as shown in Figure 5.

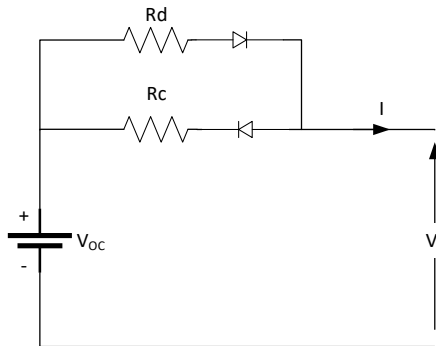


Figure 5. Simple battery model considering charging and discharging resistances.

Diodes shown in Figure 5 are supposed to be ideal and are aimed at activating the correct resistance. Thus, terminal voltage is given by:

$$\text{Charging : } V_T = V_{OC} + R_c \cdot I, \quad (2)$$

$$\text{Discharging : } V_T = V_{OC} - R_d \cdot I. \quad (3)$$

When charging, the diode associated with R_c is directly polarized and will conduct, but the diode associated with R_d is reversely polarized, avoiding current circulation. When discharging, R_d will be activated and R_c blocked, so that only one resistance will be activated in each process. This model has the same drawbacks as the previous one, but improves accuracy, and is used in hybrid and EVs [25].

2.1.3. Enhanced Simple Battery Model

Figure 6 shows the enhanced simple battery model, which considers the effect of the SoC in the resistance.

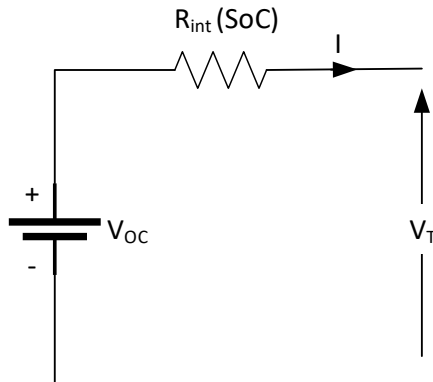


Figure 6. Simple battery model considering power fade (PF).

In this model, terminal voltage is given by:

$$V_T = V_{OC} - R_{int}(SoC) \cdot I \quad (4)$$

where internal resistance can be expressed as [26]:

$$R_{int}(SoC) = \frac{R_0}{SoC^K} \quad (5)$$

where R_0 , SoC , and k are initial internal resistance, current SoC, and a capacity factor calculated from manufacturer load curves, respectively. The current SoC is given as:

$$SoC = 1 - \frac{A \cdot h}{C_{10}} \quad (6)$$

where A is the equivalent demanded current, h is the operation time in hours, and C_{10} is capacity for 10 hours operation at reference temperature. Since actual capacity is dependent on the current, it also will be the error.

However, some authors change the internal resistance calculation method while maintaining the same schematic model, but including a resistance with non-linear behavior, given as:

$$R_{int}(SoC) = R_{int} + \frac{k}{SoC} \quad (7)$$

where R_{int} (SoC) is the variable internal resistance, k is a polarization constant, and SoC is the state of charge.

This model has been historically used by several manufacturers for batteries monitoring purposes in stationary stages, as well as for traction simulation in Pb-acid batteries [27]. Additionally, it can also be applied to lithium batteries. Among drawbacks, it does not reduce capacity when load increases, so it is not valid for dynamic systems or transient states. Although resistance varies, it does not vary as a function of the temperature, which is one of the major drawbacks of EVs.

This model can be improved in case a SoC -controlled voltage source V_{OC} is considered. Real battery V_{OC} variation is shown in Figure 7, which includes the usual hysteresis effect between charging and discharging.

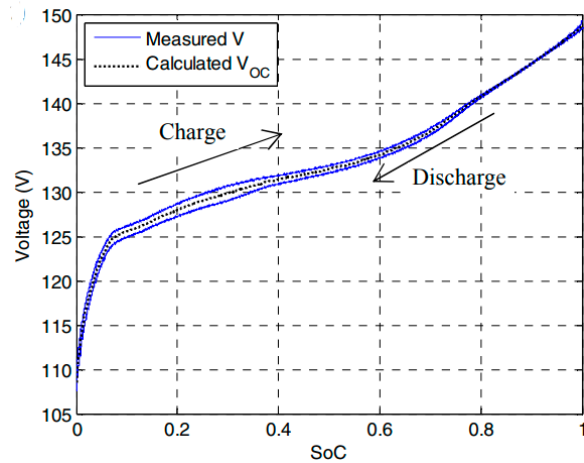


Figure 7. V_{OC} variation with SoC in NMC [28].

Terminal voltage V_T is given by [29]:

$$V_T = V_{OC}(SoC) - R_{int}(SoC) \cdot I, \quad (8)$$

$$V_{OC}(SoC) = V_O - k \cdot SoC, \quad (9)$$

$$R_{int}(SoC) = R_{int} - k_R \cdot SoC \quad (10)$$

where $V_{OC}(SoC)$ is the SoC-dependent open-circuit voltage, $R_{int}(SoC)$ is the SoC-dependent resistance, I is the current, V_O is the open-circuit voltage when the battery is fully charged, R_{int} is the internal resistance when the battery is fully charged, SoC is the state of charge, and k and k_R are empirically obtained constants.

Even though this model improves accuracy, it is very limited in terms of energy released, temperature consideration, and is not valid for simulation of transient states. To improve the accuracy, temperature and SoH can be considered in the voltage source and resistance, but only for steady-state analyses [17].

2.1.4. Voltage Sources-Based Model

The voltage sources-based model is based on the connection of several voltage sources, which represent different phenomena. The general scheme for this model is shown in Figure 8.

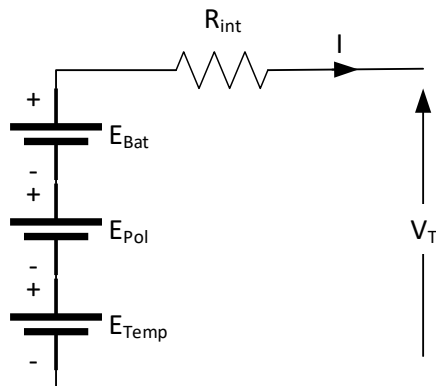


Figure 8. Voltage sources-based model.

The terminal voltage V_T is given by:

$$V_T = E_{bat} + E_{Pol} + E_{Temp} - R_{int} \cdot I \quad (11)$$

where E_{bat} is a voltage source representing cells internal voltage, E_{Pol} is a voltage source representing polarization effect caused by the active material, E_{Temp} is a voltage source representing temperature effect, R_{int} is the internal resistance, and I is the current.

Each voltage source value is experimentally determined by the relation between each effect and voltage, at each SoC value. This model can be applied to Pb-acid, Ni-Cd, and Li-Ion batteries, and is used in EV and hybrid vehicles driving simulation [30].

On one hand, the accuracy of this model relies on the accuracy of the relation specified in each voltage source. On the other hand, there is an inherent error by the consideration of each variable separately instead of considering them in a coupled manner.

2.1.5. Resistor-Capacitor (RC) or Dynamic Model

The RC or dynamic model is shown in Figure 9. It was first developed in 2000 by SAFT Battery Company for the NREL.

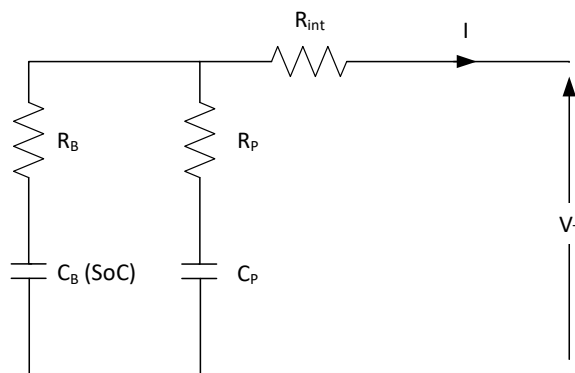


Figure 9. Resistor-capacitor (RC) or dynamic model.

This model includes a capacitor C_B , which represents the stored capacity, a series resistance R_B , which represents the propagation effect, a capacitor C_P , and a current dependent resistance R_P , which represent the polarization and diffusion effects, respectively, and an internal resistance R_{int} . The value of C_P is very small, while the value of C_B usually takes very large values. Generally, the self-discharge resistance is neglected in Li-Ion batteries [31,32]. SoC value is represented in the voltage variation through the capacitor C_B . The equations that govern its operation are:

$$V_T = V_{OC} - I_B \cdot R_B - R_{int} \cdot I, \quad (12)$$

$$V_T = V_{CP} - I_P \cdot R_P - R_{int} \cdot I. \quad (13)$$

This model is the preferred one among simple models in automotive simulations. Usually, it is used for SoC estimation [33–35], as it is accurate and complex enough.

2.2. Thevenin-Based Battery Models

None of the models presented above are valid for transient state simulations. In order to simulate transients, some phenomena as polarization must be considered. In this subsection, some of the most used models for transient state simulation are explained.

2.2.1. (First-Order) Thevenin Model

The simplest Thevenin model, commonly called first order or one time constant (OTC) [17], is composed by a voltage source V_{OC} , an internal resistance R_{int} , and a RC pair (R_1 and C_1) representing the capacitance effect between two parallel plates and the contact resistance. This model is shown in Figure 10.

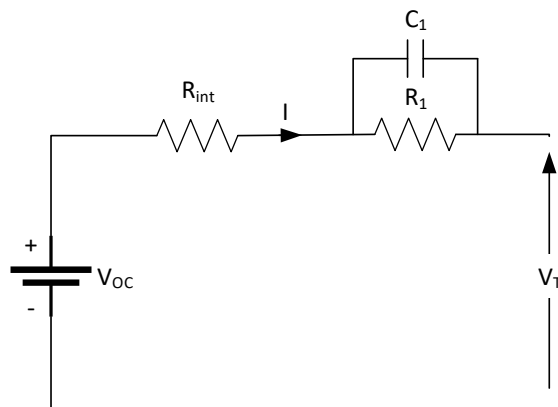


Figure 10. (First-order) Thevenin model.

The aim of adding a RC pair to the simple linear model is to represent transient phenomena. The main drawback of the Thevenin model is that all the parameters are considered to be constant. However, it is known that parameters are dependent on SoC, C-Rate, temperature, SoH, etc.

An improvement for transient state simulation can be made by considering SoC in the voltage source V_{OC} , that is, the open-circuit voltage V_{OC} is related to the SoC of the cell. Among classic applications of this model are dynamic voltage resistor (DVR) [36] with Pb-acid batteries, but it can also be used in Li-Ion batteries.

An application of this model can be found in [32], where authors present a SoC estimation method for an LCO battery. The self-discharge resistance is neglected, as these losses are minimum in Li-Ion technology (2–10% per month). Authors of [37] apply this model in their stability analysis and SoC estimation method design for a Li-Ion battery. Authors of [38], however, apply this model in their study of batteries parallelization. In [39], in addition to the SoC, a SoH estimation method in Li-Ion cells is also proposed.

Some authors consider the SoC influence in all the parameters, which improves the results accuracy. The authors of [40], for example, apply it in their study of a power train of an EV.

It is also possible to derive this model in the so-called “EP-Thevenin”, as developed in [41]. In this paper, authors consider the polarization effect in a deeper way and validate their model in LIFEPO cells.

Among the characteristics of Li-Ion cells, their low hysteresis effect can be highlighted. In [42], a model development considering this hysteresis effect, as well as the effect of the temperature and the SoC, can be found. Although considering hysteresis improves model accuracy, this type of model is surpassed by the second-order Thevenin model [42].

The correct adjustment of the parameters involved is a key factor when comes to achieve a good precision in the model, for which it is common to use different tests. In [43], a set of charge-discharge pulses are used, and a prediction error-minimization (PEM) algorithm is applied. Although the SoC is discretely estimated online using a neuro-fuzzy inference method, the model obtained is fast enough for real-time operation. In [44], however, moving-window least-square method is used for parameter estimation in frequency domain. In both papers, only SoC is considered, and other relevant variables, such as temperature and aging effects, are neglected in their estimation. In this sense, the models obtained still show some room for improvement.

2.2.2. Second-Order Thevenin Model

The second-order model, two time constants (TTC), or dual polarization model, adds a second RC pair (R_2 and C_2) with a larger time constant (Figure 11) to the previous model. Thus, it is possible to accurately represent the terminal voltage when the current is zero, which was not possible for the OTC [17].

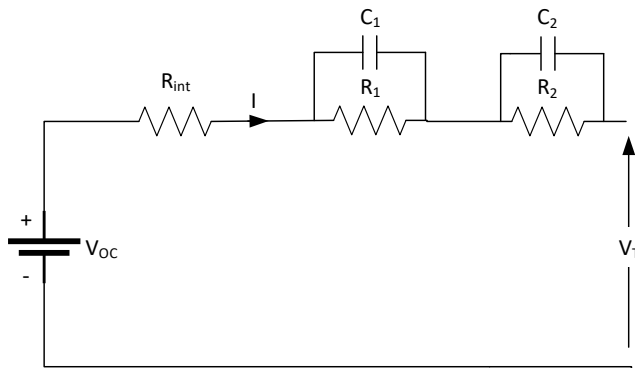


Figure 11. Second-order Thevenin model.

Therefore, the first RC pair has a low time constant for describing short-term transient effects, while the second RC pair has a larger time constant for describing long-term transient effects. These transient effects are related to electrochemical and concentration polarization effects, including charge transfer effect, diffusion, and other factors.

Equations that govern its operation are:

$$V_T = V_{OC} - R_{int} \cdot I - V_{C1} - V_{C2} \quad (14)$$

where:

$$\dot{V}_{C1} = -\frac{1}{R_1 \cdot C_1} \cdot V_{C1} + \frac{1}{C_1} \cdot I \quad (15)$$

$$\dot{V}_{C2} = -\frac{1}{R_2 \cdot C_2} \cdot V_{C2} + \frac{1}{C_2} \cdot I. \quad (16)$$

A development of this model can be found in [45], where a second-order Thevenin model is used for capacity fading (CF) characterization. In this, R_{int} is divided into two elements, the original resistance R_{series} , and the resistance $R_{cycling}$, which considers the cycling of the cell. All parameters are defined considering the SoC and temperature.

The authors of [46] apply this model in their SoC estimation method based on a combination of the least-squares method and an extended Kalman filter. They only consider the SoC, neglecting temperature and SoH. In [47], however, SoC, SoH, and SoF are considered.

Thevenin models can be used in combination with others to create a multidisciplinary model. The study performed in [48] develops a model considering three aspects: (i) Electrical model, (ii) thermal model, and (iii) degradation model for Li-Ion batteries installed in EVs. Authors apply a modified particle swarm optimization (PSO) for parameter defining and results are validated experimentally. In [49], an online parameter identification method is proposed based on several offline tests. Since temperature is considered to be a great source of error, a temperature compensation is added as an offset. SoH is calculated according to the rate of change of several parameters but is not used for the parameters identification.

2.2.3. Third-Order Thevenin Model

The third-order Thevenin model is obtained by adding a third RC pair, as can be shown in Figure 12.

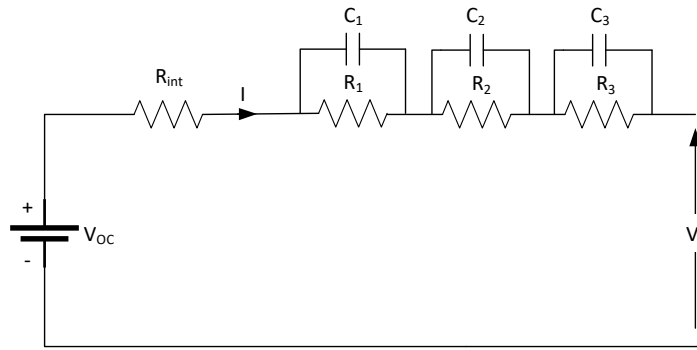


Figure 12. Third-order Thevenin model.

Terminal voltage V_T is given by:

$$V_T = V_{OC} - I \cdot R_{int} - V_{C1} - V_{C2} - V_{C3} \quad (17)$$

where:

$$\dot{V}_{C1} = -\frac{1}{R_1 \cdot C_1} \cdot V_{C1} + \frac{1}{C_1} \cdot I, \quad (18)$$

$$\dot{V}_{C2} = -\frac{1}{R_2 \cdot C_2} \cdot V_{C2} + \frac{1}{C_2} \cdot I, \quad (19)$$

$$\dot{V}_{C3} = -\frac{1}{R_3 \cdot C_3} \cdot V_{C3} + \frac{1}{C_3} \cdot I. \quad (20)$$

The most interesting applications of the third-order Thevenin model within electromobility include the parametric modelling of the battery [50] and the Vehicle-to-Grid (V2G) operation studies [51].

It is possible to increase the complexity of the model for higher accuracy, but the computation cost is not worth the improvement. Therefore, it is not usual to find higher order models, assuming that their application in electromobility would be unfeasible for real-time control.

2.3. PNGV Models

2.3.1. (First-Order) PNGV Model

A partnership for a new generation of vehicles (PNGV), composed of a cooperative research program between U.S. government and the three major domestic auto corporations (DaimlerChrysler, Ford, and General Motors), proposed the PNGV model, which is shown in Figure 13.

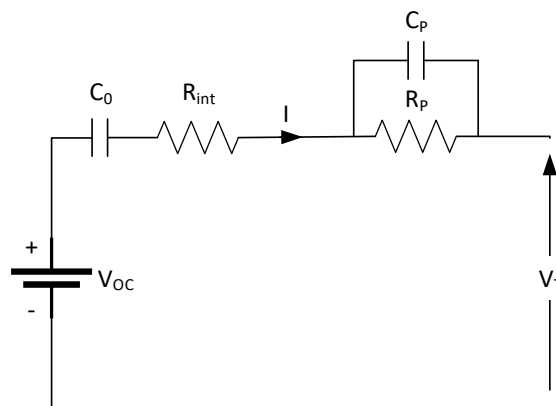


Figure 13. (First-order) partnership for a new generation of vehicles (PNGV) model.

This model is obtained by adding a series capacitance C_0 to the Thevenin model. Here, V_{OC} is the open-circuit voltage source, R_{int} is the internal ohmic resistance, R_P and C_P are the polarization resistance and the capacitance given by polarization (due to the gradient concentration), respectively, and C_0 is the capacitance that represents the changes in the open-circuit voltage (OCV) due to the integration of the current I .

When the Li-Ion battery is in a charging or discharging state, the integration of current with time causes the SoC to change, which in turn, changes the OCV of the battery, which is represented by the voltage changes on the capacitor C_0 . In this model, the capacitance C_0 not only represents the capacity of the Li-Ion battery, but also its direct current response. In addition, the effect of hysteresis is partly described by C_0 , thereby compensating some of the deficiencies of the Thevenin model. Parameter identification experiments based on current pulses can easily be conducted, with this model being among the most frequently adopted models.

Terminal voltage in this model is given by:

$$V_T = V_{OC} - I \cdot R_{int} - V_{C0} - V_{C_P} \quad (21)$$

where:

$$\dot{V}_{C0} = \frac{1}{C_0} \cdot I \quad (22)$$

$$\dot{V}_{C_P} = -\frac{1}{R_P \cdot C_P} \cdot V_{C_P} + \frac{1}{C_P} \cdot I. \quad (23)$$

However, the PNGV standard model does not consider the cycle number or C-rate effects. In turn, polarization effect, polarization, and activation as a whole, are considered. The OCV only depends on total current throughout, which conducts to an increasing error with time [52].

In the current literature, this model is used in SoC as well as in SoH estimation [53,54].

An improvement of this model can be found in [55]. In this, authors have related the parameters to SoC and temperature to improve its accuracy. They also consider the hysteresis effect and the non-linearity when operating under high currents.

2.3.2. Second-Order PNGV Model

The first-order PNGV model, as the first-order Thevenin model, is not very accurate when the cell is fully charged or fully discharged [56]. The PNGV model can be extended to a second-order one, which is shown in Figure 14.

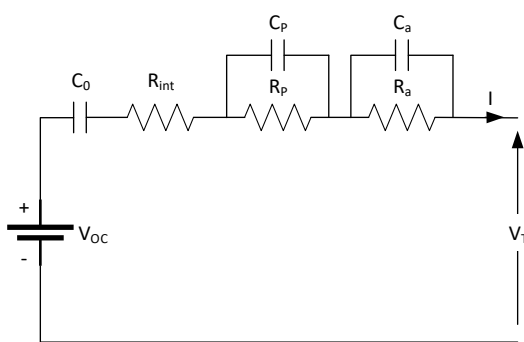


Figure 14. Second-order PNGV model.

In this model, R_P and C_P represent polarization effects by concentration, as in classic PNGV, but R_a and C_a are added to represent polarization effects by activation. The general equation that governs its operation is:

$$V_T = V_{OC} - I \cdot R_{int} - V_{C0} - V_{C_P} - V_{C_a} \quad (24)$$

where:

$$\dot{V}_{C_0} = \frac{1}{C_0} \cdot I \quad (25)$$

$$\dot{V}_{C_P} = -\frac{1}{R_P \cdot C_P} \cdot V_{C_P} + \frac{1}{C_P} \cdot I \quad (26)$$

$$\dot{V}_{C_a} = -\frac{1}{R_a \cdot C_a} \cdot V_{C_a} + \frac{1}{C_a} \cdot I. \quad (27)$$

An advantage of this second-order model is the accuracy improvement in transient and stationary state compared to the first-order PNGV and first-order Thevenin [57], but considering that computational requirements are too high, it is poorly used.

2.4. Noshin's Battery Models

Generally, battery models do not consider the hysteresis effect. Noshin's model is a derivation from the Thevenin model, which considers this hysteresis effect and the nonlinearity of the internal parameters.

Parameters of the Thevenin and PNGV models are obtained by a hybrid pulse power characterization (HPPC) test [58] and, generally, making several assumptions, such as same charging and discharging resistances, or same charging and standing resistances. However, these resistances do vary in a real battery, and therefore, it may be necessary to consider all them to obtain a high accuracy model. Figure 15 shows the Noshin's model electrical scheme.

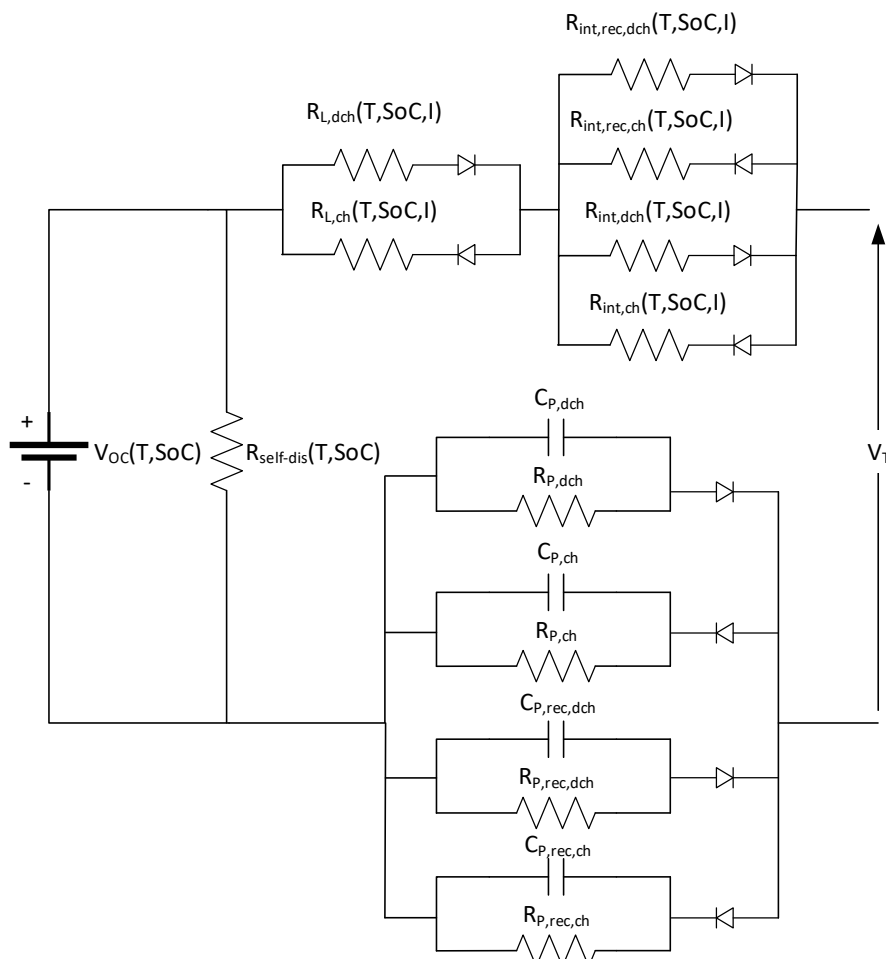


Figure 15. Noshin's model.

In this model, the internal resistance during charging $R_{int,ch}$, is different from the internal resistance during discharging $R_{int,dch}$. Furthermore, $R_{L,ch}$ and $R_{L,dch}$ are added to represent the resistance increase due to the cycle aging, and four RC pairs, which represent the polarization effects, two during cycling and two during resting. Finally, a self-discharge resistance $R_{self-dis}$ can be considered for more accuracy. A development of this model can be found in [58].

3. Impedance Models

One of the most commonly used techniques for parameter determination in ECM refers to electrochemical impedance spectroscopy (EIS) [59]. The electrochemical impedance is defined as the response of an electrochemical system to an applied voltage. In this technique, an impedance sweep in frequency spectrum is performed, easing a model definition. Therefore, an impedance is got at each frequency value. Test results are graphed in a Nyquist diagram, depicting the resistance in abscise axis and the reactance in y-axis.

In frequency spectrum, it is common to find constant phase elements (CPEs). These elements have a constant phase independent from frequency value and are commonly used in Li-Ion battery modelling [60–63].

The impedance of a CPE can be expressed in fractional calculus as:

$$Z_{CPE}(s) = \frac{1}{Ws^\alpha} \quad (28)$$

where Z_{CPE} is the impedance of the CPE; s is the Laplace operator; W is the fractional coefficient; and α is the fractional order, $0 \leq \alpha \leq 1$. Note that the CPE represents a resistance when $\alpha = 0$ and represents a capacitance when $\alpha = 1$.

A typical circuit obtained though EIS tests for Li-Ion batteries is the so-called Randle's Circuit, which is shown in Figure 16. Some authors prefer to draw the Warburg impedance Z_W out of the parallel branch, in series with R_{int} , but the difference between these two models is negligible [64].

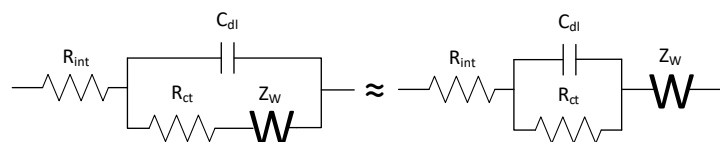


Figure 16. Randle's circuit and its approximation.

The internal resistance R_{int} used to represent the electric conductivity of the electrolyte, separator, and electrodes, matches with horizontal displacement, that is, where the curve meets the x-axis. The Z_{ARC} impedance element is composed of a parallel association of the charge transfer resistance R_{ct} and the double-layer capacitance C_{dl} , which represent the activation polarization voltage drop, and is graphed as a semicircle, while Z_W is a specific CPE, which models the diffusion effects, and is graphed as a line with 45-degree slope at very low frequencies [59]. These parameters are shown in Figure 17, in a commonly used circuit in these studies, and its Nyquist diagram with its corresponding physical interpretation.

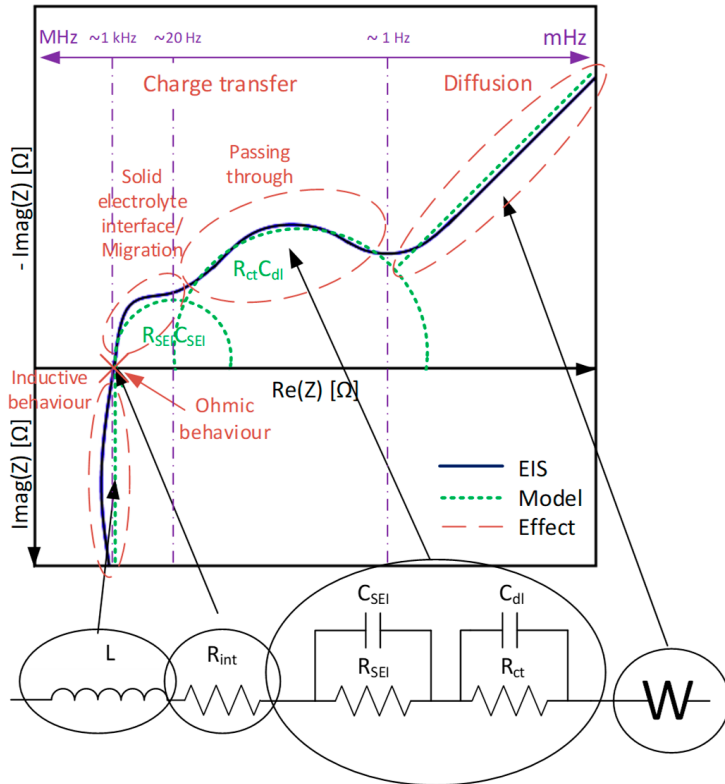


Figure 17. An impedance model of Li-Ion battery.

The analytical expression is as follows:

$$Z_{model}(s) = Ls + R_{int} + \frac{R_{SEI}}{1 + R_{SEI}C_{SEI}} + \frac{R_{ct}}{1 + R_{ct}C_{dl}s} + \frac{1}{Q_W s^{1/2}} \quad (29)$$

where Z_{model} denotes the impedance of the equivalent circuit model; L and R_{int} are the inductance and resistance in the high-frequency region, respectively; R_{SEI} and R_{ct} are the resistances in the middle-frequency region; C_{SEI} is a CPE modelled as a capacitor; C_{dl} is another CPE modelled as a capacitor; and Q_W is the fractional coefficient of the Warburg impedance.

The effects of this Warburg impedance can also be reproduced by using multiple resistor-capacitor (RC) networks in series [65]. Although for an exact equivalence an infinite RC pairs network is needed, the circuit can often be modelled precise enough over some frequency range by using a small number of RC pairs. In addition, double layer capacitance C_{dl} is often omitted, as its impact is predominant only at very high frequencies [66]. If C_{dl} is removed and Warburg impedance is replaced by a small finite number of RC pairs, the cell model becomes the Thevenin model explained in Section 2.2.

EIS is recommended to be performed in stationary state and considering low input signal to avoid non-linearity effects. Besides, very low currents must not be used to avoid noise in results. This test must be repeated for each case of interest (SoC, temperature, current, etc.), as it is necessary to wait until stationary state. Some EIS analysis can be found in [67,68]. Figure 18 [69–71] shows the results dependency on temperature, SoC, and SoH.

The direct effect that the temperature has on all the parameters can be observed, greater in Z_{ARC} , enlarging the radius of the circle in Nyquist diagram. The SoC has its larger effect in R_{int} , while the SoH affects all the parameters similarly.

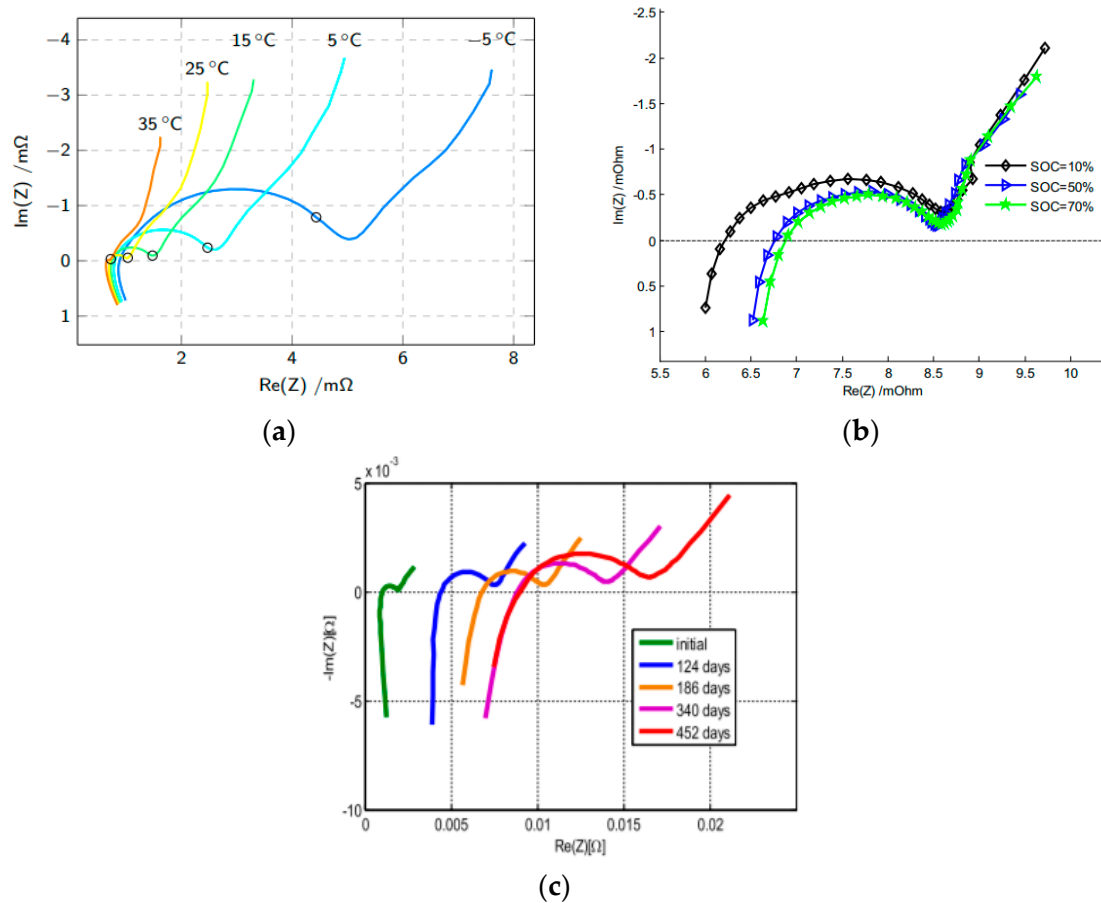


Figure 18. Nyquist plot of electrochemical impedance spectroscopy (EIS) measurements on (a) different temperatures; for each temperature, the 1 Hz point is marked; (b) different SoC state; (c) several ages.

Impedance models can be very useful in Li-Ion cell diagnosis. Thus, identifying the cell-aging reason is possible by observing the larger variation parameter. R_{int} is a contact or an ohmic resistance, and its variation means conductivity loss, collector corrosion, or side reactions in electrolyte. An increase in R_{SEI} and C_{SEI} means an increase in the solid electrolyte interface, which together with an increase of the R_{CT} , means a loss of lithium in the cell. A variation in Warbug impedance, in turn, is normally due to a loss of active material [72]. The number of semi-circles before the Warburg tail depends on the usage history of the cell as they are originated from SEI and the electronic properties of materials [73].

Several models derived of this technique can be found in the literature [74–77].

4. Runtime Models

4.1. Simple Runtime Models

The models introduced above are able to represent the voltage and current evolution. However, runtime data are not provided. Figure 19 shows a runtime model, which is commonly used for runtime simulation of a battery under a fixed average current.

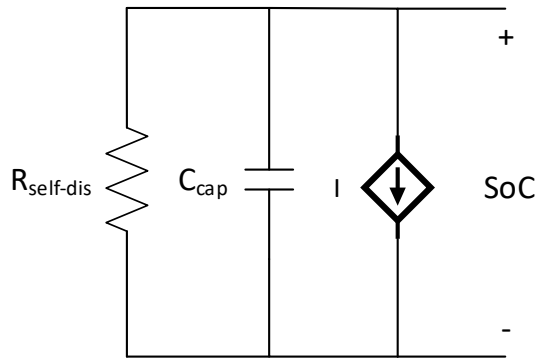


Figure 19. Runtime model.

where $R_{self-dis}$ is the self-discharge resistance, C_{Cap} is the capacitor that represents the charge stored in the battery (capacity), and $I(t)$ is a current source that represents the operating current.

Since the voltage of a battery is dependent on the SoC, this model simulates the SoC and is commonly used in combination with other models.

4.2. Runtime-Combined Models

Runtime-combined models are generally composed by two sub-circuits connected to each other. Generally, a runtime model combined with a Thevenin one is widely used. In Figure 20, a typical circuit based on the third-order Thevenin is shown.

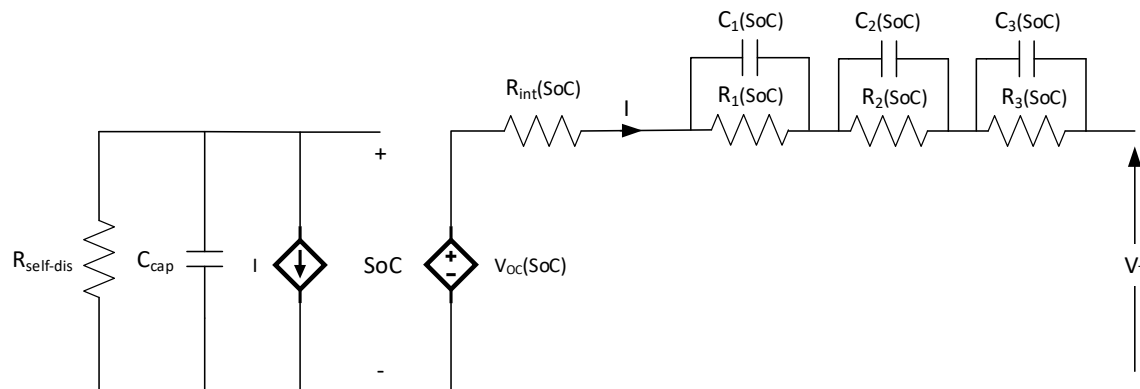


Figure 20. Runtime-combined typical model.

In the first sub-circuit, $R_{self-dis}$ is a self-discharge resistance, C_{Cap} is a capacitor representing the charge stored in battery, and $I(t)$ is a current controlled current source, measuring the current flowing in sub-circuit 2. The first sub-circuit is designed for energetic considerations, such as SoC measurement, remaining capacity, or self-discharge ratio. The second sub-circuit is composed of a third-order Thevenin model but replacing the voltage source by a voltage-controlled voltage source, measuring voltage (SoC-dependent) from the first sub-circuit. The second sub-circuit is designed for simulating I-V performance.

Several works focused on the development of this model for electromobility application can be found in the current literature, the most usual being those composed of a second-order Thevenin model [13,78] and a third-order Thevenin model [5,79,80].

5. V-I Performance

For better comprehension, below are the performance differences from the main ECMs analyzed in Section 3 are explained. Figure 21 shows the typical behavior of a Li-Ion cell during a discharge-charge cycle.

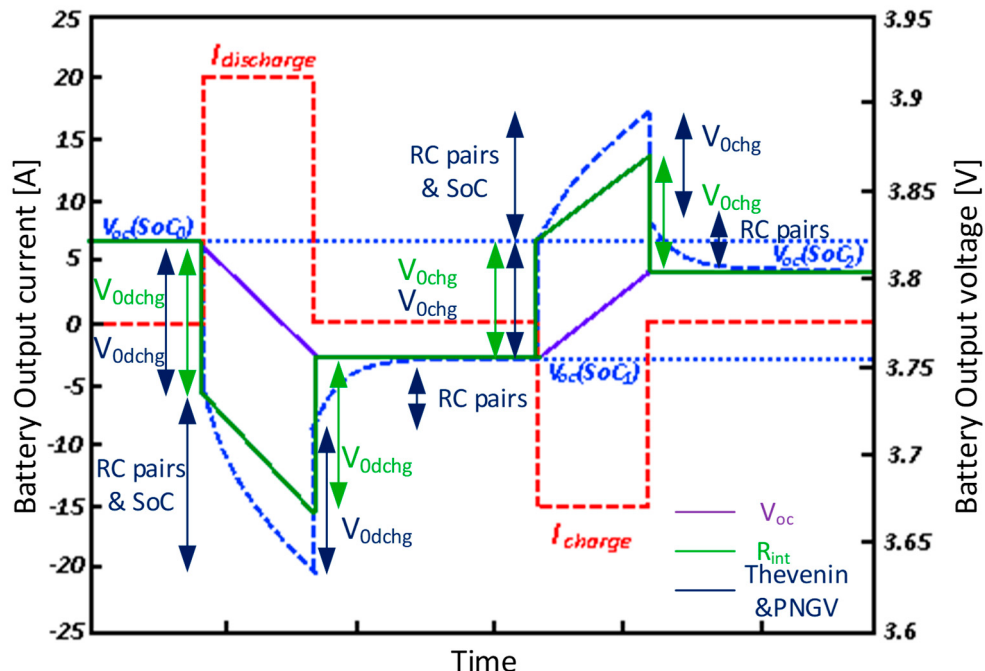


Figure 21. Li-Ion voltage and current in a cycle.

Starting from SoC_0 , an instantaneous voltage drop V_{odch} happens when the discharge is started due to R_{int} (Electrolyte resistance majorly). Then, voltage goes on decreasing exponentially, due to a combination of RC pairs (diffusion and surface reactions) and SoC decrease in the voltage source. Voltage drop V_{odch} is recovered instantaneously when current falls to zero, and due to RC pairs, voltage needs some time to be stabilized in a new SoC state, SoC_1 . When the charging state starts, an instantaneous voltage increase V_{ochg} happens due to R_{int} , followed by an exponential increase due to RC pairs and SoC variation in voltage source. Finally, when the charging stops, an instantaneous voltage drop happens due to R_{int} , and an exponential decrease due to RC pairs, until final SoC is reached, SoC_2 . Thevenin and PNGV models are more accurate when RC pairs are increased and can model these effects. However, when using an ideal model with SoC consideration, as it can be seen in Figure 21, V_{oc} graphed in purple only considers part of the dynamic: Voltage variation with SoC variation. The enhanced simple model with SoC consideration is more accurate, since it considers the instantaneous voltage drops too, graphed in green in Figure 21. Therefore, a linear model cannot be considered for SoC direct measurement, as it does not consider SoC in the voltage variation [17].

Consequently, Thevenin and PNGV models are best considered for most applications. Based on the characteristics of the study, the most-used RC pairs number in Thevenin and PNGV models are between 1 and 2. Its waveform is graphed in blue. A greater number of RC pairs increases computational effort without providing a reasonable enough accuracy increase [81]. In design or diagnosis applications, where simulation speed is not important, it is common to use three RC pairs. Therefore, the number of RC pairs is defined by accuracy and complexity dilemma [59]. The values of the elements of the RC pairs are usually obtained by experimental results.

Within Thevenin and PNGV models, the first-order one can represent transient state approximately and it is enough for most studies, especially those where simulation speed is a priority. Second-order models can represent transient state fairly accurate, and therefore, it is applicable in SoC estimation. Within electromobility, a second-order model is considered appropriate, even better if it is combined with a runtime model [78].

Table 3 [57] gathers the accuracy results of a comparative study among different models.

Table 3. Comparison of the error in percentage [%] among electrical equivalent circuits.

Test	50% SoC, 1C DoD [%]	Pulse Test			DDP Test			Capacity Test 1C			Capacity Test 5C		
		0–5	5–90	90–100	0–5	5–90	90–100	0–5	5–90	90–100	0–5	5–90	90–100
Rint	0.2	4.5	7	14	5	15	20	3	5	18	8	9	19.2
RC	0.3	8	2	55	5	5	46	7	2	58	6	5	50
Thevenin	0.2	3.5	5	17	4	4	15	2	1	20	2	7	19
PNGV	0.2	2	1.5	25	4	3.5	19	2	1.5	29	6	12	18
2nd order PNGV	0.1	2	2	19	2.5	2	14	2	2	25	4	14	35
3rd order PNGV	0.2	1.5	2	17	3	1	13	2	2	23	3	12	28
Noshin	0.2	2	1.5	13.5	2.5	3	14	2	1	16.5	2	2	12.5

Although all the models are very accurate under standard fixed conditions (5–90% Depth of Discharge (DoD)), results depend on operating current, but, overall, on DoD, reaching an error of 58%.

The batteries are operated typically with a 60% DoD when cycled near the middle of the SoC. In these applications, the Thevenin or PNGV models are usually accurate enough, while maintaining a high computational speed. In case large computation resources are available and if the application would demand a charging/discharging profile more similar to dynamic discharging profile (DDP), a third-order PNGV model would be the most accurate, as well as RC model for the pulse test profile.

Nevertheless, batteries operating in deep cycles are a critical application for current models. The Noshin model seems to offer better results in those tests that aim to measure the capacity of a battery, independently from the DoD.

Table 4 gathers analyzed literature with electromobility application.

Table 4. Analyzed literature summary.

Model	Objective	Considerations		Battery Type	Year	Ref
		Effects	Parameters			
Simple	Ideal	Model	V _{OC}	Li-Ion	1997	[15]
	Linear	Energy management	SoC, T	LFP (Li-Ion)	2017	[22]
		HEV Simulation	SoC	V _{OC} , R _{int}	2007	[23]
		SoC estimation		Li-Ion	2017	[24]
		Model	C _{cap} , R _{int}	Lead-Acid	2001	[25]
	RC	SoC estimation	Pol, Prop, SoC	LFP (Li-Ion)	2013	[82]
ECM	1 Order	SoC estimation		Li-Ion	2013	[33]
		Stability analysis and SoC estimation	Pol, SoC	LCO (Li-Ion)	2018	[32]
		Batteries parallelization			2015	[37]
		SoC and SoH model	Pol, SoC, SoH, T	Li-Ion	2016	[38]
		Power Electronic			2011	[39]
		EP-Thevenin model	Pol, SoC,	V _{OC} , R _{int} , R _P , C _P	2013	[40]
	Order	Life model	Pol, SoC, T	LFP (Li-Ion)	2011	[41]
		System design		LFP (Li-Ion)	2017	[83]
	Thev	Parameter regression	Pol, SoC, T, Hyst	Pb-acid, NiMH, Li-ion	2002	[84]
Thev	2 order	Model	T, CF		2009	[45]
		SoC estimation	Pol, SoC	Li-Ion	2016	[46]
		SoC, SoH, and SoF estimation	SoC, SoH, SoF		2018	[47]
		Model	Pol, SoC, SoH, T	NMC (Li-Ion)	2018	[48]
		Characterization		V _{OC} , R _{int} , 2RC	NMC, LFP, LTO (Li-Ion)	[18]
		Model	Pol, SoC, T		2018	[86]
	3 order	Fault diagnosis	Pol, SoC	NMC (Li Ion)	2016	[87]
		Life model	Pol, SoC, T, SoH		2018	[88]
		Model	SoC, Pol	Li-Ion	2013	[89]
		Model for V2G	SoC, Pol, T, Hyst	V _{OC} , R _{int} , 3RC	2017	[90]

Table 4. Cont.

PNGV	1 order	SoH estimation	Pol, ID, SoC, Pol, ID, SoH, SoC, T	V_{OC} , R_{int} , C_0 , RC	LFP (Li-Ion)	2018	[53]	
			Model		LFP and NMC (Li-Ion)	2016	[54]	
		2 order	Life model	Pol, ID, Hyst, SoC, T	LFP (Li-Ion)	2014	[55]	
Freq	2 order	Noshin	Model	Pol, SoC, SoH, T	V_{OC} , R_{int} , R_p , C_p	Li-Ion	2012	[58]
		Kinetics Study Characterization Model	Model	Pol Pol, SoC, T Pol, SoC	V_{OC} , R_{int} , $2Z_{Arc}$ V_{OC} , L, R_{int} , $2Z_{Arc}$	LFP (Li-Ion) NMC (Li-Ion) Li-Ion	2015 2014 2014	[74] [75] [77]
		3 order	Model	Pol	V_{OC} , L, R_{int} , $3Z_{Arc}$	Li-Ion	2012	[76]
RT	Thev	2 order	Model Model for EV	Pol, SoC, T, cycles	V_{OC} , R_{int} , $2RC$, C_{cap}	Li-Ion, Ni-MH LFP (Li-Ion)	2006 2011	[13] [92]
		3 order	Model for EV	Pol, SoC, T, cycles	V_{OC} , R_{int} , $3RC$, C_{cap}	Li-Ion Li-Ion, Ni-MH Li-Ion, Lead acid, Ni-MH	2011 2008 2016	[5] [79] [80]

CF: Capacity fade, ECM: Equivalent circuit model; Freq: Frequency, Hyst: Hysteresis, ID: Ion-diffusion, Pol: Polarization, Prop: Propagation, RT: Runtime, SoC: State of charge, SoF: State of function, SoH: State of health, T: Temperature, Thev: Thevenin.

Power variation studies, so-called power fade (PF), and capacity variation studies, so-called CF, are within the most usual and interesting current applications of battery models in electromobility. These studies represent the capacity or power variation when a battery is aged. It is known that average current, temperature, DoD, and average SoC are most influent variables in battery degradation by cycling [93]. However, an adequate model is required to know the performance differences, as can be a runtime-combined model with a first-order Thevenin considering hysteresis, second-order Thevenin, or Noshin model. This model should not only consider the current and the SoC, but also the SoH and the temperature in its parameters (R_{int} , V_{OC} , etc.). Therefore, it would be possible to predict a battery performance when it is degraded by the use and charging events. Indeed, charging events can be optimized if degradation is foreseen.

The definition of the parameters is, perhaps, the most expensive process in terms of time and effort. For this purpose, experimental tests to analyze the evolution of the parameters depending on the behavior to be characterized are necessary. These tests may consist of cycling a series of cells at different currents, temperatures, and DoDs, as well as in the continuous recording of their behavior until the end of their lifetime.

While V_{oc} and R_{int} are easily characterized by measuring the open-circuit voltage and the instantaneous voltage drop when the cells start discharging, characterizing their capacity at different SoH points requires specific capacity tests. Since these tests are carried out discretely, it may be necessary to interpolate the values obtained to calculate intermediate solutions.

An analysis of the contribution of each variable to the evolution of each parameter would allow a greater accuracy when extrapolating the results of the tests. Although these tests are carried out at constant current, it would be possible to apply the superposition method to emulate a real variable cycle.

Although these tests may involve a large time and computational cost, they are worth it since it would be possible to optimize the BMS of the vehicle that incorporates the tested cells.

6. Conclusions

Battery models can be classified into several categories; generally, these categories are electrochemical models, mathematical models, and electrical models.

Electrochemical model are the most accurate ones in emulating all the internal phenomena. However, they consume excessive computational resources and are very slow. Therefore, they are suitable for battery design, but not for real-time control or emulation purposes.

Mathematical models are appropriate for certain calculus or prediction parameters, such as statistical cycle life based on experimental tests.

Finally, electrical models are the most appropriate for real-time control or emulation purposes and are the best solution to be implemented in actual battery management systems (BMSs), chargers, or similar devices. These models are composed of simple elements, such as resistances and capacitors, which are characterized based on the influence of several parameters (temperature, current, etc.).

In this paper, several Li-Ion battery electric models available for automotive applications have been analyzed and categorized, showing their advantages and drawbacks.

Simple models are sufficient for those studies where the battery is not the focus. Thevenin and PNGV models are adequate when the battery works in a certain SoC range, however they are not suitable for DC response analysis or runtime prediction. It is common to use variable resistances and capacitors, which consider SoC or temperature for improving these deficiencies, but it increases the computational requirement. These models are appropriate for transient state analysis, but AC response is limited. Impedance models, in turn, are appropriate for AC response analysis, as they are developed in the impedance domain. However, their transient state response is very limited. Runtime models offer a DC and runtime response simultaneously with an average fixed current. At last, combined models also combine the models' advantages, improving accuracy by decreasing simulation speed.

The estimation of the parameters is another key aspect. While variables such as SoC or SoH have to be measured online, the estimation of the parameters can be done offline, and adjusted online if desired. In case an offline estimation of SoC or SoH based on laboratory tests is performed, and therefore not relating the parameters to the actual cycling of the battery, a high error in the results would be obtained.

An optimal model to be implemented in an EV must match a series of considerations:

1. Accuracy: An accurate model, and with consideration of enough general aspects is required. These general aspects can be:
 - a. Electrical model: Knowing the I-V behavior of a battery is essential for any study associated with its operation.
 - b. Thermal model: Since a battery resistance varies inversely with temperature, it is common to have accuracy errors in performance simulation and runtime estimation when temperature is neglected.
 - c. Runtime model: Necessary for those studies considering battery runtime, capacity increasing, or effects derived.
2. Computational simplicity: A simpler model is preferred easing real-time operation as simulation speed is increased.
3. Configuration simplicity: A simple model to be configured is preferred, with the lowest parameters to be identified and defined.
4. Interpretability: An interpretable model would ease the identification of the origin if any issue would appear in the battery.

Author Contributions: Conceptualization, G.S. and F.J.A.; formal analysis, G.S.; writing—original draft preparation, G.S.; writing—review and editing, F.J.A. and O.O.; visualization, O.O.; supervision, J.I.S.M. and I.Z.; project administration, J.I.S.M and I.Z.; funding acquisition, J.I.S.M. and I.Z.

Funding: The authors thank the support from the Gipuzkoa Provincial Council (project Etorkizuna Eraikiz 2019 DGE19/03), the Basque Government (GISEL research group IT1083-16), as well as from the University of the Basque Country UPV/EHU (PES16/31 and PES17/08).

Conflicts of Interest: The authors declare no conflict of interest.

References

1. Zamora, I.; San Martín, J.I.; García, J.; Asensio, F.J.; Oñederra, O.; San Martín, J.J.; Aperribay, V. PEM fuel cells in applications of urban public transport. *Renew. Energy Power Qual. J.* **2011**, *1*, 599–604. [CrossRef]

2. Yan, J.; Li, C.; Xu, G.; Xu, Y. A novel on-line self-learning state-of-charge estimation of battery management system for hybrid electric vehicle. In Proceedings of the 2009 IEEE Intelligent Vehicles Symposium (IVS), Xi'an China, 3–5 June 2009; pp. 1161–1166.
3. Shen, J.; Dusmez, S.; Khaligh, A. An advanced electro-thermal cycle-lifetime estimation model for LiFePO₄ batteries. In Proceedings of the 2013 IEEE Transportation Electrification Conference and Expo (ITEC), Detroit, MI, USA, 16–19 June 2013; pp. 1–6.
4. Eddahech, A.; Briat, O.; Vinassa, J. Real-Time SOC and SOH Estimation for EV Li-Ion Cell Using Online Parameters Identification. In Proceedings of the 2012 IEEE Energy Conversion Congress and Exposition, Raleigh, NC, USA, 15–20 September 2012.
5. Hentunen, A.; Lehmuspelto, T.; Suomela, J. Electrical battery model for dynamic simulations of hybrid electric vehicles. In Proceedings of the 2011 IEEE Vehicle Power and Propulsion Conference (VPPC), Chicago, IL, USA, 6–9 September 2011; pp. 1–6.
6. Lombardi, L.; Tribioli, L.; Cozzolino, R.; Bella, G. Comparative environmental assessment of conventional, electric, hybrid, and fuel cell powertrains based on LCA. *Int. J. Life Cycle Assess.* **2017**, *22*, 1989–2006. [[CrossRef](#)]
7. Thomas, C.E. Fuel cell and battery electric vehicles compared. *Int. J. Hydrog. Energy* **2009**, *34*, 6005–6020. [[CrossRef](#)]
8. Hu, X.; Zou, C.; Zhang, C.; Li, Y. Technological Developments in Batteries: A Survey of Principal Roles, Types, and Management Needs. *IEEE Power Energy Mag.* **2017**, *15*, 20–31. [[CrossRef](#)]
9. Wang, Y.; Ying, H.; Huang, S. Comparison of lithium-ion battery cathode materials and the internal stress development. In Proceedings of the ASME 2011 International Mechanical Engineering Congress & Exposition IMECE2011, Denver, CO, USA, 11–17 November 2011.
10. An, Z.; Jia, L.; Ding, Y.; Dang, C.; Li, X. A Review on Lithium-ion Power Battery Thermal Management Technologies and Thermal Safety. *J. Therm. Sci.* **2017**, *26*, 391–412. [[CrossRef](#)]
11. Cheng, K.W.E.; Divakar, B.P.; Wu, H.; Ding, K.; Ho, H.F. Battery-Management System (BMS) and SOC Development for Electrical Vehicles. *IEEE Trans. Veh. Technol.* **2011**, *60*, 76–88. [[CrossRef](#)]
12. Chaturvedi, N.A.; Klein, R.; Christensen, J.; Ahmed, J.; Kojic, A. Algorithms for Advanced Battery-Management Systems. *CSM* **2010**, *30*, 49–68.
13. Chen, M.; Rincon-Mora, G.A. Accurate electrical battery model capable of predicting runtime and I-V performance. *TEC* **2006**, *21*, 504–511. [[CrossRef](#)]
14. Hageman, S.C. Simple PSpice models let you simulate common battery types. *Electron. Des. News* **1993**, *38*, 117.
15. Gold, S. A PSPICE macromodel for lithium-ion batteries. In Proceedings of the Twelfth Annual Battery Conference on Applications and Advances (BCAA), Long Beach, CA, USA, 14–17 January 1997; pp. 215–222.
16. Jongerden, M.R.; Haverkort, B.R. Which battery model to use? *IET Softw.* **2009**, *3*, 445–457. [[CrossRef](#)]
17. Rahmoun, A.; Biechl, H. Parameters identification of equivalent circuit diagrams for li-ion batteries. In Proceedings of the 11th International Symposium PÄRNU “Topical Problems in the Field of Electrical and Power Engineering” and “Doctoral School of Energy and Geotechnology”, Pärnu, Estonia, 16–21 January 2012.
18. Zhang, R.; Xia, B.; Li, B.; Lai, Y.; Zheng, W.; Wang, H.; Wang, W.; Wang, M. Study on the Characteristics of a High Capacity Nickel Manganese Cobalt Oxide (NMC) Lithium-Ion Battery—An Experimental Investigation. *Energies* **2018**, *11*, 2275. [[CrossRef](#)]
19. Nikolian, A.; Firouz, Y.; Gopalakrishnan, R.; Timmermans, J.; Omar, N.; van den Bossche, P.; van Mierlo, J. Lithium Ion Batteries—Development of Advanced Electrical Equivalent Circuit Models for Nickel Manganese Cobalt Lithium-Ion. *Energies* **2016**, *9*, 360. [[CrossRef](#)]
20. Ceraolo, M. New dynamical models of lead-acid batteries. *IEEE Trans. Power Syst.* **2000**, *15*, 1184–1190. [[CrossRef](#)]
21. Puleston, P.F.; Valenciaga, F.; Battaiotto, P.E.; Mantz, R.J. Passivity/sliding mode control of a stand-alone hybrid generation system. *IEE Proc. Control Theory Appl.* **2000**, *147*, 680–686.
22. Zhu, T.; Min, H.; Yu, Y.; Zhao, Z.; Xu, T.; Chen, Y.; Li, X.; Zhang, C. An Optimized Energy Management Strategy for Preheating Vehicle-Mounted Li-ion Batteries at Subzero Temperatures. *Energies* **2017**, *10*, 243. [[CrossRef](#)]
23. Tremblay, O.; Dessaint, L.; Dekkiche, A. A Generic Battery Model for the Dynamic Simulation of Hybrid Electric Vehicles. In Proceedings of the 2007 IEEE Vehicle Power and Propulsion Conference (VPPC), Arlington, TX, USA, 9–12 September 2007; pp. 284–289.

24. Baboselac, I.; Hederić, Z.; Bensić, T. MatLab simulation model for dynamic mode of the Lithium-Ion batteries to power the EV. *Teh. Glas.* **2017**, *11*, 7–13.
25. Pang, S.; Farrell, J.; Du, J.; Barth, M. Battery state-of-charge estimation. In Proceedings of the 2001 American Control Conference. (Cat. No. 01CH37148), Arlington, VA, USA, 25–27 June 2001; Volume 2, p. 1649.
26. Cun, J.P.; Fiorina, J.N.; Fraisse, M.; Mabboux, H. The experience of a UPS company in advanced battery monitoring. In Proceedings of the Intelec'96-International Telecommunications Energy Conference, Boston, MA, USA, 6–10 October 1996; pp. 646–653.
27. Chan, H.L. A new battery model for use with battery energy storage systems and electric vehicles power systems. In Proceedings of the 2000 IEEE Power Engineering Society Winter Meeting. Conference Proceedings (Cat. No.00CH37077), Singapore, 23–27 January 2000; p. 475.
28. Berrueta, A.; Irigaray, V.; Sanchis, P.; Ursua, A. Lithium-ion battery model and experimental validation. In Proceedings of the 17th European Conference on Power Electronics and Applications (EPE'15 ECCE-Europe), Geneva, Switzerland, 8–10 September 2015; pp. 1–8.
29. Kim, Y.H.; Ha, H.D. Design of interface circuits with electrical battery models. *IEEE Trans. Ind. Electron.* **1997**, *44*, 81–86. [[CrossRef](#)]
30. Marcos, J.; Lago, A.; Penalver, C.M.; Doval, J.; Nogueira, A.; Castro, C.; Chamadoira, J. An approach to real behaviour modeling for traction lead-acid batteries. In Proceedings of the 2011 IEEE 32nd Annual Power Electronics Specialists Conference (IEEE Cat. No.01CH37230), Vancouver, BC, Canada, 17–21 June 2001; p. 624.
31. Sen, C.; Kar, N.C. Battery pack modeling for the analysis of battery management system of a hybrid electric vehicle. In Proceedings of the Battery pack modeling for the analysis of battery management system of a hybrid electric vehicle, Dearborn, MI, USA, 7–10 September 2009; pp. 207–212.
32. Ali, M.; Kamran, M.; Kumar, P.; Himanshu; Nengroo, S.; Khan, M.; Hussain, A.; Kim, H. An Online Data-Driven Model Identification and Adaptive State of Charge Estimation Approach for Lithium-ion-Batteries Using the Lagrange Multiplier Method. *Energies* **2018**, *11*, 2940. [[CrossRef](#)]
33. Kim, D.; Koo, K.; Jeong, J.; Goh, T.; Kim, S. Second-Order Discrete-Time Sliding Mode Observer for State of Charge Determination Based on a Dynamic Resistance Li-Ion Battery Model. *Energies* **2013**, *6*, 5538–5551. [[CrossRef](#)]
34. Kim, I.S. Nonlinear State of Charge Estimator for Hybrid Electric Vehicle Battery. *IEEE Trans. Power Electron.* **2008**, *23*, 2027–2034.
35. Ting, T.O.; Man, K.L.; Lim, E.G.; Leach, M. Tuning of Kalman Filter Parameters via Genetic Algorithm for State-of-Charge Estimation in Battery Management System. *Sci. World J.* **2014**, *2014*, 176052. [[CrossRef](#)] [[PubMed](#)]
36. Zhan, C.; Wu, X.G.; Kromlidis, S.; Ramachandaramurthy, V.K.; Barnes, M.; Jenkins, N.; Ruddell, A.J. Two electrical models of the lead–acid battery used in a dynamic voltage restorer. *IEE Proc. Gener. Transm. Distrib.* **2003**, *150*, 175. [[CrossRef](#)]
37. Yuan, S.; Wu, H.; Ma, X.; Yin, C. Stability Analysis for Li-Ion Battery Model Parameters and State of Charge Estimation by Measurement Uncertainty Consideration. *Energies* **2015**, *8*, 7729–7751. [[CrossRef](#)]
38. Bruen, T.; Marco, J. Modelling and experimental evaluation of parallel connected lithium ion cells for an electric vehicle battery system. *J. Power Sources* **2016**, *310*, 91–101. [[CrossRef](#)]
39. Jonghoon, K.; Cho, B.H. State-of-Charge Estimation and State-of-Health Prediction of a Li-Ion Degraded Battery Based on an EKF Combined With a Per-Unit System. *IEEE Trans. Veh. Technol.* **2011**, *60*, 4249–4260.
40. Hegazy, O.; Barrero, R.; Van Mierlo, J.; Lataire, P.; Omar, N.; Coosemans, T. An Advanced Power Electronics Interface for Electric Vehicles Applications. *IEEE Trans. Power Electron.* **2013**, *28*, 5508–5521. [[CrossRef](#)]
41. Xiong, R.; He, H.; Guo, H.; Ding, Y. Modeling for Lithium-Ion Battery used in Electric Vehicles. *Procedia Eng.* **2011**, *15*, 2869–2874. [[CrossRef](#)]
42. Han, H.; Xu, H.; Yuan, Z.; Zhao, Y. Modeling for lithium-ion battery used in electric vehicles. In Proceedings of the 2014 IEEE Conference and Expo Transportation Electrification Asia-Pacific (ITEC Asia-Pacific), Beijing, China, 31 August–3 September 2014.
43. Fotouhi, A.; Propp, K.; Auger, D.J. Electric vehicle battery model identification and state of charge estimation in real world driving cycles. In Proceedings of the 2015 7th Computer Science and Electronic Engineering Conference, Colchester, UK, 24–25 September 2015; p. 243.

44. Rahimi-Eichi, H.; Chow, M.Y. Adaptive parameter identification and State-of-Charge estimation of lithium-ion batteries. In Proceedings of the IECON 2012-38th Annual Conference on IEEE Industrial Electronics Society, Montreal, QC, Canada, 25–28 October 2012; pp. 4012–4017.
45. Erdinc, O.; Vural, B.; Uzunoglu, M. A dynamic lithium-ion battery model considering the effects of temperature and capacity fading. In Proceedings of the 2009 International Conference on Clean Electrical Power, Capri, Italy, 9–11 June 2009; pp. 383–386.
46. Guo, X.; Kang, L.; Yao, Y.; Huang, Z.; Li, W. Joint Estimation of the Electric Vehicle Power Battery State of Charge Based on the Least Squares Method and the Kalman Filter Algorithm. *Energies* **2016**, *9*, 100. [[CrossRef](#)]
47. Shen, P.; Ouyang, M.; Lu, L.; Li, J.; Feng, X. The Co-estimation of State of Charge, State of Health, and State of Function for Lithium-Ion Batteries in Electric Vehicles. *IEEE Trans. Veh. Technol.* **2018**, *67*, 92–103. [[CrossRef](#)]
48. Mesbahi, T.; Rizoug, N.; Bartholomeus, P.; Sadoun, R.; Khenfri, F.; Le Moigne, P. Dynamic Model of Li-Ion Batteries Incorporating Electrothermal and Ageing Aspects for Electric Vehicle Applications. *IEEE Trans. Ind. Electron.* **2018**, *65*, 1298–1305. [[CrossRef](#)]
49. Chaoui, H.; El Mejdoubi, A.; Gualous, H. Online Parameter Identification of Lithium-Ion Batteries With Surface Temperature Variations. *IEEE Trans. Veh. Technol.* **2017**, *66*, 2000–2009. [[CrossRef](#)]
50. Cheng, X.; Yao, L.; Xing, Y.; Pecht, M. Novel Parametric Circuit Modeling for Li-Ion Batteries. *Energies* **2016**, *9*, 539. [[CrossRef](#)]
51. Guenther, C.; Barillas, J.K.; Stumpp, S.; Danzer, M.A. A dynamic battery model for simulation of battery-to-grid applications. In Proceedings of the 2012 3rd IEEE PES Innovative Smart Grid Technologies Europe (ISGT Europe), Berlin, Germany, 14–17 October 2012; pp. 1–7.
52. Dong, B.; Tian, Y.; Zhou, C. One Estimating Method of the State of Charge of Power Battery for Electronic Vehicle. In Proceedings of the 2014 Sixth International Conference on Measuring Technology and Mechatronics Automation, Zhangjiajie, China, 10–11 January 2014; pp. 439–442.
53. Liu, X.; Li, W.; Zhou, A. PNGV Equivalent Circuit Model and SOC Estimation Algorithm for Lithium Battery Pack Adopted in AGV Vehicle. *Access* **2018**, *6*, 23639–23647. [[CrossRef](#)]
54. Ozkurt, C.; Camci, F.; Atamuradov, V.; Odorry, C. Integration of sampling based battery state of health estimation method in electric vehicles. *Appl. Energy* **2016**, *175*, 356–367. [[CrossRef](#)]
55. Uddin, K.; Picarelli, A.; Lyness, C.; Taylor, N.; Marco, J. An Acausal Li-Ion Battery Pack Model for Automotive Applications. *Energies* **2014**, *7*, 5675–5700. [[CrossRef](#)]
56. U.S. Department Secretary of Energy FreedomCAR Battery Test Manual for IDAHO. Available online: https://avt.inl.gov/sites/default/files/pdf/battery/freedomcar_manual_04_15_03.pdf (accessed on 5 May 2019).
57. Omar, N.; Widanage, D.; Abdel Monem, M.; Firouz, Y.; Hegazy, O.; Van den Bossche, P.; Coosemans, T.; Van Mierlo, J. Optimization of an advanced battery model parameter minimization tool and development of a novel electrical model for lithium-ion batteries. *Int. Trans. Electr. Energy Syst.* **2014**, *24*, 1747–1767. [[CrossRef](#)]
58. Omar, N.; Daowd, M.; Bossche, P.v.d.; Hegazy, O.; Smekens, J.; Coosemans, T.; Mierlo, J.v. Rechargeable Energy Storage Systems for Plug-in Hybrid Electric Vehicles—Assessment of Electrical Characteristics. *Energies* **2012**, *5*, 2952–2988. [[CrossRef](#)]
59. Fotouhi, A.; Auger, D.J.; Propp, K.; Longo, S.; Wild, M. A review on electric vehicle battery modelling: From Lithium-ion toward Lithium-Sulphur. *Renew. Sustain. Energy Rev.* **2016**, *56*, 1008–1021. [[CrossRef](#)]
60. Deng, Z.; Zhang, Z.; Lai, Y.; Liu, J.; Li, J.; Liu, Y. Electrochemical Impedance Spectroscopy Study of a Lithium/Sulfur Battery: Modeling and Analysis of Capacity Fading. *J. Electrochem. Soc.* **2013**, *160*, A558. [[CrossRef](#)]
61. Alavi, S.M.M.; Birk, C.R.; Howey, D.A. Time-domain fitting of battery electrochemical impedance models. *J. Power Sources* **2015**, *288*, 345–352. [[CrossRef](#)]
62. Troxler, Y.; Wu, B.; Marinescu, M.; Yufit, V.; Patel, Y.; Marquis, A.J.; Brandon, N.P.; Offer, G.J. The effect of thermal gradients on the performance of lithium-ion batteries. *J. Power Sources* **2014**, *247*, 1018–1025. [[CrossRef](#)]
63. Dai, H.; Jiang, B.; Wei, X. Impedance Characterization and Modeling of Lithium-Ion Batteries Considering the Internal Temperature Gradient. *Energies* **2018**, *11*, 220. [[CrossRef](#)]
64. Huang, J.; Li, Z.; Liaw, B.Y.; Zhang, J. Graphical analysis of electrochemical impedance spectroscopy data in Bode and Nyquist representations. *J. Power Sources* **2016**, *309*, 82–98. [[CrossRef](#)]

65. Kollmeyer, P.; Hackl, A.; Emadi, A. Li-ion battery model performance for automotive drive cycles with current pulse and EIS parameterization. In Proceedings of the 2017 IEEE Transportation Electrification Conference and Expo (ITEC), Chicago, IL, USA, 22–24 June 2017; pp. 486–492.
66. Plett, G. *Battery Management Systems, Volume I: Battery Modeling*; Artech House: Norwood, UK, 2015.
67. Jespersen, J.L.; Tønnesen, A.E.; Nørregaard, K.; Overgaard, L.; Elefsen, F. Capacity Measurements of Li-Ion Batteries using AC Impedance Spectroscopy. *World Electr. Veh. J.* **2009**, *3*, 127–133. [CrossRef]
68. Birk, C.R.; Howey, D.A. Model identification and parameter estimation for LiFePO₄ batteries. In Proceedings of the IET Hybrid and Electric Vehicles Conference 2013 (HEVC 2013), London, UK, 6–7 November 2013.
69. Schmalstieg, J.; Sauer, D.U. Full Cell Parameterization of a High-Power Lithium-Ion Battery for a Physico-Chemical Model: Part II. Thermal Parameters and Validation. *J. Electrochem. Soc.* **2018**, *165*, A3819. [CrossRef]
70. Xu, J.; Mi, C.C.; Cao, B.; Cao, J. A new method to estimate the state of charge of lithium-ion batteries based on the battery impedance model. *J. Power Sources* **2013**, *233*, 277–284. [CrossRef]
71. Eddahech, A.; Briat, O.; Vinassa, J. Performance comparison of four lithium-ion battery technologies under calendar aging. *Energy* **2015**, *84*, 542–550. [CrossRef]
72. Pastor-Fernández, C.; Uddin, K.; Chouchelamane, G.H.; Widanage, W.D.; Marco, J. A Comparison between Electrochemical Impedance Spectroscopy and Incremental Capacity-Differential Voltage as Li-ion Diagnostic Techniques to Identify and Quantify the Effects of Degradation Modes within Battery Management Systems. *J. Power Sources* **2017**, *360*, 301–318. [CrossRef]
73. Barai, A.; Chouchelamane, G.H.; Guo, Y.; McGordon, A.; Jennings, P. A study on the impact of lithium-ion cell relaxation on electrochemical impedance spectroscopy. *J. Power Sources* **2015**, *280*, 74–80. [CrossRef]
74. Heubner, C.; Schneider, M.; Michaelis, A. Investigation of charge transfer kinetics of Li-Intercalation in LiFePO₄. *J. Power Sources* **2015**, *288*, 115–120. [CrossRef]
75. Olofsson, Y.; Groot, J.; Katrašnik, T.; Tavčar, G. Impedance spectroscopy characterisation of automotive NMC/graphite Li-ion cells aged with realistic PHEV load profile. In Proceedings of the 2014 IEEE International Electric Vehicle Conference (IEVC), Florence, Italy, 17–19 December 2014; pp. 1–6.
76. Osaka, T.; Momma, T.; Mukoyama, D.; Nara, H. Proposal of novel equivalent circuit for electrochemical impedance analysis of commercially available lithium ion battery. *J. Power Sources* **2012**, *205*, 483–486. [CrossRef]
77. Li, S.E.; Wang, B.; Peng, H.; Hu, X. An electrochemistry-based impedance model for lithium-ion batteries. *J. Power Sources* **2014**, *258*, 9–18. [CrossRef]
78. Zhang, H.; Chow, M.H. Comprehensive dynamic battery modeling for PHEV applications. In Proceedings of the IEEE PES General Meeting, Providence, RI, USA, 25–29 July 2010; pp. 1–6.
79. Kroeze, R.C.; Krein, P.T. Electrical battery model for use in dynamic electric vehicle simulations. In Proceedings of the 2008 IEEE Power Electronics Specialists Conference, Rhodes, Greece, 15–19 June 2008; pp. 1336–1342.
80. Cao, Y.; Kroeze, R.C.; Krein, P.T. Multi-timescale Parametric Electrical Battery Model for Use in Dynamic Electric Vehicle Simulations. *IEEE Trans. Transp. Electr.* **2016**, *2*, 432–442. [CrossRef]
81. Huria, T.; Ceraolo, M.; Gazzarri, J.; Jackey, R. High fidelity electrical model with thermal dependence for characterization and simulation of high power lithium battery cells. In Proceedings of the 2012 IEEE International Electric Vehicle Conference, Greenville, SC, USA, 4–8 March 2012; pp. 1–8.
82. Blanco, C.; Sánchez, L.; Gonzalez, M.; Anton, J.C.; Gacia, V.; Viera, J.C. An Equivalent Circuit Model With Variable Effective Capacity for LiFePO₄ Batteries. *IEEE Trans. Veh. Technol.* **2014**, *63*, 3592–3599. [CrossRef]
83. Mathew, M.; Kong, Q.H.; McGrory, J.; Fowler, M. Simulation of lithium ion battery replacement in a battery pack for application in electric vehicles. *J. Power Sources* **2017**, *349*, 94–104. [CrossRef]
84. Gao, L.; Liu, S.; Dougal, R.A. Dynamic lithium-ion battery model for system simulation. *IEEE Trans. Compon. Packag. Technol.* **2002**, *25*, 495–505.
85. Verbrugge, M.; Koch, B. Generalized Recursive Algorithm for Adaptive Multiparameter Regression. *J. Electrochem. Soc.* **2006**, *153*, A187. [CrossRef]
86. Nikolian, A.; Jaguemont, J.; de Hoog, J.; Goutam, S.; Omar, N.; Van Den Bossche, P.; Van Mierlo, J. Complete cell-level lithium-ion electrical ECM model for different chemistries (NMC, LFP, LTO) and temperatures (−5 °C to 45 °C)—Optimized modelling techniques. *Int. J. Electr. Power Energy Syst.* **2018**, *98*, 133–146. [CrossRef]

87. Mesbahi, T.; Khenfri, F.; Rizoug, N.; Chaaban, K.; Bartholomeüs, P.; Le Moigne, P. Dynamical modeling of Li-ion batteries for electric vehicle applications based on hybrid Particle Swarm-Nelder-Mead (PSO-NM) optimization algorithm. *Electr. Power Syst. Res.* **2016**, *131*, 195–204. [[CrossRef](#)]
88. de Hoog, J.; Jaguemont, J.; Abdel-Monem, M.; Van Den Bossche, P.; Van Mierlo, J.; Omar, N. Combining an Electrothermal and Impedance Aging Model to Investigate Thermal Degradation Caused by Fast Charging. *Energies* **2018**, *11*, 804. [[CrossRef](#)]
89. Sidhu, A.; Izadian, A.; Anwar, S. Adaptive Nonlinear Model-Based Fault Diagnosis of Li-Ion Batteries. *IEEE Trans. Ind. Electron.* **2015**, *62*, 1002–1011. [[CrossRef](#)]
90. Yuksel, T.; Litster, S.; Viswanathan, V.; Michalek, J.J. Plug-in hybrid electric vehicle LiFePO₄ battery life implications of thermal management, driving conditions, and regional climate. *J. Power Sources* **2017**, *338*, 49–64. [[CrossRef](#)]
91. Omar, N.; Monem, M.A.; Firouz, Y.; Salminen, J.; Smekens, J.; Hegazy, O.; Gaulous, H.; Mulder, G.; Van den Bossche, P.; Coosemans, T.; et al. Lithium iron phosphate based battery—Assessment of the aging parameters and development of cycle life model. *Appl. Energy* **2014**, *113*, 1575–1585. [[CrossRef](#)]
92. Lam, L.; Bauer, P.; Kelder, E. A practical circuit-based model for Li-ion battery cells in electric vehicle applications. In Proceedings of the 2011 IEEE 33rd International Telecommunications Energy Conference (INTELEC), Amsterdam, Netherlands, 9–13 October 2011; pp. 1–9.
93. Thompson, A.W. Economic implications of lithium ion battery degradation for Vehicle-to-Grid (V2X) services. *J. Power Sources* **2018**, *396*, 691–709. [[CrossRef](#)]



© 2019 by the authors. Licensee MDPI, Basel, Switzerland. This article is an open access article distributed under the terms and conditions of the Creative Commons Attribution (CC BY) license (<http://creativecommons.org/licenses/by/4.0/>).

**SELF EVALUATION REPORT OF KRISHNADAS BABU FOR THE MONTH OF
MARCH 2021**
INTERNS BATCH NO. 2

(TO BE FILLED AND uploaded BY EACH CANDIDATE)

1	Name of the candidate	Krishnadas Babu
2	Institution	Govt. Model Engineering College
3	Assessment Period (Month Year)	March 2021
<i>All below information is to be respective of the Assessment Period mentioned</i>		
4	Primary mode of team communication	ONLINE
5	Apps used for communication w/ other team members <i>(include all that is applicable)</i>	Signal, Google Meet
6	Technology/Stack focused in learning	Django, MySQL
7	Resources used to learn the focused technology/stack <i>(include all that is applicable)</i>	YouTube, Django documentations, Udemy
8	Satisfied in the resources that you use to learn? (Y/N)	Y
9	Any particular portion/concept that is difficult to understand in the focused technology/stack requires addl. training <i>(include all that is applicable)</i>	Nil
10	Received any resources from the company? (Y/N)	Y
11	Details of any tests attended (SL / Name of the test / Date / Outcome)	1. Nil
12	Number of team meetings conducted	5
13	Number of team meetings attended	3
14	How will you describe your contribution to the team? (> 100 words)	Contributing to the team by bringing enthusiasm and sharing knowledge. Continuous peer to peer learning in the backend stack
15	Challenges faced by the team or yourself (if any, elaborate)	Person to person contact and communication
16	Satisfied in the technologies used? (Y/N)	Y

17	Are you satisfied with the team lead? (Y/N)	Y
18	Do you have any complaints? (if yes, elaborate)	Nil

19	How helpful / knowledgeable is your other team members	Helpful in providing resources and support oriented towards the project
20	A team member that you contact when you have a doubt/question as part of learning <i>(Mention their name)</i>	Soorya Krishnanunni
21	How helpful / knowledgeable are they?	Very helpful and keen on sharing doubts and knowledge
22	Have you ever faced any form of discrimination and or less consideration and or ever felt that way while working in the team? (Including company officials) <i>(if Yes, elaborate)</i> (Y/N)	N

23	Satisfied in the technologies used? (Y/N) (if no, describe)	Y
24	Any other technology/stack that you want to use in the current project <i>(if any)</i>	Nil
24	Any other comments <i>(if any)</i>	Nil

25	Any personal projects that you are currently working on? Explain <i>(if any, include all that is applicable)</i>	Nil
26	Would you like to receive any aid like server resources (AWS/GCP/Azure/DigitalOcean) from the company to back your personal projects? <i>(if any, write a short pitch statement)</i>	N
27	Would you like to get any learning resources from the company?	N

	(Y/N) (if yes, please elaborate)	
--	----------------------------------	--

I hereby confirm that the above provided information are correct and sincere to the best of my efforts and knowledge.

Batch: 2
Date: 29-05-2021

Krishnadas Babu

On Date: 29-05-2021



(Image of Signature)

**SELF EVALUATION REPORT OF KRISHNADAS BABU FOR THE MONTH OF
APRIL 2021**

INTERNS BATCH NO. 2

(TO BE FILLED AND uploaded BY EACH CANDIDATE)

1	Name of the candidate	Krishnadas Babu
2	Institution	Govt. Model Engineering College
3	Assessment Period (Month Year)	April 2021
<i>All below information is to be respective of the Assessment Period mentioned</i>		
4	Primary mode of team communication	ONLINE
5	Apps used for communication w/ other team members <i>(include all that is applicable)</i>	Signal, Google Meet
6	Technology/Stack focused in learning	Django, MySQL
7	Resources used to learn the focused technology/stack <i>(include all that is applicable)</i>	YouTube, Django documentations, Udemy
8	Satisfied in the resources that you use to learn? (Y/N)	Y
9	Any particular <i>portion/concept</i> that is difficult to understand in the focused technology/stack requires addl. training <i>(include all that is applicable)</i>	Nil
10	Received any resources from the company? (Y/N)	Y
11	Details of any tests attended (SL / Name of the test / Date / Outcome)	<ol style="list-style-type: none"> 1. Related Technologies Test/19-04-2021/Pass 2. SQL Test/22-04-2021/Pass
12	Number of team meetings conducted	17
13	Number of team meetings attended	17
14	How will you describe your contribution to the team? (> 100 words)	Contributing to the team by bringing enthusiasm and sharing knowledge. Continuous peer to peer learning in the backend stack
15	Challenges faced by the team or yourself (if any, elaborate)	Person to person contact and communication

16	Satisfied in the technologies used? (Y/N)	Y
17	Are you satisfied with the team lead? (Y/N)	Y
18	Do you have any complaints? (if yes, elaborate)	Nil

19	How helpful / knowledgeable is your other team members	Helpful in providing resources and support oriented towards the project
20	A team member that you contact when you have a doubt/question as part of learning <i>(Mention their name)</i>	Soorya Krishnanunni
21	How helpful / knowledgeable are they?	Very helpful and keen on sharing doubts and knowledge
22	Have you ever faced any form of discrimination and or less consideration and or ever felt that way while working in the team? (Including company officials) (if Yes, elaborate) (Y/N)	N

23	Satisfied in the technologies used? (Y/N) (if no, describe)	Y
24	Any other technology/stack that you want to use in the current project (if any)	Nil
24	Any other comments (if any)	Nil

25	Any personal projects that you are currently working on? Explain (if any, include all that is applicable)	Nil
26	Would you like to receive any aid like server resources (AWS/GCP/Azure/DigitalOcean) from the company to back your personal projects? (if any, write a short pitch statement)	N

27	Would you like to get any learning resources from the company? (Y/N) <i>(if yes, please elaborate)</i>	N
----	---	---

I hereby confirm that the above provided information are correct and sincere to the best of my efforts and knowledge.

Batch: 2
Date: 29-05-2021

Krishnadas Babu

On Date: 29-05-2021



(Image of Signature)